GEOLOGICA ULTRAIECTINA

Mededelingen van de
Faculteit Aardwetenschappen
Universiteit Utrecht

No. 117

GEODYNAMICS IN THE BAMBLE AREA DURING GOTHIAN- AND SVECONORWEGIAN TIMES

A COMPARATIVE PETROLOGICAL STUDY OF TWO GABBROS

Bas Dam

GEOLOGICA ULTRAIECTINA

Mededelingen van de
Faculteit Aardwetenschappen
Universiteit Utrecht

No. 117

GEODYNAMICS IN THE BAMBLE AREA DURING GOTHIAN- AND SVECONORWEGIAN TIMES

A COMPARATIVE PETROLOGICAL STUDY OF TWO GABBROS

Bas Dam

CIP-GEGEVENS KONINKLIJKE BIBLIOTHEEK, DEN HAAG

Dam, Bastiaan Pieter

Geodynamics in the Bamble area during Gothian- and Sveconorwegian times: (A comparative petrological study of two gabbros) / Bastiaan P. Dam. -Utrecht : Faculteit Aardwetenschappen, Universiteit Utrecht. -(Geologica Ultraiectina, ISSN 0072-1026; No. 117)

Proefschrift Universiteit Utrecht. Met lit. opg -Met samenvatting in het Nederlands.

ISBN 90-71577-71-6

Trefwoorden: Noorwegen ; geodynamica / gesteenten.

GEODYNAMICS IN THE BAMBLE AREA DURING GOTHIAN- AND SVECONORWEGIAN TIMES

A COMPARATIVE PETROLOGICAL STUDY OF TWO GABBROS

GEODYNAMICA IN HET BAMBLE GEBIED TIJDENS DE GOTISCHE- EN SVECONORWEGISCHE PERIODE

EEN VERGELIJKEND PETROLOGISCH ONDERZOEK AAN TWEE GABBRO'S

(MET EEN SAMENVATTING IN HET NEDERLANDS)

PROEFSCHRIFT

TER VERKRIJGING VAN DE GRAAD VAN DOCTOR AAN DE UNIVERSITEIT UTRECHT OP GEZAG VAN DE RECTOR MAGNIFICUS, PROF.DR. J.A. VAN GINKEL INGEVOLGE HET BESLUIT VAN HET COLLEGE VAN DECANEN IN HET OPENBAAR TE VERDEDIGEN OP WOENSDAG 18 JANUARI 1995 DES MIDDAGS OM 14.30 UUR.

Door

Bastiaan Pieter Dam

Geboren op 4 Januari 1964, te Heerjansdam

PROMOTOREN: **PROF. DR. B.M.W.S. DE JONG**
PROF. DR. J.L.R. TOURET

Met mijn bimbam hamertje
sla ik op mijn kamertje
alle steentjes kort en klein
want dat vind ik reuzefijn

W.F. Hermans, 1975

TABLE OF CONTENT

DANKWOORD\ACKNOWLEDGEMENT

Vele mensen hebben zijn of haar steentje bijgedragen om dit proefschrift tot de huidige status te verheffen. Sommigen hebben een klein steentje bijgedragen, andere een enorm rotsblok. Echter alle stenen zijn van grote waarde geweest. De steentjes zijn niet alleen geologisch van aard; er zitten ook heel veel sociale steentjes bij. Ik wil bij deze iedere donateur heel hartelijk danken. Een aantal wil ik met name noemen omdat deze of een hele grote of een hele mooie steen hebben bijgedragen.

Allereerst is daar mijn eerste promotor, Prof. B. de Jong. Hij heeft mij de juiste stenen aangerijkt en er op toegezien dat bij de opbouw van dit proefschrift elk steentje de juiste plaats kreeg. Door zijn vernieuwende kennis binnen de geologie heeft mij kunnen motiveren om dit onderzoek passend af te sluiten.

Bernhard, bedankt !

Ten tweede wil ik mijn andere promotor, de immer enthousiaste Prof. J. Touret bedanken. Hij heeft naast vele constructieve opmerkingen mij in de wereld van de vloeistof insluitseltjes geïntroduceerd. Vervolgens wil ik de initiator van dit project, Cees Mayer, bedanken. Zijn kennis van de klassieke petrologie is van grote waarde geweest voor dit proefschrift. Een grote groep mensen, die ik hier niet allemaal met name zal noemen wil ik hier toch graag bedanken voor een fijne tijd. Deze groep bestaat uit:

(ex)collega's, (ex)promovendi, analisten, (N)WP'ers, hardlopers, zwemmers, fietsers, squashers, skiers, een enkele touwtrekker, zeilers en een ieder die zich niet in dit rijtje kan plaatsen maar zich toch aangesproken voelt.

I would also like to thank the members of the examining committees. They pointed out the imperfections of a previous version of my thesis and helped me to correct this.

De aangename tijd die ik met mijn bimbam hamertje op mijn warande kamertje heb doorgebracht is mede veroorzaakt door het prettige gezelschap van:

Peter, Marc V, Nelleke, Reinier, Willeke, Ruud, Annemiek en last but not least Draadje.

De onvoorwaardelijke steun die ik van mijn familie heb gekregen, heeft me zeker in de wat 'moeilijkere' perioden, veel goed gedaan.

SAMENVATTING

Algemeen onderzoekskader

De vorming van continenten is een zeer dynamisch proces. Zo wordt op de ene plaats nieuw continent gevormd; op de andere wordt het gedeeltelijk weer afgebroken. De motor achter dit proces is de warmtehuishouding van de aarde. De aarde probeert zich van haar warmte te ontdoen door heet gesmolten gesteente naar buiten te stuwen waar het kan afkoelen. Een dergelijke stuw kan zo intens zijn dat de bovenliggende aardkorst breekt en uit elkaar wordt getrokken. Er ontstaan platen die op de ene plaats van elkaar af bewegen en op de andere tegen elkaar botsen of onder elkaar schuiven. Botsende en onderschuivende platen kunnen nieuw continent vormen. Dit gehele proces staat bekent onder de naam plaattektoniek en is waarschijnlijk al miljarden jaren actief. Of de processen achter de plaattektoniek gedurende de gehele aardse geschiedenis hetzelfde zijn gebleven is nog maar de vraag. Immers de warmtehuishouding van de aarde zal in de loop van de tijd aanzienlijk verandert zijn. De geologie onderzoekt de processen die aan de plaattektoniek gerelateerd zijn of waren en probeert ze te begrijpen.

De faculteit Geologie en Geofysica te Utrecht, afdeling Petrologie heeft zich onder andere jarenlang bezig gehouden met de continentvormende processen in zuid Noorwegen, een gebied met een ouderdom variërend van 1,7 tot 0,9 miljard jaar. Mijn bijdrage aan dit grootschalig onderzoek heeft zich geconcentreerd in een gebied in het zuidoosten van Noorwegen. In dit gebied, Bamble genaamd, zijn twee continentvormende perioden te herkennen. Deze perioden worden aangeduid met de Gotische en Sveconorwegische periode en zijn respectievelijk 1,6 en 1,1 miljard jaar oud. Wat precies de geologische omstandigheden in het Bamble gebied zijn geweest tijdens deze twee perioden is lange tijd een discussie geweest. Deze discussie is de aanleiding geweest tot het definiëren van mijn onderzoek.

Doel van het onderzoek

Het doel wat ik met dit onderzoek heb willen bereiken is tweeledig:

1) karakterisering van de geologische processen tijdens de continentvorming in het Bamble gebied.
2) vaststellen van criteria waarop beide continentvormende perioden in het Bamble gebied onderscheiden kunnen worden.

Geologische inleiding

Uit voorgaande studies is gebleken dat de twee continentvormende processen in het Bamble gebied gepaard zijn gegaan met het indringen van gesmolten gesteenten, gabbro's genaamd, in de bovenliggende aardkorst. Dergelijke gabbroïde smelten worden diep in de aardkorst, of zelfs nabij de mantel, gevormd en hebben een temperatuur van ongeveer 1200°C. Deze smelten kunnen vervolgens tot verschillende niveaus in de bovengelegen aardkorst dringen. Komt zo'n smelt aan het aardoppervlak, dan ontstaat er een vulkaan; blijft hij halverwege steken en kristalliseert hij daar uit dan ontstaat er een gabbro. De gabbro's uit het Bamble gebied zijn waarschijnlijk op een diepte van ongeveer 24 km blijven steken. Daar zijn ze uitgekristalliseerd en onderdeel van het continent geworden. Het zal duidelijk zijn dat dergelijke gabbro's belangrijke informatie bevatten over de warmtehuishouding van de aarde.

SAMENVATTING

Door grootschalige opheffing en erosie van onder andere het Bamble gebied is een diepe gedeelte van de aardkorst aan de oppervlakte gekomen. In het Bamble gebied kunnen we dus processen onderzoeken die zich zo'n 1,6 miljard jaar op een diepte van 24 km onder het aardoppervlak hebben afgespeeld.

Onderzoeksmethode

De methode die ik gebruikt heb om de twee continentvormende perioden in het Bamble gebied te karakteriseren is het vergelijken van twee gabbro lichamen, een oude van ca. 1,7 miljard jaar oud en een 'jonge' van ca. 1,1 miljard jaar oud. Deze gabbro's worden respectievelijk met de Jomasknutene en Dale gabbro aangeduid. De Dale gabbro heeft alleen de Sveconorwegische continentvormende periode meegemaakt; de Jomasknutene zowel de Gotische als de Sveconorwegische. Door beide gabbro's met elkaar te vergelijken moet men in principe het verschil tussen de twee continentvormende perioden kunnen bepalen. Omdat er al relatief veel bekend was van de Dale gabbro heb ik me voornamelijk op het onderzoek van de Jomasknutene gabbro toegelegd en de gegevens van de Dale gabbro gebruikt als vergelijkingsmateriaal.

Allereerst heb ik de Jomasknutene gabbro gedetailleerd gekarteerd en bemonsterd. De monsters heb ik chemisch geanalyseerd en hun mineralogie bepaald. Vervolgens heb ik een aantal specifieke onderwerpen geselecteerd die de mogelijke sleutel vormen voor mijn probleemstelling.

Resultaten

In dit proefschrift laat ik zien dat het verschil tussen de twee continentvormende processen in het Bamble gebied zich slechts door kleine subtiele verschillen manifesteert. Ik noem hier de drie belangrijkste:

1) Uit modelberekeningen blijkt dat er tijdens beide perioden sprake was van extra warmte toevoer vanuit het onderliggende gebied. De vorming van de gabbroïde smelten is hier waarschijnlijk het gevolg van. Deze warmte toevoer was tijdens de Sveconorwegische periode iets groter dan tijdens de Gotische.
2) In de Jomasknutene gabbro zijn er aanwijzingen dat na het kristalliseren van de smelt zure chloorrijke vloeistoffen door het gesteente migreerden. Deze vloeistoffen hebben plaatselijk zowel de gabbro als het nevengesteente van samenstelling doen veranderen. Dergelijke processen zijn niet in de Dale gabbro te herkennen.
3) Na het kristalliseren van de Dale gabbro is er een substantiële drukverlaging geweest bij constante temperatuur met als resultaat dat er bepaalde waterhoudende mineralen dehydrateerden. Dit fenomeen is niet in de Jomasknutene gabbro gevonden.

De conclusie die ik uit deze resultaten trek is dat met mijn onderzoeksmethode geen eenduidige criteria gevonden worden waarop ik een onderscheid zou kunnen maken tussen de Gotische en Sveconorwegische continentvormende periode in het Bamble gebied.

SUMMARY

Continents started to grow already at an early stage of the earth history. Some of these early continents were preserved from major destroying forces and are now recognized as cratons. What make these cratons unique is that they contain useful information about the continent building mechanism at an early time of the earth history. I focus in this thesis on such continent building mechanism occurring in the southwestern part of the Baltic Shield, the Bamble area, in a period between 1.8 Ga and 0.9 Ga ago. This area is one of the youngest parts of the Baltic Shield and exhibits two distinct periods of continental growth. The oldest is known as the Gothian period (between 1.75 Ga and 1.50 Ga); the youngest as the Sveconorwegian (between 1.25 and 0.9 Ga).

The method I used to investigate this continent building mechanism at late proterozoic times is by comparing the geology of two gabbros i.e. the Jomasknutene and Dale gabbro. The Jomasknutene gabbro has been dated at 1.77 Ga $\pm$0.19 Ga and must contain information about the Gothian and Sveconorwegian period. The Dale gabbro has been dated at 1.11 Ga $\pm$0.14 Ga and must contain information about the Sveconorwegian period only.

In the period the Bamble area was subjected to continental growth, between 1.75 Ga and 0.9 Ga ago, the reigning metamorphic conditions in this area were characterized by a continuous high heat flow from the area below. In terms of geotectonic setting, this can be interpreted as a discontinuous active rift system. At least two periods of gabbroic intrusions were initialized in this rift environment. True rifting was probably opposed by, compressional, orogenic activity. That the geotectonic setting in the Bamble area did not change much between 1.75 Ga and 0.9 Ga ago is accentuated by the geological similarity between the Gothian Jomasknutene and the Sveconorwegian Dale gabbro. They appear to have a similar whole rock chemistry, magmatic fractionation trend, magmatic and, in less extent, metamorphic mineralogy. The most prominent results of this study, based on the comparison of the two gabbros, are listed below.

SUMMARY

I It is not possible to distinguish unequivocally between the Gothian and Sveconorwegian metamorphic period in the central part of the Bamble area.

II Both metamorphic periods can be characterized by a high heat flow from the underlying area. Uplift of the Bamble area at the end of the Sveconorwegian period was probably accompanied an increasing heat flow.

III Only limited mass transfer occurred during metamorphism of the Jomasknutene and the Dale gabbro. This is born out by the comparison of "fresh" and "altered" gabbroic rocks, by metamorphic mineral chemistry and by the isochemical character of olivine coronas.

IV Typical grain size variations and concomitantly the magmatic structure of the Jomasknutene and Dale gabbro seems to be a discriminating feature between Gothian and Sveconorwegian gabbros in the Bamble area. To explain their grain size variation a new concept in the magmatic petrology is introduced and is illustrated in a Time-Temperature-Transformation diagram.

V The olivine corona texture of the Dale gabbro exhibit dehydration textures of its amphibole outer rim probably due to decompression at about 850°C. This dehydration reaction is of Sveconorwegian age.

VI The hydration of augite in the Jomasknutene gabbro is accompanied by aqueous brine like and high density CO_2-N_2 fluids. Estimation of the partial water pressure during the amphibolitization of the intercumulus augite is about 1 kbar.

VII The acid chlorine rich metamorphic fluid penetrating the Jomasknutene gabbro de-aluminized locally amphibole.

CHAPTER I
THE ROLE OF THE BAMBLE AREA IN THE EVOLUTION OF THE BALTIC SHIELD

1.1 SCOPE OF THIS THESIS

This thesis concerns the geological characterization and comparison of two continent-building periods in the south-western part of the Baltic Shield viz. the Bamble area, south-east Norway, between circa 1.75 Ga and 0.90 Ga ago (mid- to late Proterozoic). The oldest continent-building period is known as the Gothian period (between 1.75 Ga and 1.50 Ga); the youngest as the Sveconorwegian period (between 1.25 Ga and 0.90 Ga).

The method I used to characterize these two periods of continental growth is by comparing the 1.77 Ga $\pm$0.19 Ga old Jomasknutene gabbro with the 1.11 Ga $\pm$0.14 Ga old Dale gabbro. Both age estimates were carried out by de Haas 1992 using the Sm/Nd isotope dating method. The geological information stored in these two gabbros are the result of syn and post intrusion conditions. Thus the Jomasknutene gabbro provides most likely information about the geological conditions during Gothian and Sveconorwegian times whereas the Dale gabbro provides information about the Sveconorwegian period only.

The subject of this thesis fits in the whole of continental growth of Precambrian cratons, the Baltic craton in particular. Therefore I start discussing a model concerning the growth of continents at Precambrian times and discuss the regional geology of the Baltic Shield briefly. As the subject of this thesis covers only a small episode in the history of the continental growth of the Baltic Shield viz. between 1.75 and 0.90 Ga ago I shall zoom in on this particular period and focus on the Bamble area, the area I carried out my study.

1.2 EVOLUTION OF THE BALTIC SHIELD

The Baltic Shield comprises the Scandinavian main land with an extension to the Kola Peninsula in the north-western part of Russia. This Shield has been divided into three main domains of Precambrian age and two of Palaeozoic age. This subdivision is based on absolute age determinations and illustrates the growth of the Baltic Shield with time.

The Baltic Shield is illustrated in figure 1.1. The oldest domain, an Archean protocontinent (1) was formed between 3.5 Ga and 2.65 Ga ago. A mechanism to form such a protocontinent is described by Vlaar (1985). This mechanism is based on the earths' heat dissipation in which solidified basaltic material at the earths' surface is continuously resorbed by an underlying melt. This resorption process generated tonalitic-like magmas which intruded and accumulated to protocontinents. As this way of continent-building proceeded, the thermal and dynamic state of the earth changed (Richter 1988) to such extent that another, less effective heat dissipating mechanism (Hargraves 1986) became operational in the early Proterozoic. This mechanism is probably the precursor for the present day plate tectonics (Vlaar 1985). A characteristic of such post Archean geodynamic evolution is the recycling of older continental material. Claesson et al. (1991) dated 3.4 Ga old detrital zircons from sediments from the Karelian-Svecofennian domain (2) in the Baltic Shield. Apparently, continental material from the Archean protocontinent was recycled to the sediments deposited in the Karelian-Svecofennian domain, between 2.65 Ga and 1.75 Ga ago (Gaál and Gorbatschev, 1987, Lindh, 1987 and Ward, 1987). After the formation of the Karelian-Svecofennian Domain the growth of the Baltic Shield proceeded by forming the Gothian-Sveconorwegian

Domain designated by area 3 and 4 in figure 1.1 (Gorbatschev and Gaál 1987, Åhäll and Daly 1989, Falkum 1990). Sediments probably derived from the Karelian-Svecofennian mainland were deposited here somewhere between 1.75 Ga and 0.90 Ga ago. The western and north-western part of the Baltic Shield are partly covered with Caledonian rocks, designated 5. These Caledonian rocks varying in age between 0.6 Ga and 0.4 Ga, represent some of the youngest accretional features encountered in this region. Locally Palaeozoic sediments ageing between 0.6 Ga and 0.4 Ga and magmatic rocks of Permian age (0.25 Ga old), designated 6, are present in the Gothian Sveconorwegian domain.

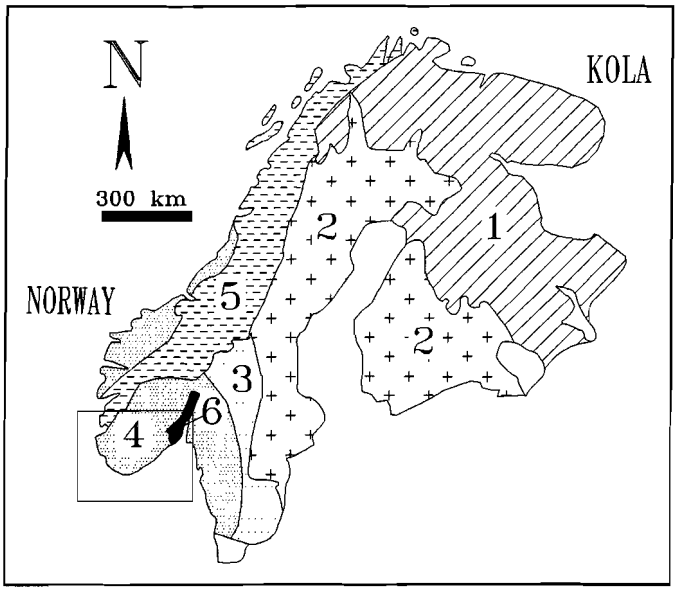

Figure 1.1

The Baltic Shield (modified after Lindh 1987) subdivided in six domains. These domains are based on absolute age determinations. Four of them are of Precambrian age; two of Phanerozoic age.

1 = Archean domain (3.5 to 2.65 Ga).
2 = Karelian/Svecofennian domain (2.75 to 1.75 Ga).
3,4 = Gothian/Sveconorwegian domain (1.75 to 0.90 Ga).
5 = Caledonides (0.6 to 0.4 Ga).
6 = Early Palaeozoic and Permian rocks (0.6 to 0.4 and ~0.25 Ga).
The south-western part of the Shield, indicated by the rectangle, is enlarged in figure 1.2.

The two principal conclusions concerning the history of the Baltic Shield are:

1) The Baltic shield becomes progressively younger towards the south-west
2) Plate tectonism must have been active already at the beginning of the Proterozoic period (Gorbatschev and Gaál 1987).

1.3 EVOLUTION OF THE SOUTH-WESTERN PART OF THE BALTIC SHIELD

The south-western part of the Gothian Sveconorwegian domain, marked by the rectangle in figure 1.1, is enlarged in figure 1.2. The units designated in figure 1.2 are mainly tectonically defined. The Proterozoic rocks (units 1, 2, 4, 5 and 6) in this area have formed mainly between circa 1.75 Ga and 0.90 Ga ago as obtained from review papers from Starmer (1985), Verschure (1985) and Gaál and Gorbatschev (1987). The Phanerozoic rocks (unit 3 and 7) cover locally the Proterozoic basement. I shall concentrate on the late Proterozoic evolution in the south-western part of the Baltic Shield and emphasise the role of the Bamble area (1) in it. The various geological events which played a considerable role in the evolution of the Bamble area are summarized in table 1.1. This table presents the basic relations between the age and character of main tectonic events in the Bamble area emphasising the role of the Jomasknutene and Dale gabbro in this scheme. I distinguished five major periods:

1) > 1.75 Ga — Pre Gothian period
2) 1.75 Ga - 1.50 Ga — Gothian orogenic period
3) 1.50 Ga - 1.25 Ga — Anorogenic period
4) 1.25 Ga - 0.90 Ga — Sveconorwegian orogenic period
5) < 0.90 Ga — Post Sveconorwegian period

(PRE)GOTHIAN OROGENIC PERIOD

Initial deposition of sediments in the south Norwegian area must have occurred in pre and early Gothian times (Pasteels and Michot 1975, Wahlgren 1981). Although exact age determination of these sediments appears to be difficult, Jacobson and Heier (1978) suggested a maximum age of 1.65 Ga for sediment deposition in the Kongsberg area. Considering the age of the presumably 1.77 Ga $\pm$0.19 Ga old Jomasknutene gabbro (de Haas 1992), the oldest rocks ever dated in the Bamble area, supracrustals from this area (figure 1.3) must have been deposited at least more than 1.58 Ga ago. More precise age determinations of granitic and charnockitic plutonic rocks yield a minimum age of the supracrustals of about 1.60 Ga $\pm$0.02 Ga (Lamb et al. 1986, O'Nions and Baadsgaard 1971). The substratum, a Svecofennian basement, on which these supracrustals must have been deposited has never been found in the Bamble area. Before major thrusting of these supracrustals occurred, large gneiss regions, among which the Telemark Banded Gneiss Complex (included in unit 2 in figure 1.2) formed a rigid protocontinent (Falkum 1985, Falkum and Petersen 1980, Starmer 1985, Starmer 1993) west of the Bamble and Kongsberg area (unit 1 and 5 respectively). The inferred presence of such rigid protocontinent is based on the oldest Gothian deformation structures found in both the Kongsberg and Bamble area. Sediments from the Bamble and Kongsberg area were squeezed between the Telemark Banded Gneiss Complex in the west and the Svecofennian continent in the east in a general east west compressional regime. The Bamble and Kongsberg area acted as an area in which most of the deformation was absorbed. This east west compression resulted in a westward thrusting of the Bamble and Kongsberg sediments over the Telemark Banded Gneiss Complex. Upper amphibolite to granulite facies metamorphism accompanying deformation occurred, according to Field et al. (1985), some 1.54 Ga ago in the Bamble area.

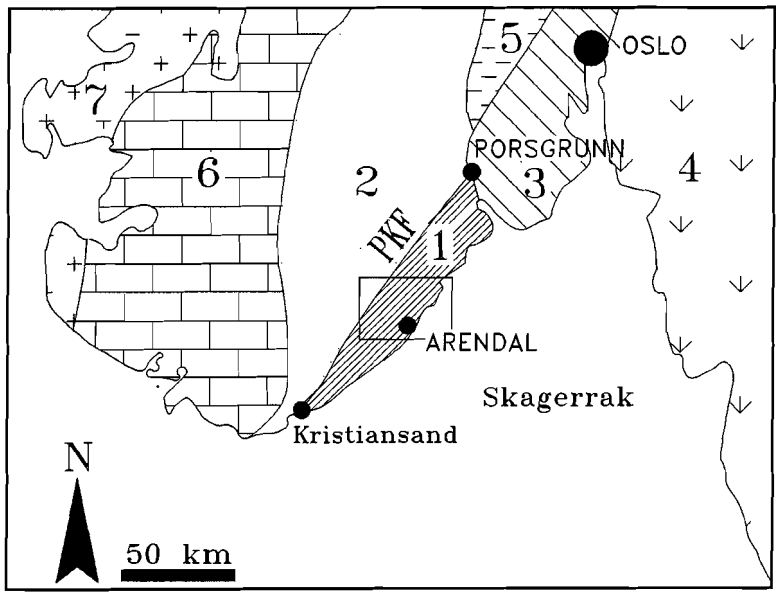

Figure 1.2

The tectonic units of the south-western part of the Baltic Shield modified after Verschure (1985).

1= Bamble area

2= Telemark gneiss region and Telemark supracrustals

3= Early Phanerozoic and Permian rocks

4= Segmented zone

5= Kongsberg area

6= Rogaland/Vest Agder area

7= Caledonian rocks

The central part of the Bamble area, indicated by the rectangle, is enlarged in figure 1.3.

ANOROGENIC PERIOD

The anorogenic period between the Gothian and Sveconorwegian orogenic events starts with the intrusion of alkaline gabbroic material and augen gneiss complexes (Hagelia 1989). The intrusion of these magmas is the result of a rift event which broke up a Proterozoic Supercontinent into the Scandinavian Baltic Shield and the Canadian Laurentia Shield (Torske, 1985). Solyom et al. (1992) interpreted the chemistry of the 1.22 Ga old dolerite intrusions (Daly et al. 1983) as being rift related. A 1.42 Ga old dike swarm in south-west Sweden (Hageskov and Petersen 1988) most likely confirms the rift model. The metamorphic conditions in the Bamble area during this period reached upper amphibolite facies conditions. Apparently, the currently exposed rocks in the Bamble area remained buried at considerable depth during this anorogenic rifting period and, as we will see below, also thereafter. At the end of this anorogenic period, and probably at the beginning of the Sveconorwegian orogenic period, the 90° clockwise rotation (Poorter 1981) of the Scandinavian Baltic Shield with respect to the Canadian Laurentia Shield did occur (Falkum 1985).

(POST)SVECONORWEGIAN OROGENIC PERIOD

Addition of new continental material to the Baltic continent during the Sveconorwegian period finds its peak in the Rogaland-Vest Agder area as discussed by Falkum (1985). The intensity of the Sveconorwegian intrusional activity increases in the south scandinavian area from east to west. Apart from this intrusional activity, the Sveconorwegian orogenic period is characterized by mobilizing pre Sveconorwegian continental material. This mobilization process occurs throughout the entire south-western part of the Baltic Shield. Deformation dated at the beginning of this period may have a direct relation with the 90° clockwise rotation of the Baltic Shield as discussed above. As a consequence of this deformation, old Gothian structures were locally transposed to the young Sveconorwegian ones.

The start of the Sveconorwegian orogenic period in the Bamble area, circa 1.25 Ga ago is marked by substantial magmatic activity (Jacobson and Heier 1978, Munz and Morvik 1991). Acid and basic magmas intruded the crust and were subsequently deformed in a north-north-west south-south-east compressional regime. The Bamble and Kongsberg area absorbed major deformation during this orogenic period and were reactivated as ductile shear zones. This period of deformation is followed by an anorogenic period (between 1.2 Ga and 1.1 Ga ago), characterized by static upper amphibolite facies metamorphism, intrusion of the main hyperite suite, among which the Dale gabbro, and a high heat flow. The start of the main Sveconorwegian orogenic period (1.1 Ga ago) following the anorogenic period is marked by granitic intrusions and an east west compressional regime which again caused thrusting of Kongsberg and Bamble over the Telemark Banded Gneiss Complex. The Sveconorwegian orogenic period ends about 0.90 Ga ago with the intrusion of post tectonic granites, among which the Herefoss (0.96 Ga $\pm$0.06 Ga, Brueckner 1972) and Grimstad granite (0.99 Ga $\pm$0.01 Ga, Kullerud and Machado 1991).

In conclusion, the south-western part of the Baltic Shield has mainly formed between 1.8 Ga and 0.9 Ga due to two orogenic periods. Remnants of the oldest, Gothian orogenic period, are found all over the south-western part of the Baltic Shield (figure 1.2) but become increasingly important towards the east. The intensity of magmatic continental accretion during the young Sveconorwegian orogenic event is strongest in the west (unit 6) and fades out towards the east (unit 4) as discussed by Verschure (1985). In a tectonic point of view, the sequence of events discussed above resembles the model of James and Ding, 1988. They suggest repeated extension and contraction tectonism, associated with magmatic activity at the turn-over from an extensional to a compressional regime, as being a common style of Proterozoic orogenisis. Their model is known as 'caterpillar tectonics'.

1.4 REGIONAL GEOLOGY OF THE BAMBLE AREA

In the foregoing, I presented a geological model for the evolution of the Baltic Shield and focused on the geotectonics of the south-western part of it in order to establish the role of the Bamble area during Gothian and Sveconorwegian times. Now I shall zoom in on the geology of the Bamble area in particular.

The Bamble area, designated 1 in figure 1.2, is a 150 km long, 30 km wide domain in the south-eastern part of Norway. In the west this area is 'traditionally' separated from the adjacent Telemark gneiss area (2) by a large tectonic structure, the Porsgrunn-Kristiansand Fault (PKF); in the east by the Skagerrak. Starmer (1991) however recognized major similarities between the southern part of the Bamble area and the Telemark Banded Gneiss Complex. The northern part of the Bamble area is covered by early Phanerozoic rocks from the Oslo rift system (3). These rocks separate the Bamble area from its northern equivalent, the Kongsberg area (5). The region I carried out my studies lies in the central part of the Bamble area west and north-west of Arendal. This area is marked by the rectangle in figure 1.2. A simplified geological map of this area is presented in figure 1.3.

In the last few decades, geological studies carried out in the Bamble area generated a complex of controversies concerning the prevailing metamorphic conditions in the Bamble area during Gothian and Sveconorwegian times. Until the early seventies only one metamorphic period in the Bamble area was recognized and thought to be of Sveconorwegian age (1.2 to 0.9 Ga). Later, Field and Råheim (1979, 1981) found evidence for the existence of upper amphibolite to granulite facies conditions in the Bamble area during Gothian times (between 1.7 Ga and 1.5 Ga ago). The orogenic phase during Sveconorwegian times was in their opinion of minor importance. Recent studies carried out by Maijer (1990), Hagelia (1989), Nijland and Senior (1991) and Nijland (1993) discuss the importance of Sveconorwegian metamorphism which has locally reached granulite facies conditions. The dominant current opinion is that the main metamorphism in the Bamble area, designated in figure 1.3, is of Sveconorwegian age (Nijland 1993). It seems likely that two high grade metamorphic periods can be recognized in the Bamble area but that they are often difficult to distinguish from each other. This difficulty is the key issue in this thesis.

LITHOLOGIES IN THE BAMBLE AREA

The rocks in the Bamble area show great diversity identified by the presence of metasediments such as quartzite, gneiss, migmatite, marble, metapelite, amphibolite as well as (meta)magmatic rocks such as gabbro granite and various migmatitic and amphibolitic rocks (Bugge 1943, Starmer 1987).

Sediments in this area were probably deposited before or in the early Gothian period, more than 1.58 Ga ago. Nijland et al. (1993) suggest a near shore or inland continental basin deposition of a huge quartzite complex in the central part of the Bamble area, known as the Nidelva Quartzite Complex (designated 1 in figure 1.3). Such sedimentary environment is inferred from structures such as cross bedding, ripples and mud cracks. This hypothesis is reinforced by the occurrence of corundum bearing gneiss, interpreted as having originated from a kaolinite bauxite weathered crust (Nijland 1993). Touret (1969) suggests a turbiditic origin for the Selås Banded Gneiss Complex (SBGC), a metasedimentary complex north of the NQC. The age relation between the NQC and the SBGC is unknown. Apparently, sediments from the Bamble area have been deposited under various conditions including deep marine and near coastal or continental environments.

Magmatic rocks such as granite, gabbro, dolerite, etc. intruded the (meta) sediments of the Bamble area. Age determination of some gabbroic rocks from the Bamble area has been carried out by de Haas (1992). He concluded from his Sm/Nd whole rock isotope study that gabbroic magmas did intrude the Bamble area during Gothian and Sveconorwegian times. Gabbros from both periods are known as hyperites, an old term used for coronitic gabbros in the Bamble area. The oldest intrusive activity resulted, among others, in the 1.77 $\pm$0.19 Ga old rhythmically layered Jomasknutene gabbro. The youngest intrusive activity resulted, among others, in the 1.11 $\pm$ 0.14 Ga old, more or less concentrically, layered Dale gabbro. The age relation of these two gabbro intrusions with respect to the orogenic periods is illustrated in table 1.1. It appears that the Dale gabbro intruded the Bamble area pre or syn the main sveconorwegian period. Therefore the Dale gabbro was probably subjected to the metamorphic conditions during the main Sveconorwegian period only. The Jomasknutene gabbro intruded the Bamble area probably before the late Gothian period. The Jomasknutene gabbro was subjected to all geological events post dating its intrusion. Therefore, if the Sm/Nd age determinations of the two gabbros are correct, the comparison of magmatic and metamorphic features stored in these two gabbroic suites provides a unique opportunity to distinguish between the conditions of crustal formation during Gothian and Sveconorwegian times in the Bamble area.

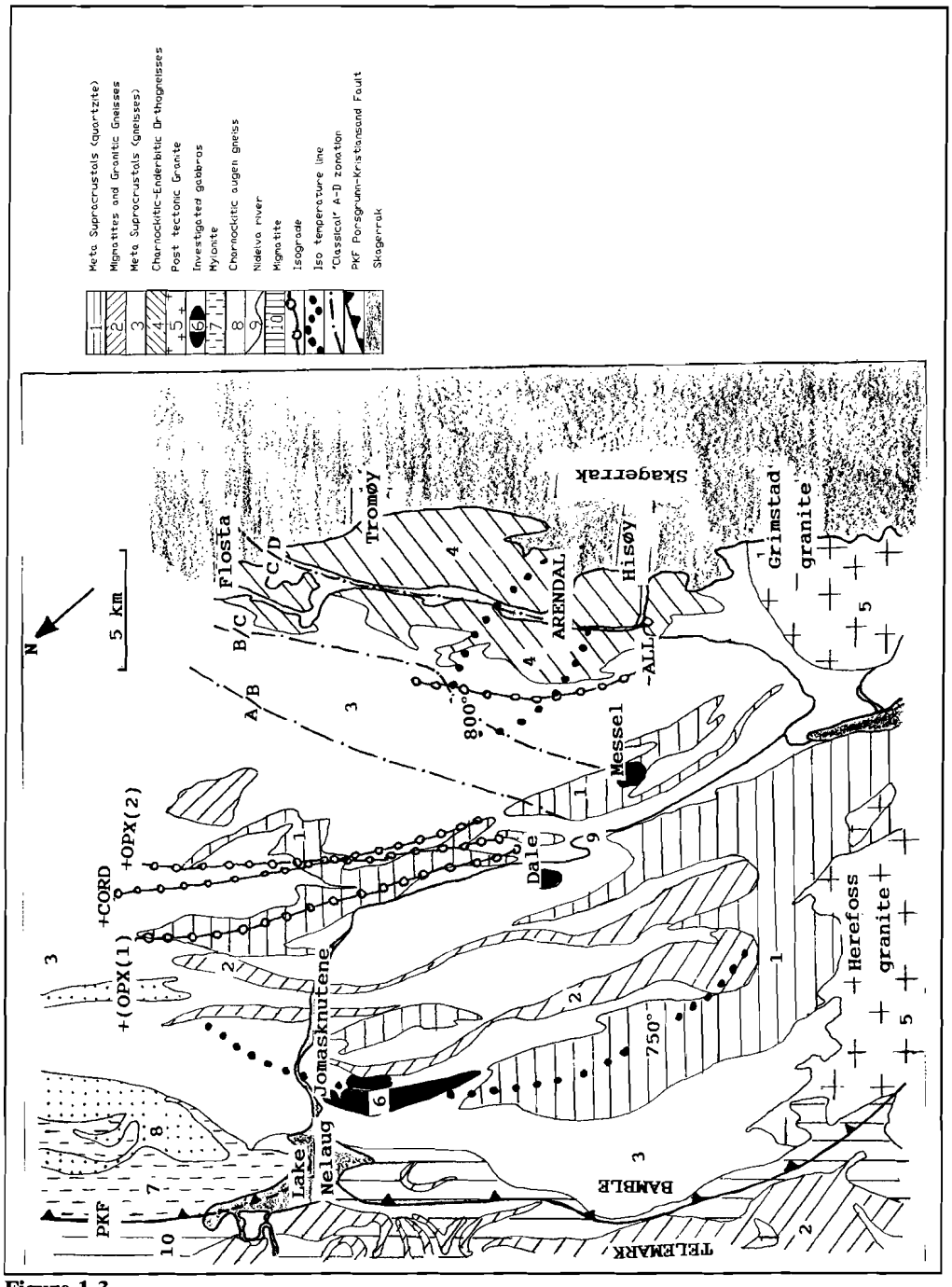

Figure 1.3

A simplified geological map of the central part of the Bamble area modified after Starmer (1985). The isograde and isotherm pattern is after Nijland (1993); the A to D zonation after Field et al. (1985).

METAMORPHISM IN THE BAMBLE AREA

The classical north-west south-east Gothian (1.54 Ga $\pm$0.21 Ga) tending metamorphic pattern in the central part of the Bamble area of Field et al. (1985) is illustrated in figure 1.3. These authors suggest peak metamorphic granulite facies conditions on Tromøy. The metamorphic zones are designated by A to D. The first three zones are based on two orthopyroxene-in isograde; one in basic rocks (A-B) and one in more acidic rocks (B-C). The C-D boundary is thought to be a tectonic line rather than a metamorphic defined boundary. Field et al. (1985) suggested that the only high grade metamorphic period took place 1.54 $\pm$0.21 Ga ago and was followed by a gentle low grade amphibolite to greenschist facies metamorphism of Sveconorwegian age. A high grade Gothian metamorphic event is confirmed by Visser (1993). Peak metamorphic P-T estimates of the Gothian metamorphism reached 600° to 700° C and 6 to 8 kbar. Although we know now from recent work of Nijland (1993) that the metamorphism at Sveconorwegian times in the central part of the Bamble area reached upper amphibolite and locally even granulite facies, it cannot be ruled out that the metamorphism at Gothian times did too.

Nijland (1993) suggests an isograde pattern of Sveconorwegian age in the central part of the Bamble area forming a thermal dome with its' centre in the Arendal area. The peak metamorphic conditions in the Arendal area reached 836 $\pm$49°C, 7.7 $\pm$0.3 kbar. Peak metamorphic conditions in the Nelaug area, north of the Jomasknutene gabbro about 15 km north-west of the Arendal area, reached 752 $\pm$34°C, 7.1 $\pm$0.4 kbar. Thus, the metamorphic grade decreases from east to west. These data imply a temperature drop of 86°C over a pressure range of 0.6 kbar with as consequence a geothermal gradient of about 43°C/km. The isotherms dip, most likely, gently away from the centre of the metamorphic dome structure.

The reason for this metamorphic dome structure is probably an elevated heat flow in the Arendal area at Sveconorwegian times possibly concomitant with the "high heat flow event" during the Sveconorwegian anorogenic period discussed in table 1.1. The sequence of the observed Sveconorwegian isograde pattern from north-west to south-east towards the centre of the dome is as follows:

1) Cordierite in isograde in metapelite
2) Orthopyroxene in isograde in amphibolite
3) Orthopyroxene in isograde in acid gneiss
4) Allanite out isograde in gneiss, metapelite and amphibolite

The peak metamorphic mineral fabric in and near the "dome" area indicate a static metamorphism whereas metamorphism at the outer margin of the dome seems to be more dynamical. Simultaneous with the peak metamorphic temperature conditions, water pressure became significantly lower in this area (Nijland, 1993) coinciding with maximum CO_2 density of fluid inclusions in the Bamble area (Touret, 1985)

STRUCTURAL ELEMENTS IN THE BAMBLE AREA

The main foliation in the central part of the Bamble area, striking north-east south-west, is probably of Sveconorwegian age (Falkum and Petersen 1980, Falkum 1985, Hagelia 1989). This Sveconorwegian foliation presumably redirected the old Gothian foliation and dips generally sub vertical towards the south-east. Some north-east south-west striking shear zones are thought to be synchronous with the, Sveconorwegian, thermal doming in the Arendal area. The age of first initiation of this metamorphic dome was created is debatable; the dome structure ceased to exist 1.15 Ga ago (Nijland 1993).

Table 1.1 *RELATION BETWEEN TECTONIC EVENTS AND THE INTRUSION OF THE JOMASKNUTENE AND DALE GABBRO IN THE BAMBLE AREA*

This time table presents the relation between the age and the character of the various tectonic events in the Bamble area, modified after Starmer (1991). Additionally the estimated age of the Dale and Jomasknutene gabbro (de Haas 1992) are plotted in order to establish the relation between the two gabbro intrusions and the tectonic history of the Bamble area.

Abbreviations: *KB* = *Kongsberg area*
B = *Bamble area*
TBGC = *Telemark Banded Gneiss Complex*

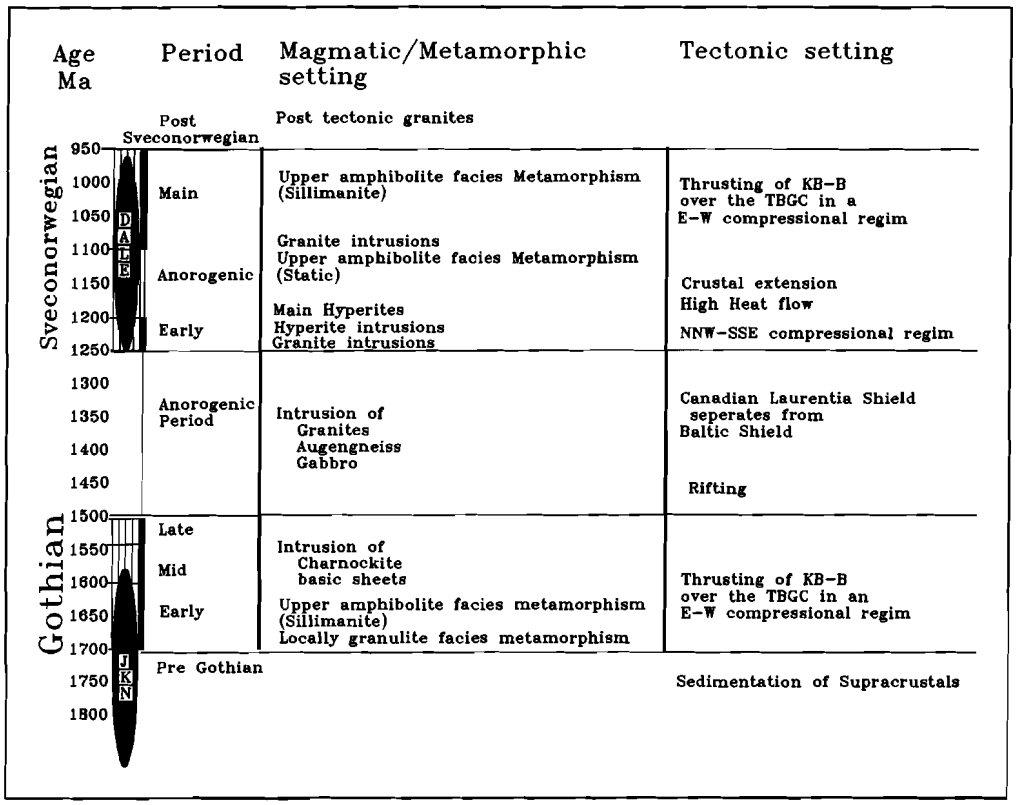

CHAPTER II
GOTHIAN AND SVECONORWEGIAN CHARACTERISTICS PRESERVED IN THE JOMASKNUTENE AND DALE GABBRO

2.1 INTRODUCTION

In the previous chapter I established a geological framework to contribute in understanding the role of the Bamble area in the late Proterozoic evolution of the Baltic Shield. I pointed out that large areas in the south-western part of the Shield have formed during pre Sveconorwegian times, among which the Gothian orogenic period. Some of these areas were mobilized during the Sveconorwegian orogenic period. Thus, the south-western part of the Baltic Shield exhibits continent-building features of both the Gothian and Sveconorwegian period. The controversies concerning the conditions during Gothian and Sveconorwegian times in the Bamble area have led to the following principal question:

What were the physical and chemical conditions in the central part of the Bamble area during the Gothian and Sveconorwegian period and (how) can they be distinguished from one another ?

In answering this question, I compared field relations, mineralogy and whole rock chemistry of two different gabbroic intrusions which are thought to be distinctively different in age. The oldest gabbro, the Jomasknutene (1.77 Ga $\pm$0.19 Ga old), must contain information about the reigning crustal conditions in the Bamble area during the syn and post Gothian period; the youngest gabbro, the Dale (1.11 Ga $\pm$0.14 Ga old) contains information from the syn and post Sveconorwegian period only. I paid more attention to the Jomasknutene gabbro because:

1) the knowledge about the geology of the Jomasknutene gabbro was poor compared to the Dale gabbro.
2) the Jomasknutene gabbro exhibit most probably Gothian characteristics. Gothian characteristics in the Bamble area are, in my opinion, far less understood than the Sveconorwegian ones.

I estimated, if possible, some physical properties of these two gabbros among which the magmatic and metamorphic P-T conditions and the viscosity of the magma. The theory of TTT-diagrams is introduced here and applied to the investigated rocks. The application of this theory to magmatic igneous petrology is innovating. It explains grain size variation in igneous rocks in terms of viscosity, temperature and residence time of magma.

2.2 FIELD RELATIONS OF THE JOMASKNUTENE AND DALE GABBRO

Field relations are of essential importance in order to understand the results of subsequent geological research. In this case it provides information about the relative sample position, internal magmatic structures, deformation structures etc.. Therefore I shall start to discuss and compare the field relations of the Jomasknutene and Dale gabbro. Most of the field related information, as well as the mineralogy and whole rock data from the Dale gabbro are obtained from the PhD thesis of de Haas (1992) and the unpublished M.Sc. thesis of Theulings and van Ditshuizen (1987). The data from the Jomasknutene gabbro were mainly collected by de Haas (1992) and myself.

2.2.1 THE JOMASKNUTENE GABBRO

The geological map of the Jomasknutene gabbro is shown in figure 2.2.1. It is one of the largest coronitic gabbros in the central part of the Bamble area (Starmer, 1985). The northern border of the gabbro is about 1.5 km south of lake Nelaug and 2 km east of the Porsgrunn-Kristiansand Fault (PKF) as shown in figure 1.3. The gabbro consists of two elongated north-east south-west striking bodies; a western body which is 5.5 km long and 1 km wide and an eastern one which is 2.1 km long and 1 km wide separated from each other by a 150 m thick north-east south-west striking shear zone. The shear zone is developed in the country rock as well as in the gabbro itself. It seems likely that these two gabbroic bodies belong to one and the same gabbro complex.

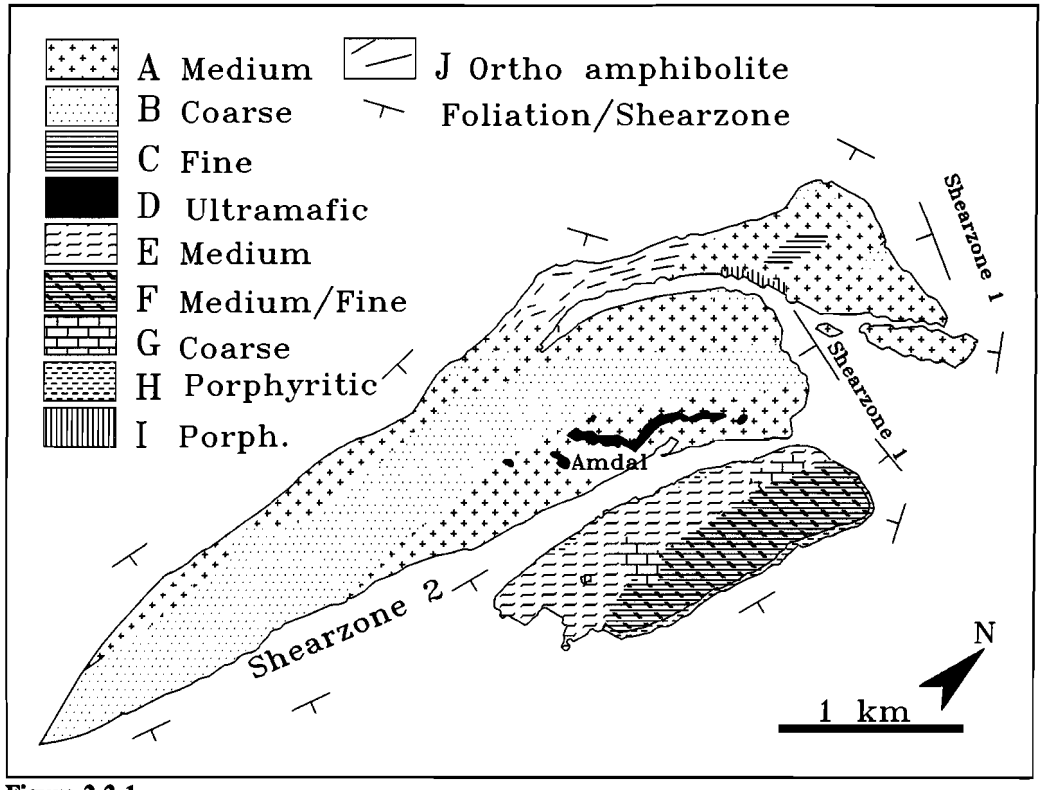

Figure 2.2.1

The geological map of the Jomasknutene gabbro. The foliation of the surrounding gneiss wraps around the gabbro. Gently south dipping shear zones (1) and steep east to south-east dipping shear zones (2) cross cut the gabbro. The various units are distinguished from one another mainly by differences in grain size. No sharp boundaries between the units can be defined on this scale.

A,E = *Medium grained gabbro.*
B,G = *Coarse grained gabbro.*
C = *Fine grained gabbro.*
D = *Folded ultramafic amphibole-orthopyroxene unit.*
F = *Medium to fine grained gabbro.*
H,I = *Porphyritic gabbro.*
J = *Ortho amphibolite.*

COUNTRY ROCK

The Jomasknutene gabbro is surrounded by metasedimentary rocks belonging to the northern extension of the Nidelva Quartzite Complex (figure 1.3). These metasediments consist of quartzite, sillimanite bearing nodular gneiss and albite actinolite gneiss with variable amounts of quartz (AAQ-gneiss). The foliation in the country rock is concordant with the gabbro-country rock contact (figure 2.2.1) and has therefore most likely formed after the intrusion. The surrounding AAQ gneiss is locally brecciated and cross cut by veins containing the same minerals in different proportions. The complete AAQ-assemblage is thought to have formed due to metasomatism of an acid fluid (chapter IV) affecting the country rock as well as part of the outer margins of the gabbro body. Whether the observed breccia is caused by the gabbro intrusion or by subsequent tectonic processes is not clear. A contact metamorphic aureole in the country rock caused by the hot intrusive gabbroic magma has never been found.

SHEAR ZONES

Two main systems of shear zones are recognized in or near the Jomasknutene gabbro designated zone 1 and 2 in figure 2.2.1. Both systems are developed in the gabbroic rocks as well as in the country rock. Shear zone 1 is a relative old gently south dipping deformation system of about 10 m thick. There are two of these shear zones found about 100 m above one another. At the base of each shear zone, the transition from non foliated gabbro at the bottom to banded amphibolite is abrupt and sub horizontal as indicated in figure 2.2.2. From this base upwards, the intensity of deformation weakens and the sub horizontal foliation shifts to a 50° south dipping foliation. The orientation of the foliation indicates a reverse fault system in which the hanging wall moved northwards. Shear zone 2 is a relative young, possibly Sveconorwegian, steep (80° to 90°) east to south-east dipping deformation system of about 150 m wide. The intensity of deformation in this shear zone is much more intense than in shear zone 1. It transposes the foliation of the old shear zone (1) towards its own shear direction. Its foliation is sub parallel to the general foliation found in the country rock in this part of the Bamble area. The major shear zone (2) is accompanied by numerous small, centimeter scaled, shear zones in the gabbro with the same orientation but with a less destructive effect. Shear zone 2 cross cuts the gabbro country rock contact.

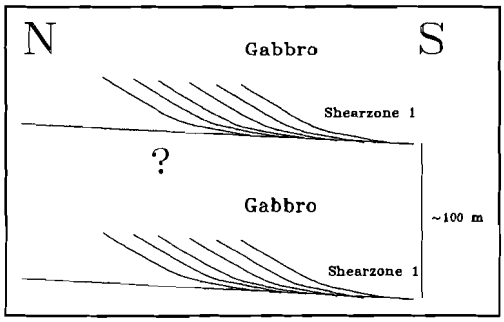

Figure 2.2.2

Schematic presentation of the oldest south dipping shear zone designated shear zone 1 in figure 2.2.1. At the base of such a shear zone the gabbro is transformed into a banded amphibolite. This base is about 10 meter thick. From the base upwards the foliation steepens and becomes less pronounced. The relation between the two shear zones is unknown as indicated by the question mark.

The transition from non foliated gabbro to banded amphibolite in this deformation system occurs within 20 m. The observed sense of shear is always sinistral. This sinistral sense of shear is opposite to the regional dextral sense of shear as suggested by Falkum (1985) for the Bamble area. The original magmatic texture and mineralogy have been transformed in both shear systems to a metamorphic one.

GABBROIC UNITS

The internal magmatic structure of the Jomasknutene gabbro emerged after detailed mapping. I distinguished nine gabbroic units, designated A to I in figure 2.2.1, based mainly on grain size differences. These grain sizes vary from larger than 1 cm in the coarse grained units to smaller than 5 mm in the fine grained ones. Medium grained gabbroic rocks have a grain size variation between 1 cm and 5 mm. Large grain size variations occur also within the units which makes it impossible to pinpoint the exact location of each unit boundary. Thus the geological map of the Jomasknutene gabbro in figure 2.2.1 illustrates an estimated grain size distribution.

Most units, A, B, D, E, F and H are sheet like and strike north-east south-west. However, it has not been possible to determine the dip of these units. The remaining units, C, G and I do not follow this sheet like trend. Unit D can be distinguished from the other units by the absence of plagioclase and the presence of magmatic rhythmic layering. Some of these magmatic layers are tightly folded as shown in figure 2.2.3. Two porphyritic gabbro units, H and I, occur locally along the contact with the country rock in the Jomasknutene gabbro. Whether these porphyritic units are genetically related to the gabbro (chilled margins) is not clear from the field observations.

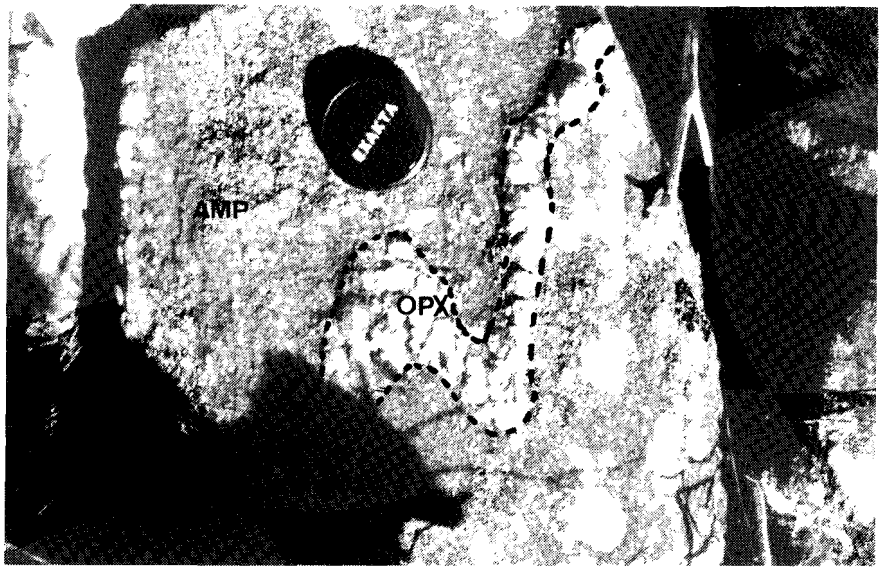

Figure 2.2.3

A tightly folded orthopyroxene layer (OPX) surrounded by amphibole matrix (AMP). This orthopyroxene layer, accentuated by dotted lines, is about 10 centimeter thick and is related to unit D of figure 2.2.1. Apparently, internal deformation occurred in the Jomasknutene gabbro.

I have distinguished three types of contacts between the nine units:

1) Irregular shaped lobate contacts as shown in figure 2.2.4. These contacts prevail in the Jomasknutene gabbro. The change in grain size is abrupt and no evidence for chilled margins or chemical exchange between the units has been found.
2) Sheared contacts as shown in figure 2.2.5. These are characterized by listric faults in the more coarse grained unit. The intensity of deformation increases towards the contact. They occur, for example, along the western border of unit A and B.
3) Fine grained contacts, separating two units. These consist of a 10 cm to 20 cm thick zone of a fine grained gabbroic rock. This type of contact is rare, poorly exposed and occurs locally along the western A-B boundary and along the E-F boundary.

Besides these well defined contacts gradual grain size variations occur in the Jomasknutene gabbro as well. There will be a further discussion on the grain size variation in chapter 2.6

The mineralogy is similar for most units except for unit D. Locally scapolitized cumulus plagioclase forms the network of the gabbroic rocks. The spaces between these plagioclase crystals are occupied by clinopyroxene and ilmenite which are in their turn locally amphibolitized. Olivine corona textures have be recognized with or without the presence of garnet. I did not find any relation between the macroscopically observed mineralogy and the various gabbroic units or geographical position. A more detailed petrographic description will be discussed below, in chapter 2.3.

Figure 2.2.4

A lobate shaped contact between a coarse (C) and medium (M) grained gabbro unit. The transition from a coarse to medium grained gabbro is abrupt and marked by the arrow. This example is taken from the western contact zone between unit A and B in figure 2.2.1.

Figure 2.2.5

A sheared contact between a coarse (C) and a medium (M) grained gabbro unit. The listric foliation, marked by the arrow, is mainly developed in the coarse grained gabbro unit. This example is taken from the western contact zone between unit A and B in figure 2.2.1.

2.2.2 THE DALE GABBRO

The Dale gabbro is one of the best documented gabbro bodies of the Bamble area due to work of petrologists from Utrecht University. The position of the Dale gabbro in the Bamble area is shown in figure 1.3 and a detailed geological map is presented in figure 2.2.6. It is much smaller than the Jomasknutene gabbro and situated near Froland, west of the Nidelva river. The gabbro is about 600 m long and 450 m wide. The elongation of the gabbro, more or less parallel to the foliation in the country rock, is not as pronounced as that of the Jomasknutene gabbro.

COUNTRY ROCK

The Dale gabbro intruded a granitic gneiss complex. According to the geological map of Starmer (1985), it seems likely that the Dale gabbro intruded the same unit as the Jomasknutene gabbro (figure 1.3). However, the country rock around the Dale gabbro has mainly a granitic composition occurring as migmatite; the country rock around the Jomasknutene gabbro is mainly composed of metasediments. The geological map of the Dale gabbro (figure 2.2.6) suggests that the foliation in the country rock is concordant along the eastern and western gabbro country rock contact but discordant along the northern part of the gabbro country rock contact. This indicates that the Dale gabbro intruded after the main foliation was already developed but was exposed to later deformation as well. Melting of the country rock occurred during the emplacement of the Dale gabbro resulting in back veining of granitic material into the solidified and fractured gabbroic rock. It resulted in a intermingling of gabbro and country rock along the margins of the gabbro.

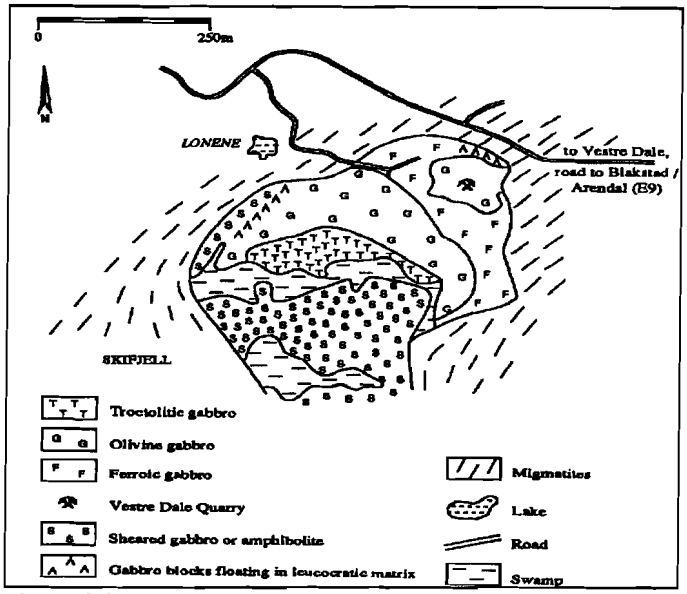

Figure 2.2.6

Geological map of the Dale gabbro (modified after Theulings and van Ditshuizen, 1986 and de Haas, 1992). This map suggests that concordant and discordant gabbro country rock contacts occur. The various units are based on grain size variation in combination with the whole rock chemistry and mineralogy. The grain size variation increases from the fine grained troctolitic unit (T) via the olivine gabbro unit (G) to the coarse grained ferroic gabbro unit (F).

SHEAR ZONES

Major deformation structures, similar to those found in the Jomasknutene gabbro, are absent in the Dale gabbro. Deformation is restricted mainly to the southern and western part of the Dale gabbro and manifests itself in the occurrence of amphibolite.

GABBROIC UNITS

The internal magmatic structure of the Dale gabbro is concentric. It consist of a fine grained core, the troctolitic unit (T). The grain size increases gradually towards the outer margin of the gabbro, finely resulting in the ferroic gabbro unit (F) which is coarse grained. This grain size variation is always gradual and the characteristically sharp contacts similar to those found in the Jomasknutene gabbro are absent as is fine scaled rhythmic magmatic layering.

The magmatic mineralogy in the Dale gabbro is similar to that observed for the Jomasknutene gabbro. Olivine occurs more frequently and the alteration of the magmatic minerals is less pronounced than in the Jomasknutene gabbro.

2.3 PETROGRAPHY AND MINERAL CHEMISTRY OF THE JOMASKNUTENE AND DALE GABBRO

The field study of the Jomasknutene gabbro has resulted in a set of about 180 samples. After an intensive petrographical study of these samples with an optical microscope I reduced this number to about 69. These 69 samples are in my opinion a representative set to study the magmatic, metamorphic and metasomatic evolution of the gabbro. A similar approach for the Dale gabbro has led to a set of 17 'fresh' gabbro samples. These two sample sets have been used for further investigation. Before discussing magmatic and metamorphic parameters of the two gabbros one has to be acquainted with their mineralogy. This chapter will present a brief description of the petrography and mineral chemistry; a base from which values of the magmatic and metamorphic parameters will be derived.

ANALYTICAL TECHNIQUE

The chemical mineral composition has mainly been determined with a fully automated TPD microprobe at the Institute of Earth Sciences at Utrecht university. The standard measurement conditions are:

Energy dispersive method, ZAF-correction, calibration using synthetic and natural standards, 15 kV acceleration voltage, 30 to 40 Na sample current, 70 to 100 seconds counting time and a probe spot diameter of about 5 μm. Additional analyses were obtained with the microprobe at the Vrije Universiteit in Amsterdam. Standard measurement conditions are:

Wavelength dispersive method, ZAF and deadtime correction 20 kV acceleration voltage, 20 nA sample current, 20 second counting time and a probe spot diameter of about 5 μm.

Spot analyses provide detailed mineral information about the mineral composition, zonation and (dis)equilibrium conditions. Additionally one can easily obtain chemical information from primary or secondary inclusions and/or exsolution phases.

2.3.1 PRIMARY MINERALS

The primary minerals in both gabbros consist of cumulus and intercumulus minerals. These minerals are listed in table 2.3.1[a,b] and will be discussed below. The chemistry of these minerals establishes the subsequent chemistry of the subsolidus and metamorphic mineralogy.

Table 2.3.1[a] *PRIMARY MAGMATIC MINERALS OF THE JOMASKNUTENE GABBRO*

Cumulus	Intercumulus
Olivine	Augite (Orthopyroxene ?)
Plagioclase	Ilmenite/Magnetite/Hercynite
	Plagioclase/K-feldspar/Quartz
	Apatite
	Zircon

Table 2.3.1[b] *PRIMARY MAGMATIC MINERALS OF THE DALE GABBRO*

Cumulus	Intercumulus
Olivine	Augite
Plagioclase	Ilmenite
	Plagioclase
	Apatite
	Zircon

JOMASKNUTENE GABBRO

Olivine is the first mineral to crystallize from the investigated gabbroic magma. It is cumulus and locally included in cumulus plagioclase. Only 5 of the 65 selected samples contain olivine occupying between 5 and 25 % of the total rock volume. Three of the five samples occur in eastern part of unit E parallel to the north-east south-west elongation of the gabbro units, one in the western part of unit E and one in the ultramafic unit (D). Olivine crystals exhibit undulatory extinction and extinction bands. The crystals are convex shaped due to subsolidus corona growth and usually surrounded by orthopyroxene $\pm$amphibole (chapter III). Cracks in olivine filled with magnetite, orthoamphibole, apatite and dendritic opaque crystals are common. Chemical analyses of only one olivine sample are available. The chemical variation of olivine in this sample is small. The mean Mg# is 52.7 $\pm$1.5. The chemical homogeneity of olivine crystals within one sample suggests that either the chemical composition of the magma and/or the physical conditions remained rather constant during the crystallization or a post cumulus process homogenized the olivine crystals. The general occurrence of olivine corona textures and the presence of orthopyroxene magnetite symplectite in the Jomasknutene gabbro indicates that olivine used to be a common constituent.

Cumulus plagioclase is the most common magmatic mineral occurring in nearly all samples (except in samples from unit D). It occupies between 5% and 70% of the total rock volume. Large twinned and tabular shaped plagioclase crystals usually form a network texture. Small, also twinned and tabular shaped, plagioclase crystals 'float' usually in a matrix of augite. Plagioclase probably started to crystallize after olivine was formed but before the crystallization of augite. In only two samples, plagioclase crystals form a laminated fabric, dipping $\sim 50^{o}$ westwards. Plagioclase crystals tend to have a normal chemical zonation i.e. high anorthite values in the core of the crystals and decreasing anorthite values towards the rim. Anorthite values vary between 5% in the rim and 70% in the core of the crystals. The composition of plagioclase indicates a fractionation process in which the gabbroic magma become progressively sodium richer. The original magmatic plagioclase composition has locally changed due to subsolidus and metamorphic processes. This will be discussed in further detail in chapter III.

Intercumulus fills the interstitial spaces between cumulus olivine and plagioclase. Augite is the most frequent intercumulus in the Jomasknutene gabbro and occurs usually as large poikilitic crystals up to 2 cm in size. Its mode ranges between 5% and 40%. The chemical composition of augite falls within the field of diopside and augite as defined by Morimoto et al. (1988) and is more or less constant within one sample. On the whole, the wollastonite component varies between 43% and 46%, the enstatite component between 30% and 42% and the ferrosillite component between 14% and 26%. All poikilitic intercumulus clinopyroxene crystals exhibit ilmenite and pigeonite exsolution textures. The latter is parallel to $[001]_{augite}$ (Dam and van Roermund 1989). The pigeonite exsolution lamellae are too small to be analyzed with the

microprobe. The chemical analyses of intercumulus clinopyroxene listed in table 2.3.2 are obtained from areas in the augite without exsolution lamellae. These microprobe data probably represent the composition of augite after exsolution rather than these of primary magmatic augite. These exsolution textures indicate that intercumulus augite has adapted its chemistry several times during subsolidus cooling or metamorphism. Comparing the Mg# of augite with that of olivine within one sample indicate that augite has always a higher Mg# than olivine (figure 2.3.1). The Mg# of augite plot generally above the line '1=1', olivine plot below it.

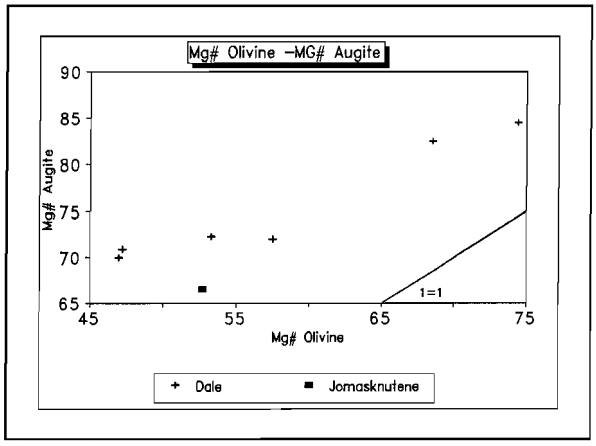

Figure 2.3.1

The Mg# of augite plotted against the Mg# of olivine from the same sample indicates that augite has always a higher Mg#.

Ilmenite±magnetite is usually present as an intercumulus. The mode does not exceed 10 volume percent. The original chemical composition has been modified during subsequent cooling resulting in a magnetite±ilmenite± hercynite intergrowth.

Plagioclase is occasionally present as an intercumulus. It exhibits undulatory extinction due to crystal deformation and is not twinned. The intercumulus plagioclase is often accompanied by varying amounts of K_feldspar, quartz, apatite and rounded augite crystals. The composition of the intercumulus plagioclase is close to albite. This intercumulus accumulation has most likely formed during the final stage of the crystallisation process.

Accessory minerals like apatite and zircon are occasionally present mainly as inclusions in the intercumulus plagioclase. Idiomorphic apatite crystals as large as 5 mm have been observed.

DALE GABBRO

The primary magmatic minerals in the Dale gabbro are similar to those occurring in the Jomasknutene gabbro. Therefore I discuss here the mineralogy of the Dale gabbro only briefly. For a detailed petrographic description of the Dale gabbro I refer to the work of de Haas (1992) and Theulings and van Ditshuizen (1986).

Olivine is more abundant (n=14) in the Dale than in the Jomasknutene gabbro. Modal olivine percentage ranges from 65% in the core to 0% in the northern part at the margin of the gabbro. The Mg# of olivine ranges from 47 to 75 but is constant within one sample. Three examples of average olivine analyses are shown in table 2.3.2.. Modal plagioclase ranges between 20% and 40%; modal clinopyroxene between 15% and 40%. Apatite and minor amounts of zircon occur mainly in the olivine poor and olivine free gabbro samples. Quartz intergrown with intercumulus plagioclase, K_feldspar and augite, as observed in the Jomasknutene gabbro, has not been found.

Table 2.3.2 *AUGITE AND OLIVINE ANALYSES FROM THE JOMASKNUTENE AND DALE GABBRO*

Average augite and olivine microprobe spot analyses from the Jomasknutene gabbro (designated Ga) and the Dale gabbro (designated WT). The oxides are in weight %; the elements in atoms per formula unit (p.f.u.). The Mg# of augite and olivine suggest a chemical fractionation in both gabbroic magmas. The whole rock magnesium number (WR Mg#) is added to demonstrate that variation of the Mg# of the minerals is positively correlated with the WR Mg#.

a) Average augite from the Jomasknutene gabbro and the Dale gabbro.

Sample	Ga153	Ga315	Ga364	WT10	WT210	WT209
n	n=9	n=6	n=6	n=4	n=4	n=3
Mineral	augite	augite	augite	augite	augite	augite
SiO_2	51.65	52.81	52.11	52.89	52.04	52.85
TiO_2	0.36	0.21	0.00	0.67	0.23	0.25
Al_2O_3	1.94	2.54	0.67	3.04	2.58	2.54
FeO	10.96	8.50	15.12	5.56	9.06	9.84
MnO	0.27	0.13	0.69	0.26	0.24	0.29
MgO	12.18	14.38	10.12	16.91	13.07	13.28
CaO	21.09	21.18	20.56	20.71	21.75	21.38
Na_2O	0.80	0.56	0.95	0.59	0.60	0.80
Negative charge	12	12	12	12	12	12
Si	1.96	1.95	2.00	1.92	1.95	1.94
Ti	0.01	0.01	0.00	0.02	0.01	0.01
Al^{IV}	0.04	0.05	0.00	0.08	0.05	0.06
Al^{VI}	0.05	0.06	0.03	0.05	0.06	0.05
Fe	0.35	0.36	0.48	0.17	0.28	0.30
Mn	0.01	0.00	0.02	0.01	0.01	0.01
Mg	0.69	0.79	0.58	0.92	0.73	0.73
Ca	0.86	0.84	0.84	0.81	0.87	0.85
Na	0.06	0.04	0.07	0.04	0.04	0.06
Mg# augite	66.5	75.2	54.4	84.4	72.3	70.9
Mg# whole rock	51.3	57.6	32.2	74.4	63.2	59.7

Table 2.3.2 *(continued)*

b) Average olivine from the Jomasknutene and the Dale gabbro.

Sample	Ga153	WT10	WT210	WT209
n	n=13	n=6	n=7	n=9
Mineral	Olivine	Olivine	Olivine	Olivine
SiO_2	35.01	39.22	35.28	34.17
FeO	39.60	23.51	39.40	43.10
MnO	0.41	0.35	0.50	0.59
MgO	24.72	37.99	25.23	21.72
NiO	0.06	0.13	0.24	0.23
Negative charge	8	8	8	8
Si	1.00	1.01	1.00	1.05
Fe	0.94	0.51	0.93	1.05
Mn	0.01	0.01	0.01	0.02
Mg	1.06	1.46	1.06	0.94
Ni	0.00	0.00	0.01	0.01
Mg# Olivine	53.0	74.1	53.3	47.2
Mg# Whole rock	51.1	74.4	63.2	59.7

CONCLUSION

The principal conclusions which can be drawn from the comparison of the primary magmatic minerals are:

1) The small variation in the magmatic minerals are striking keeping in mind that the gabbros differ considerably in age and magmatic history.
2) Olivine from the Dale gabbro crystallized probably from a more Mg rich magma than the Jomasknutene gabbro. There have been no indicators that the more Mg rich olivine and augite have formed under different physical emplacement conditions.
3) The fractionation of the Jomasknutene magma proceeded until primary magmatic quartz and K-feldspar crystallized in the intercumulus spaces. The Dale magma never reached this state.

2.3.2 SECONDARY MINERALS

Secondary minerals in the Jomasknutene and Dale gabbro are the result of adaption of the magmatic minerals to changes in physical and chemical conditions. These changes include cooling of a solidified magma, metamorphic events and metasomatic processes among which the introduction of acidic fluids. However, it is often very difficult to distinguish unequivocally what exactly caused these mineral adaption.

JOMASKNUTENE GABBRO

All primary magmatic minerals are altered to some extent. The most common metamorphic mineral is amphibole. It is formed using components from the magmatic minerals such as olivine, augite, ilmenite and plagioclase or from other, possibly metamorphic, minerals such as biotite and occasionally garnet. Amphibole analyses in table 2.3.3 demonstrate that the chemical composition of metamorphic amphiboles is strongly dependent on that of the surrounding minerals. The following general trend in Mg# of amphibole within one sample can be distinguished:

$Mg\#^{(olivine\ related\ amphibole)} > Mg\#^{(ilmenite\ related\ amphibole)}$

Augite is partially amphibolitized at the contact with plagioclase. This amphibolitization is often accompanied by the formation of quartz resulting in an amphibole quartz symplectite. Amphibole lamellae parallel to $(010)_{augite}$ have been observed in several augite crystals, probably initiated on cleavage planes.

Garnet occurs in these rocks, locally replacing amphibole in the olivine corona texture and amphibole and biotite around ilmenite. Garnet never occurs near intercumulus clinopyroxene probably due to the relatively high Mg# of the latter. Mean garnet compositions are presented in table 2.3.4. These values confirm the chemical dependency of metamorphic minerals on their chemical environment as we have already noted for amphibole.

Metamorphic orthopyroxene occurs locally in combination with amphibole and garnet. It is often difficult to discern its host but there are indications that it forms from intercumulus clinopyroxene. Chemically, a pigeonite as host would have been more likely. However there are no indications that (inverted) pigeonite has been present in the Jomasknutene gabbro. Orthopyroxene magnetite intergrowth, derived from olivine can either have a subsolidus or metamorphic origin but must have formed after the corona forming reaction as they have a corona texture similar to olivine crystals.

Plagioclase is locally replaced by scapolite either along mineral contacts, in veins or in the core of plagioclase crystals. The chemical variation of scapolite in one sample tends to be substantial. Its composition ranges between 10% to 80% meionite (average 36% meionite, n=41) based on optical determinations but has not been investigated in great detail.

The relative age sequence of the metamorphic minerals is often difficult to unravel or determine unequivocally. The following age sequence can be determined from the ilmenite corona texture:

$Age^{biotite} > Age^{amphibole} > Age^{garnet}$

Mineral relations near other textures, for example olivine coronas, tend not always to be that clear. The exception to this is garnet which seems in general to be one of the latest minerals to have formed.

Table 2.3.3 *METAMORPHIC AMPHIBOLE ANALYSES FROM THE JOMASKNUTENE GABBRO*

Average metamorphic amphibole analyses from sample Ga153 (Jomasknutene gabbro) demonstrate the dependence on the mineral surroundings. Olivine related amphibole has a higher Mg# than ilmenite related amphibole. The whole rock Mg# = 51.1.

Sample	Ga153	Ga153
n	n=6	n=9
Mineral	Amphibole	Amphibole
Surrounding mineral	Ilmenite	Olivine
Sio_2	39.13	39.15
TiO_2	2.78	0.59
Al_2O_3	14.00	16.22
FeO	18.38	14.08
MnO	0.00	0.06
MgO	7.80	10.84
CaO	11.09	11.26
Na_2O	1.95	2.20
K_2O	2.00	1.69
Cl	0.42	nd
F	0.00	nd
Negative charge	46	46
Si	6.03	5.96
Ti	0.32	0.07
Al	2.54	2.91
Al^{IV}	1.97	2.04
Al^{VI}	0.58	0.87
Fe	2.37	1.79
Mn	0.00	0.01
Mg	1.79	2.46
Ca	1.83	1.83
Na	0.58	0.65
K	0.39	0.33
Cl	0.11	nd
F	0.00	nd
Mg# amphibole	43.0	57.9

Table 2.3.4 *CHEMICAL COMPOSITION OF METAMORPHIC GARNET*

Average compositions of metamorphic garnet indicating the variability of the chemistry of garnet per sample and per chemical environment.

	Related to Ilmenite Ga153	Related to Olivine Ga153	Related to Ilmenite Ga357
Pyrope	16.9	19.9	26.9
Almandine	61.4	58.0	57.1
Grossular	18.8	18.7	11.9
Spessartine	2.9	3.4	4.1

DALE GABBRO

The secondary minerals from the Dale gabbro are on the whole similar to these found in the Jomasknutene gabbro. Two principal differences between their secondary mineral assemblages are:

1) Secondary minerals are less common in the Dale gabbro than in the Jomasknutene gabbro. There is substantial less amphibolitization whereas scapolitization seems to be absent.
2) Garnet is extremely rare in the Dale gabbro, probably because of the relatively high Mg abundances found in samples from the Dale gabbro.

CONCLUSION

The chemistry of the metamorphic minerals is strongly host dependant. The chemical variation of a metamorphic mineral in one sample can therefore be considerable. It indicates that no large scaled chemical homogenization occurred in these rocks. If equilibrium conditions were reached, it must have been on a local scale only. The metamorphic mineralogy of the Jomasknutene and Dale gabbro is similar but the intensity of metamorphism differ. This indicates that either Gothian and Sveconorwegian metamorphic conditions were similar but differed in intensity or that the Sveconorwegian overprinted the entire Gothian metamorphic mineral assemblage in the Jomasknutene gabbro and that the intensity was variable from place to place.

2.4 CRYSTALLIZATION AND METAMORPHIC CONDITIONS IN THE JOMASKNUTENE AND DALE GABBRO

Magmatic and metamorphic P-T estimations in gabbroic rocks require a well suited mineralogy, equilibrium conditions between coexisting minerals and the knowledge of other parameters which could modify the P-T estimations. In case of the Jomasknutene and Dale gabbro it seems not to be possible to pinpoint the exact magmatic P-T conditions. Metamorphic temperature conditions in the Jomasknutene gabbro can be better pinned down although comparison between them and previous metamorphic temperature estimates in the same area from Nijland and Maijer (1992), suggest that they probably do not reflect peak metamorphic conditions.

2.4.1 MAGMATIC P-T CONSTRAINTS

Several authors, among which de Haas (1992) and Brickwood and Craig (1987) have suggested that the pressure during crystallization of magmas in the central part of the Bamble area does not exceed 8 kbar. Their suggestion is based on the presence of plagioclase as the main magmatic Al-rich mineral in gabbroic rocks instead of spinel or garnet (Carmichael et al. 1974). Temperature estimates are even more difficult and highly debatable. Using the binary phase diagrams of Bowen and Schairer (1935), Kushiro (1973) and Huebner and Turnock (1980), which are constructed for 1 atmosphere in a dry system, the estimated crystallization temperatures ranges between 1400°C and 1600°C for the crystallization of olivine, between 1350°C and 1125°C for plagioclase and between 1250°C and 1110°C for augite. Especially the crystallization temperature for olivine is unrealistically high.

2.4.2 METAMORPHIC TEMPERATURE CONSTRAINTS IN THE JOMASKNUTENE GABBRO

The secondary minerals, discussed previously, have formed after the solidification of the gabbroic magma. Some of those minerals have a subsolidus origin whereas other have a metamorphic origin. However it is often difficult to distinguish whether a secondary mineral has a subsolidus or metamorphic origin.

A mineral may equilibrate chemically with its environment under specific P-T conditions in a permeable system; a system in which element are able to redistribute. Changing the P-T conditions causes a shift in equilibrium until it is re-established or the chemical system is frozen i.e. the exchange reaction stopped. Thus, in principle, values obtained from geothermometers and geobarometers do not necessarily need to represent peak metamorphic conditions but may reflect "closure conditions". Whether or not equilibrium conditions between mineral pairs were reached can be visualized in a Kd-diagram. In such diagram element ratios of the minerals concerned are plotted and linked by tie lines. Parallel running tie lines indicate equilibrium conditions. Such diagram is constructed in figure 2.4.1 indicating that equilibrium conditions between orthopyroxene and garnet and between orthopyroxene and biotite were reached. I used these mineral pairs to calculate equilibration temperatures. The results of these calculations are listed below in table 2.4.1 and 2.4.2.

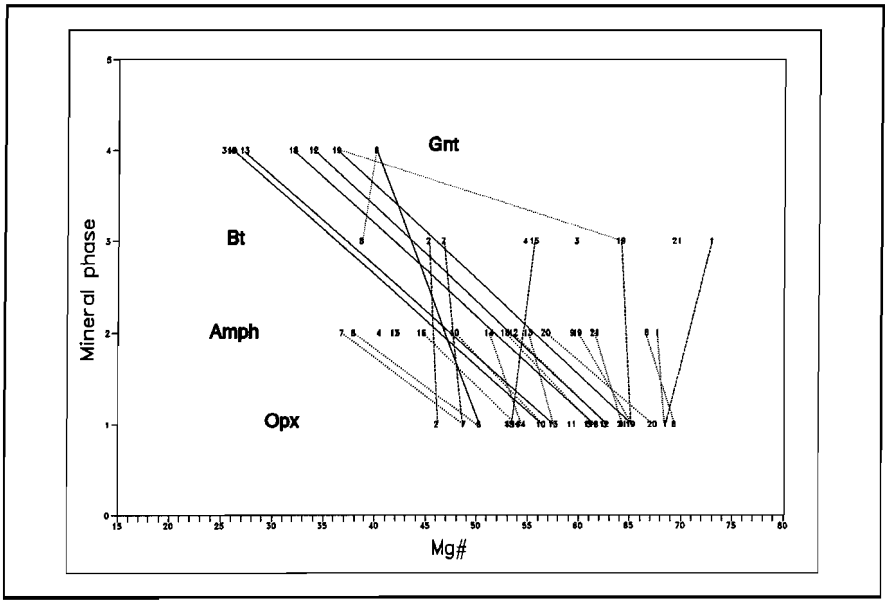

Figure 2.4.1

Kd plots (Mg#) of four Fe-Mg minerals. Each tie line represent contacting minerals. The Mg# are average values. Parallel lines between two minerals indicate equilibrium.

Gnt= garnet, Bt= biotite, Amph= amphibole, Opx= orthopyroxene.

ORTHOPYROXENE GARNET GEOTHERMOMETRY

The mean estimated equilibrium temperature for orthopyroxene garnet pairs, summarized in table 2.4.1, are based on the iron magnesium distribution coefficient between the two minerals. The estimated mean temperatures conditions during equilibration range between 665°C ±29 (Harley, 1984) and 721°C ±38 (Sen and Bhattacharya, 1984).

Table 2.4.1 *ORTHOPYROXENE GARNET THERMOMETRY FROM THE JOMASKNUTENE GABBRO*

Mean estimated equilibration temperature of coexisting orthopyroxene garnet pairs from the Jomasknutene gabbro.

	Ga315	Ga336	Ga357
Lee & Ganguly 1988	687°	630°	683°
Sen & Bhattacharya 1984	715°	693°	735°
Harley 1984	663°	636°	676°

ORTHOPYROXENE BIOTITE GEOTHERMOMETRY

The estimated equilibrium temperatures for orthopyroxene biotite pairs are summarized in table 2.4.2. The mean estimated temperature for equilibrium conditions, based on the geothermometer of Sengupta et al. (1990), is 671°C (±32).

Table 2.4.2 *ORTHOPYROXENE BIOTITE THERMOMETRY FROM THE JOMASKNUTENE GABBRO*

Mean estimated equilibration temperature of coexisting orthopyroxene biotite pairs from the Jomasknutene gabbro.

	Ga148	Ga159	Ga358
Sengupta et al.1990	671°	702°	579°

Temperature estimates obtained from both mineral pairs are in general lower then the peak metamorphic temperature (752°C ±34°) for this area stated by Nijland and Maijer (1992). This discrepancy may have two reasons:

1) The estimated metamorphic temperatures in the Jomasknutene gabbro are of Gothian age and have not been reset thereafter. This would imply that the metamorphic temperature conditions in the Nelaug area were slightly lower at Gothian times than at Sveconorwegian times
2) The estimated temperature conditions in the Jomasknutene gabbro are closure conditions and do not represent peak metamorphic conditions at Sveconorwegian times.

AMPHIBOLE QUARTZ SYMPLECTITE; A THERMODYNAMIC CONSIDERATION

The reaction between plagioclase and intercumulus augite generated amphibole and quartz in samples from the Jomasknutene gabbro. The reaction was accompanied by fluids. These fluids were trapped in the quartz grains. I shall discuss the nature of these fluid in more detail in chapter IV. The two most important conclusions from that study are:

1) The fluid is an aqueous salt bearing solution containing in addition, carbon dioxide and nitrogen
2) The fluid has a metamorphic origin

The first conclusion implies a partial water pressure during the quartz producing reaction substantial lower than the total pressure. The reaction which describes the formation of the amphibole quartz symplectite is:

$$NaCa_2Mg_4Al_3Si_6O_{22}(OH)_2 + SiO_2 \rightleftharpoons CaMgSi_2O_6 + 2Ca_{0.5}Na_{0.5}Al_{1.5}Si_{2.5}O_8 + H_2O + 3MgO$$

Pargasite + Quartz ⇌ Diopside + Plagioclase + Water + Periclase

This reaction equation is idealized. Besides the fact that I used nominal mineral compositions I also added the mineral periclase to the system to balance the equation. However, no periclase has been found in the investigated samples. The mineral formula with its corresponding thermodynamic values are obtained from the work of Holland and Powell (1990). The thermodynamic potential at 298 K for each component is calculated via the following equation:

$$U(298) \approx H(298) - T \times S(298)$$

This equation leads to table 2.4.3.

Table 2.4.3 *THERMODYNAMIC POTENTIAL AT 298K*

	H(298)	S(298)*10^{-3}	V(298)	U(298)
Diopside	-3200.2	142.7	66.2	-3242.7
Plagioclase	-4086.3	203.4	100.4	-4146.9
Water	-241.8	188.8	1.0	-298.1
Periclase	601.41	26.9	11.3	-609.4
Pargasite	12719.8	519.0	272.1	-12874.5
Quartz	910.8	41.5	23.0	-923.2

$\Delta U = 134.85$

$\Delta S = 258.4*10^{-3}$

$\Delta V = 5.7$

The temperature dependence of the thermodynamic potential is expressed in the following equation:

$$\mu(T) = \mu(298) + S(298) \times \Delta T$$

At equilibrium conditions, the summation of the thermodynamic potential of the products is equal to the summation of the thermodynamic potential of the reactants. Neglecting the pressure dependence on the thermodynamic potential of solid phases the following equation presents the water pressure as functions of temperature.

$$\sum \mu(T) = -R \times T \times Ln(P_{H_2O})$$

$$Ln(P_{H_2O}) = \frac{-\sum \mu(T)}{R \times T}$$

This equation leads to table 2.4.4.

These P_{H2O} and T values are plotted in figure 2.4.2. The reaction line represent the breakdown of augite, plagioclase and periclase to amphibole and quartz. If the P_{H2O} is equal to the estimated metamorphic pressure concerning this part of the Bamble area of 7.1 kbar (Nijland and Maijer 1992) temperature conditions must have reached 875°C. This metamorphic temperature is much too high. No evidence for such high grade metamorphism in this part of the Bamble area has been found. On the other hand, if we assume the metamorphic temperature to be 751°C the corresponding partial water pressure would be in the order of 1 kbar; 7 times lower than the total pressure. This would also elucidate the presence of other fluid/gaseous phases viz. CO_2 and N_2.

Table 2.4.4 *PARTIAL WATER PRESSURE*

Temperature T in °C; Partial water pressure P_{H2O} in kbar

T	μ(T)	Ln(P)	P_{H2O}	T	μ(T)	Ln(P)	P_{H2O}
127	108.5	-32.6	< 0.1	627	-20.7	2.8	<0.1
227	82.7	-19.9	< 0.1	727	-46.55	5.6	0.3
327	56.8	-11.4	< 0.1	827	-72.4	7.9	2.7
427	31.0	-5.3	< 0.1	877	-85.3	8.9	7.5
527	5.1	-0.8	<0.1	927	-98.23	9.85	19.0

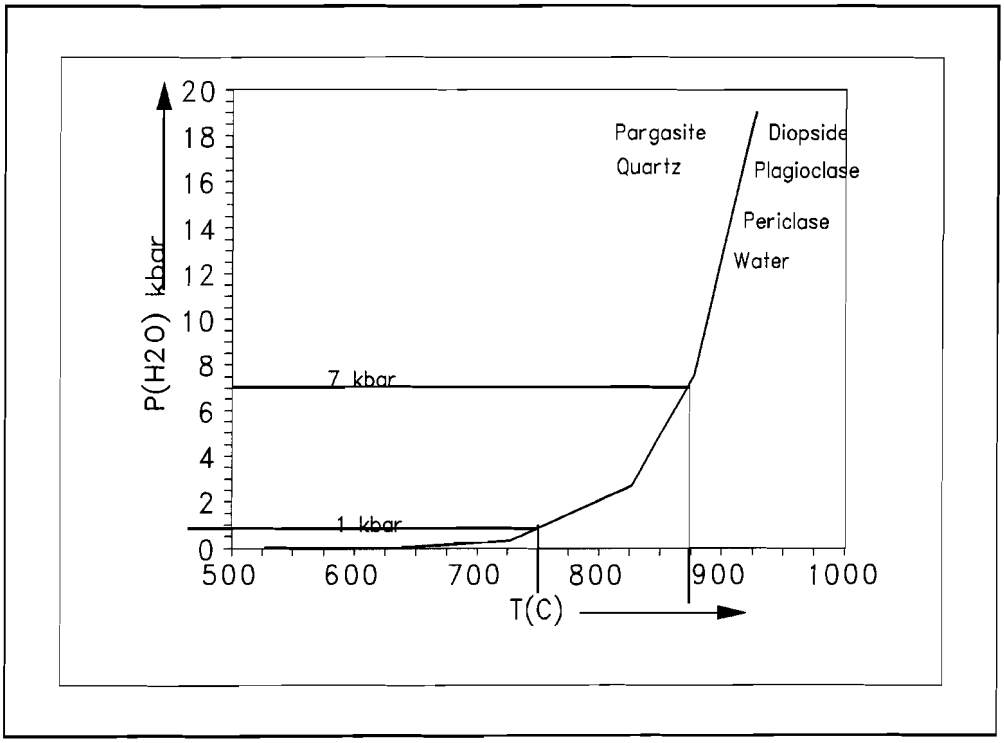

Figure 2.4.2

The theoretical P-T curve of the breakdown reaction of augite, plagioclase, periclase and water to amphibole and quartz.

2.5 WHOLE ROCK CHEMISTRY OF THE JOMASKNUTENE AND THE DALE GABBRO

Whole rock chemistry of gabbroic rocks provide useful information about the crystallization of the magma and the chemical effect of subsequent metamorphism and metasomatism. By comparing the whole rock chemistry of only slightly altered gabbroic samples from the Jomasknutene with the Dale gabbro we might get an idea about the differences and similarities of their magmatic history. By comparing the whole rock chemistry of 'fresh' gabbroic rock with metamorphosed or metasomatized ones we might get an idea about the character of the metamorphic process.

ANALYTICAL TECHNIQUE

A group of samples selected on the basis of their mineralogical characteristics (chapter 2.3) have been analyzed in order to determine the whole rock chemistry. X-ray fluorescence analyses were carried out at the Institute of Earth Sciences, Utrecht university. The following standard preparation and measurement conditions were used:

- About 3 kg sample material was broken in a tungsten-carbide coated jaw-crusher and homogenized. From this sample about 75 gr was grounded in a tungsten coated swing-mill.
- About 2.5 gr. of the grounded sample was ignited for four hours at 900°C.
- Glass beads were made by fusing a mixture of $LiBO_4/Li_2B_4O_7$ (66/34) spectroflux with ignited sample material in a ratio of 10:1 at 1000°C.
- Pressed pellets were made by mixing about 8 gr. of the grounded sample with Elvacite as cementing medium.
- The glass beads were used for major element analyses; the pressed pellets for trace elements analyses. All samples were analyzed by a Philips 1450/AHP automatic spectrometer.

The complete 'raw' data set concerning the whole rock chemistry of the Dale and Jomasknutene gabbro is presented in appendix A.

WHOLE ROCK MG# AS FRACTIONATION INDEX

The whole rock Mg# is generally used as a fractionation index for mafic rocks. There are however some often overlooked factors which influence the absolute values of the whole rock Mg#. Two of these factors are discuss below.

The whole rock Mg# is composed of two mineral related variables i.e. the Mg# of the individual ferromagnesian minerals and their relative abundances. These two variables changes due to fractionation during magma solidification. The Fe content of the minerals increases relatively to Mg with increasing fractionation as indicated in binary phase diagrams. I have drawn in figure 2.5.1 two of such phase diagrams; one for olivine (after Bowen and Schairer 1935) and one for Ca rich clinopyroxene (after Huebner 1980). These minerals appear to be the main magmatic Fe-Mg minerals in the Jomasknutene and Dale gabbro. Figure 2.5.1 demonstrates that a crystallizing magma with a specific Mg# produces minerals with different Mg#. In this example the $Mg\#^{augite} > Mg\#^{olivine}$.

To illustrate the chemical behaviour of augite and olivine in the Jomasknutene and Dale gabbro I have plotted their Mg# against the whole rock Mg#. The results are shown in figure 2.5.2 and 2.5.3 respectively. In these figures the reference line '1=1' represents equality of mineral and whole rock Mg#. It appears that the Mg# of augite is in general higher than the whole rock Mg# whereas the Mg# of olivine is in general lower than that of the whole rock. It is clear that the whole rock Mg# is a combination of the augite Mg# and the olivine Mg# and does not automatically imply an absolute fractionation index value of the magma. However, the positive correlation between the Mg# of the minerals and that of the whole rock suggests that the whole rock Mg# may be used as a relative fractionation index value.

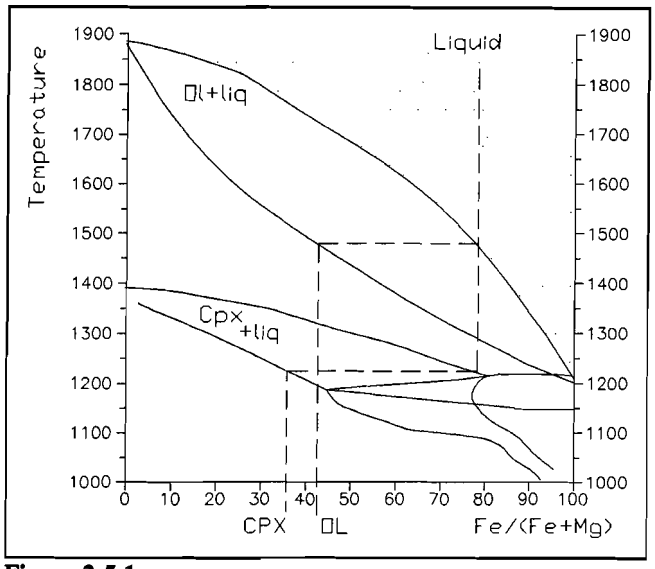

Figure 2.5.1

Two phase diagrams; one of olivine and one of augite (modified after Bowen and Schairer, 1935 and Huebner and Turnock, 1980). This figure shows that crystallizing clinopyroxene has a higher Mg# then crystallizing olivine for a specific starting liquid composition.

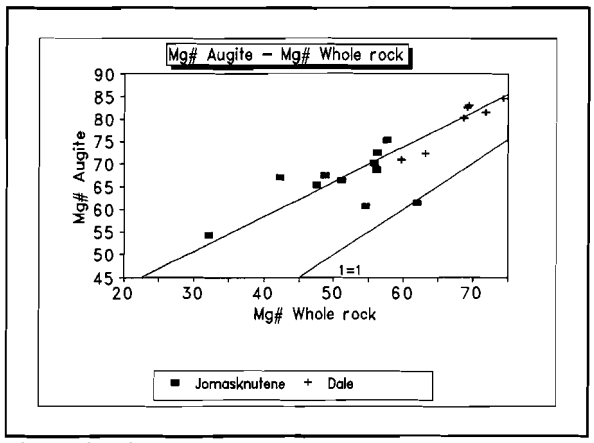

Figure 2.5.2

The Mg# of augite from the Jomasknutene gabbro and the Dale gabbro plotted against the whole rock Mg#. The increase of the Mg# of augite runs more or less parallel to the '1=1' line. The Mg# of augite is higher than the corresponding Mg# of the whole rock.

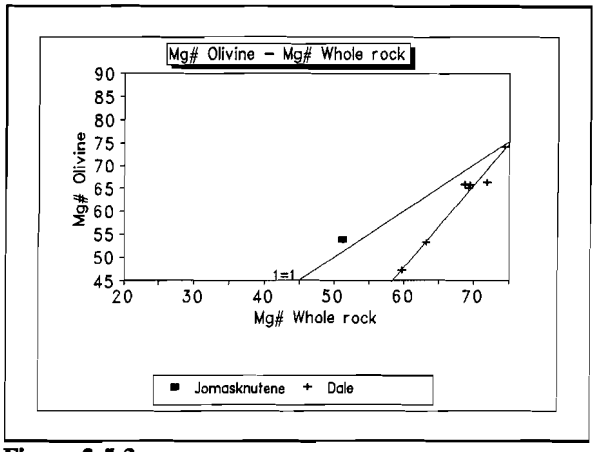

Figure 2.5.3

The Mg# of olivine from the Jomasknutene gabbro and the Dale gabbro plotted against the whole rock Mg#. The increase of the Mg# of olivine runs steeper than '1=1' line. The Mg# of olivine is in general lower than the corresponding Mg# of the whole rock. An exception to this rule is the sample from the Jomasknutene gabbro.

An other aspect, which is often overlooked in the cause of determining the whole rock Mg# as fractionation index, is the presence of iron-oxides which do not contain Mg. The whole rock Mg# as fractionation index, which is based on the Mg# of the ferro magnesium minerals, will be perturbed if large quantities of ilmenite or magnetite are present in the rock. The effect of these large quantities is two fold:

1) It considerably lowers the whole rock Mg#.
2) It lowers the relative amount of all other elements except iron and titanium. This is known as the 'closure effect'.

To avoid these perturbing factors in graphical whole rock diagrams I employed a correction factor on the 'raw' whole rock chemical data. Values in the whole rock tables are not corrected except for their Mg#. To correct for these 'raw' data I used the following procedure:

1) Calculate the molar properties of the whole rock analysis and normalize it to 100.
2) Calculate the normative ilmenite content (for simplicity I ignored normative magnetite).
3) Subtract the normative amount of ilmenite multiplied by its chemical molar composition from the whole rock analysis and normalize it to 100 again.
4) Finely recalculating the new whole rock Mg#.

2.5.1 ORTHOGABBROS FROM THE JOMASKNUTENE AND DALE GABBRO

It is a general characteristic of orthogabbros that they exhibit a (sub)ofitic texture and that primary magmatic minerals did not change much in spite of metamorphism and local deformation. Any chemical variation between orthogabbroic samples is thus primarily magmatic in origin. Although there are many ways to classify a magmatic rock or to illustrate its' crystallization history, I confine the discussion here to three schemes:

1) The Harker diagram, which illustrates the crystallization and chemical evolution in terms of the corrected Mg# as fractionation index.

2) AFM-classification, which illustrates the crystallization and chemical evolution of a magmatic rock in terms of its FeO, MgO and Na_2O+K_2O content.
3) Projection of the normative mineral content in a basalt tetrahedral which classifies gabbroic magmas in terms of its silica saturation.

Table 2.5.1 gives a summary of the chemical analyses, Mg# and normative mineral data from 17 orthogabbroic samples from the Dale gabbro and 23 orthogabbroic samples from the Jomasknutene gabbro. Two examples illustrating the chemical variations in both gabbros are presented in figure 2.5.4 and 2.5.5. Here the Mg# is plotted against molar percentage SiO_2 and Al_2O_3 respectively. It appears that, although some overlap in Mg# occurs, the fractionation trend for the Jomasknutene gabbro starts where it ends for the Dale gabbro.

Classification of the orthogabbroic rocks of both gabbro bodies via an AFM-diagram is illustrated in figure 2.5.6. It appears that most chemical whole rock analyses of the Jomasknutene and Dale gabbro plot on or close to the "iron enrichment branch" of this classification diagram which separates the tholeiitic suite from the calc alkaline suite. Samples from the Jomasknutene gabbro are in general iron and alkali richer than those from the Dale gabbro.

The major chemical whole rock differences between orthogabbroic rocks from the Jomasknutene and Dale gabbro can be summarized as follows:

1) The Dale gabbro shows generally well defined chemical fractionation trends whereas those in the Jomasknutene gabbro tend to scatter more.
2) Titanium, zirconium and sodium contents are slightly higher in the Jomasknutene gabbro than in the Dale gabbro. Magnesium and nickel contents are lower in the Jomasknutene gabbro than in the Dale gabbro.
3) The calcium content increases during fractionation of the Dale gabbro whereas it decreases during fractionation of the Jomasknutene gabbro.

Another way of characterizing gabbroic magmas is to plot the mineral content, obtained from the CIPW norm calculations, in the basalt tetrahedron of Yoder and Tilley (1962). Figure 2.5.7 demonstrates such characterization. Samples from the Jomasknutene gabbro plot in general just on the nepheline side of the critical plane of silica undersaturation whereas samples from the Dale plot in general just on the hypersthene or quartz side.

Norm calculations lead to the following differences:

1) Samples from the Jomasknutene gabbro are usually nepheline normative whereas samples from the Dale gabbro are not. Samples from the Dale gabbro are usually hypersthene normative whereas samples from the Jomasknutene gabbro are not. These norm calculations indicate that the Dale gabbro is usually silica saturated whereas the Jomasknutene is not. This is however not in accordance with occurrence of quartz in the Jomasknutene gabbro.
2) The normative olivine concentration is higher in the Dale gabbro than in the Jomasknutene. This coincides with the modal olivine content discussed in chapter 2.3.

I did not account for magnetite in the norm calculations because of unknown Fe_2O_3 contents in the gabbros. Because the Jomasknutene gabbro contains besides ilmenite also magnetite an error is introduced in the norm calculations. This error may very well be the reason why the Jomasknutene gabbro is in general nepheline normative (silica undersaturated) whereas the Dale gabbro is not.

Table 2.5.1 *CHEMICAL ANALYSES OF ORTHOGABBROS FROM THE JOMASKNUTENE AND DALE GABBRO*

A compilation of the chemical data, in mole %, from orthogabbroic samples from the Dale gabbro designated (D) and the Jomasknutene gabbro designated (J). The Dale sample WT221 is chemically similar to the Jomasknutene gabbro sample Ga159. Furthermore the average, maximum and minimum values are added. The Mg# is corrected for ilmenite. CIPW norms have been calculated. Ap = apatite, Ilm = ilmenite, Or = K-feldspar, Ab = albite, An = anorthite, Di = diopside, Hy = hypersthene, Ol = olivine, Ne = nepheline.

	Mol% WT221 (D)	Avg Mol% (D)	Max Mol% (D)	Min Mol% (D)	Mol% GA159 (J)	Avg Mol% (J)	Max Mol% (J)	Min Mol% (J)
SiO_2	50.64	47.22	52.91	39.38	50.23	50.37	54.80	43.90
Al_2O_3	11.76	8.45	11.76	4.80	12.05	10.64	14.87	6.13
TiO_2	0.71	0.65	1.51	0.20	0.84	1.71	4.86	0.84
FeO	9.00	10.66	13.57	8.31	9.06	11.44	21.92	6.67
MnO	0.16	0.18	0.24	0.14	0.17	0.21	0.37	0.13
MgO	13.11	20.59	36.60	11.02	13.50	10.37	21.35	4.94
CaO	12.02	10.13	13.18	5.37	10.73	11.18	14.28	9.32
Na_2O	2.05	1.82	2.65	0.69	3.00	3.60	5.17	1.99
K_2O	0.55	0.29	0.60	0.07	0.34	0.40	0.72	0.16
P_2O_5	0.00	0.00	0.05	0.00	0.07	0.10	0.21	0.05
Total	100.00				100.00			
Mg#[1]	61	65	74	53	62	51	62	31
Ni(ppm)	136	253	499	59	39	80	203	29
Zr(ppm)	59	51	71	18	94	106	258	65
Ap	0.00	0.12	0.23	0.00	0.32	0.12	0.24	0.00
Ilm	1.72	2.09	3.71	0.47	1.95	6.84	11.72	1.95
Or	4.87	3.02	5.46	0.57	2.88	3.75	6.14	1.36
Ab	17.03	11.63	22.61	0.65	21.81	19.21	28.80	9.62
An	40.44	28.87	40.44	17.30	36.84	32.82	45.87	19.76
Di	10.69	15.93	27.04	4.81	6.48	16.48	26.48	6.48
Hy	2.81	2.19	4.37	0.00	0.00	0.48	0.96	0.00
Ol	22.89	41.28	69.78	12.77	27.95	27.11	43.94	10.28
Ne	0.00	2.21	4.42	0.00	1.17	4.65	9.30	0.00

[1] Ilmenite corrected

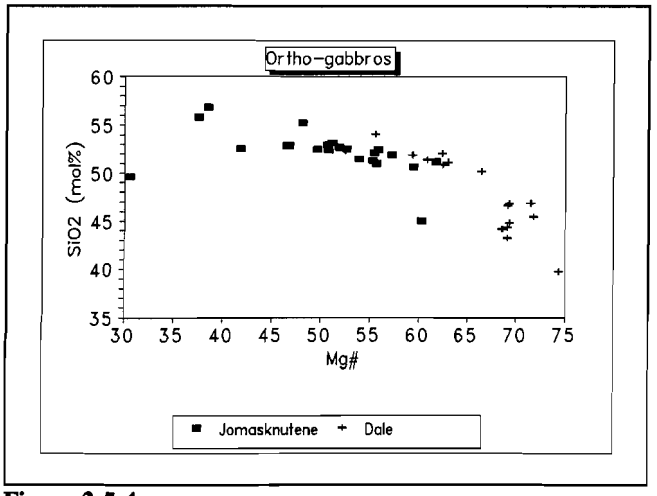

Figure 2.5.4

The normalized molar SiO_2 content of the Jomasknutene and Dale orthogabbros plotted against the whole rock Mg# as fractionation index. The values are normalized with respect to ilmenite. Both gabbros have a comparable SiO_2 content which increases with increasing fractionation index.

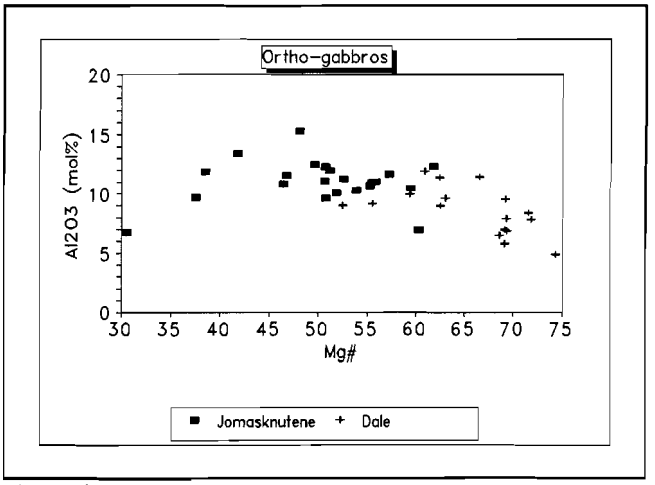

Figure 2.5.5

The normalized molar Al_2O_3 content of the Jomasknutene and Dale orthogabbros plotted against the whole rock Mg# as fractionation index. The values are normalized with respect to ilmenite. Both gabbros have a comparable Al_2O_3 content which depends on the fractionation index. The Al_2O_3 content increases in the beginning of the fractionation both for the Dale and Jomasknutene gabbro process whereas it decreases in the Jomasknutene gabbro only at the end of the fractionation process.

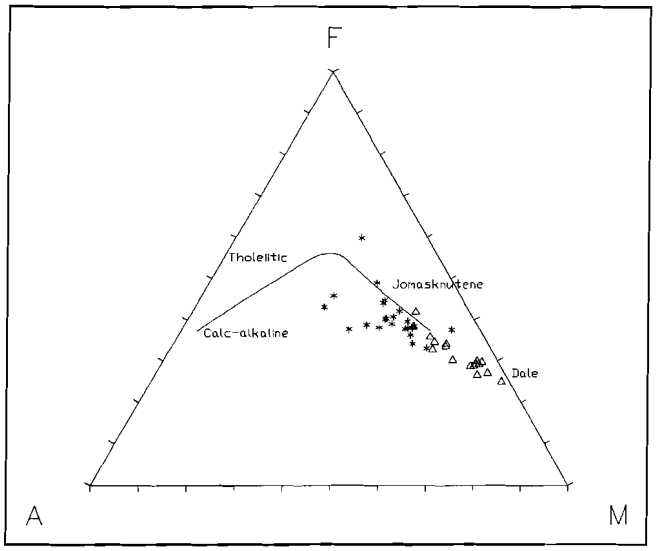

Figure 2.5.6

The alkali, iron and magnesium variation (in Wt%) in samples from the Jomasknutene and Dale gabbro, designated with stars and triangles respectively. A = Na_2O + K_2O, F = FeO, M = MgO. This figure demonstrates the similarities in fractionation process of the two gabbroic magmas, tending towards iron enrichment.

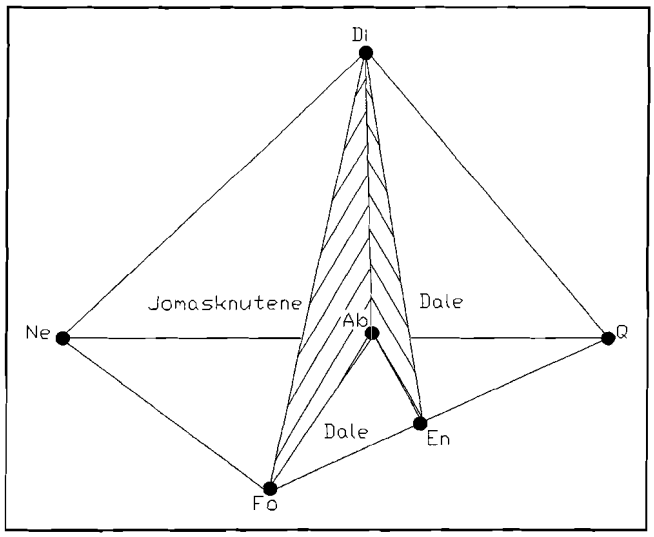

Figure 2.5.7

The normative basalt tetrahedron modified after Yoder and Tilley (1962). It classifies the whole rock chemistry of the Jomasknutene and Dale gabbro. The samples from the Jomasknutene gabbro plot on the nepheline site; the samples from the Dale gabbro plot on the quartz site of the forsterite diopside albite plane.

In conclusion, the whole rock chemistry of the Dale and the Jomasknutene orthogabbros do not differ much although the Dale gabbro is just silica saturated whereas the Jomasknutene gabbro is slightly silica undersaturated. The normative mineral composition which does not directly relate to the modal mineral composition in the investigated gabbro samples. The magma from which both gabbros originate is thought to be similar (de Haas 1992) although the Jomasknutene gabbro is qua Mg# slightly more evolved due to fractional crystallization than the Dale gabbro. The scattering of the fractionation trends in the Jomasknutene gabbro may have several causes among which:

1) The more complex intrusive character of this gabbro with respect to that of the Dale gabbro.
2) The more intensive metamorphic alteration of the primary magmatic minerals of the Jomasknutene gabbro in contrast to the Dale gabbro.

2.5.2 ORTHO- AND METAGABBRO IN THE JOMASKNUTENE GABBRO

Orthogabbroic rocks may have changed due to deformation and mineralogical alteration to metagabbroic rocks or even to orthoamphibolitic rocks. Metagabbro is characterized by alteration of the primary magmatic mineral assemblage to a metamorphic one. This alteration consists mainly of amphibolitization and scapolitization. The orthogabbroic subofitic texture still tends to be present. In ortho amphibolite rocks both the primary magmatic texture and mineralogy has been changed to a metamorphic one. Amphibole, plagioclase and scapolite are the main constituents and exhibit usually a banded or foliated texture.

To demonstrate the effect of this alteration process of the primary magmatic minerals on the whole rock chemistry, I have compared 17 orthogabbros and 39 metagabbros from the Jomasknutene gabbro. The results of this comparison are illustrated in figure 2.5.8 to 2.5.11 and listed in table 2.5.2 in which the chemical analyses of one meta- and one orthogabbro are presented. The 56 chemical analyses indicate that ortho- and metagabbros tend to be, with the possible exception of potassium, similar in chemical composition despite intensive alteration. Apparently, neither Gothian nor Sveconorwegian metamorphism significantly influenced the elements presented in the whole rock chemistry of the Jomasknutene gabbro. It is clear from figure 2.5.10 and 2.5.11 that intensive scapolitization did not significantly affect the whole rock chemistry either.

2.5.3 METASOMATIZED GABBROS FROM THE OUTER MARGIN OF THE JOMASKNUTENE GABBRO

The most intense alteration of gabbroic rocks in the Jomasknutene gabbro occur near the contact with the country rock and in or near shear zones. The original, primary magmatic minerals with their (sub)ofitic texture are usually absent and modified to a metamorphic fabric. The metasomatic process, which is responsible for the formation of the AAQ gneiss, affected only locally the outer gabbro margins. To demonstrate the influence of this metasomatic process on the whole rock chemistry of the gabbro, I compared 8 metasomatized gabbroic samples from the outer gabbro margin with 39 metagabbro and 17 orthogabbro samples. Only 3 out of 8 samples from the outer margin have a clearly higher potassium content as illustrated in figure 2.5.11. The other elements exhibit no large deviation from observed chemical trends found in orthogabbroic samples. An example of this potassium enrichment is presented in table 2.5.2. Thus, only high potassium concentrations seems to be an indicator of metasomatism in the Jomasknutene gabbro.

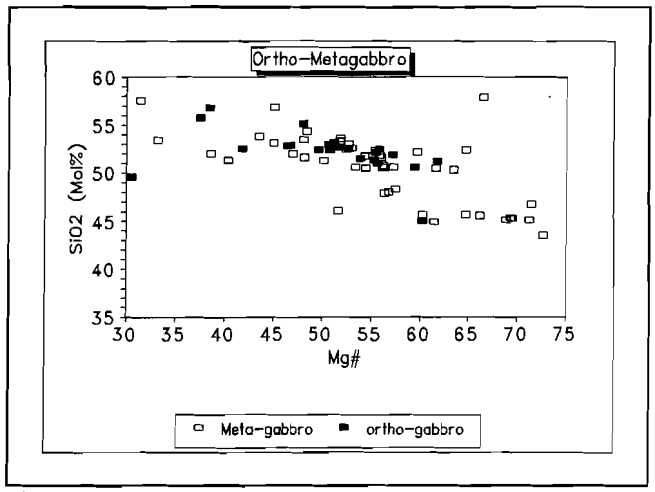

Figure 2.5.8

The normalized molar SiO_2 content of the Jomasknutene ortho- and metagabbro plotted against the whole rock Mg#. The values are normalized for ilmenite. The metagabbro has a similar chemistry as the orthogabbro and is chemically indistinguishable with respect to SiO_2 and the Mg#.

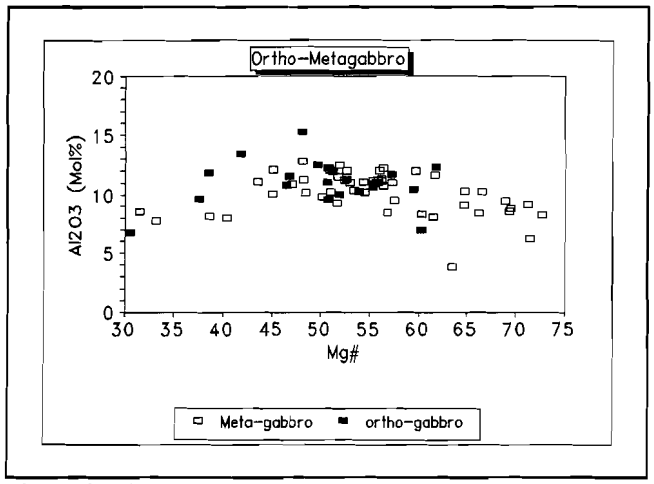

Figure 2.5.9

The normalized molar Al_2O_3 content of the Jomasknutene ortho- and metagabbro plotted against the whole rock Mg#. The values are normalized with respect to ilmenite. The metagabbro has a similar chemistry as the orthogabbro and is chemically indistinguishable with respect to Al_2O_3 and the Mg#.

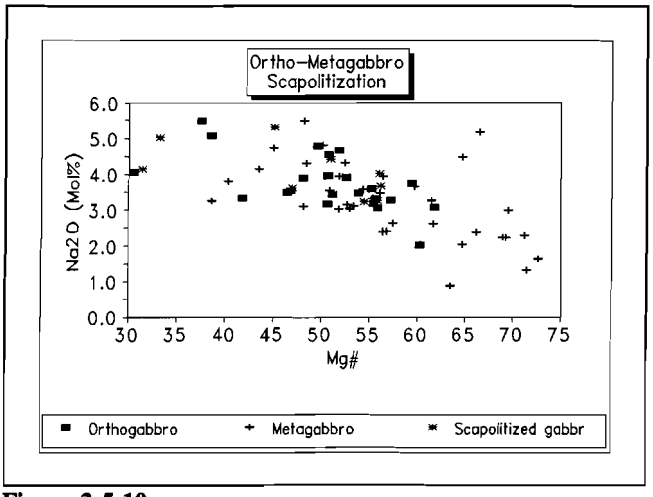

Figure 2.5.10

The normalized molar Na_2O content of meta and scapolitized gabbro samples compared with orthogabbro samples from the Jomasknutene gabbro. The values are normalized with respect to ilmenite. Scapolitization and other alterations of the gabbro do not significantly influence the sodium content of the whole rock.

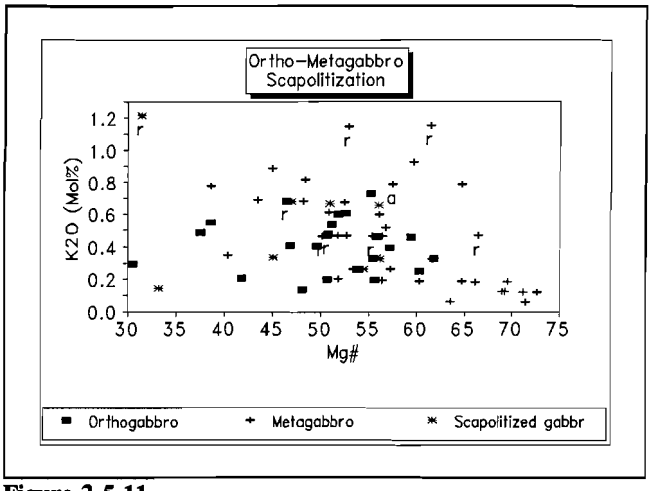

Figure 2.5.11

The normalized molar K_2O content of meta and scapolitized gabbro samples compared with orthogabbro samples. The values are normalized with respect to ilmenite. Samples close to the outer margin of the Jomasknutene gabbro are designated as 'r'. 'a' represent amphibolite from the Jomasknutene gabbro. The K_2O content of the outer margin samples tend to be slightly higher than the K_2O content of the orthogabbro.

Table 2.5.2 *CHEMICAL ANALYSES OF ORTHO-, META- AND METASOMATIZED GABBRO FROM THE JOMASKNUTENE GABBRO*

Chemical data, in mole % of sample Ga179 representing a metagabbro, Ga159 representing an orthogabbro and Ga394 representing a sample near the outer margin of the Jomasknutene gabbro. The metagabbro and orthogabbro are similar in chemistry whereas the outer margin sample is higher in potassium due to metasomatic processes along this margin. Abbreviations are the same as those used in table 2.5.1.

	Mol% Ga179 Meta gabbro	Mol% Ga159 Ortho gabbro	Mol% Ga394 Metasomatized gabbro
SiO_2	49.04	50.23	50.67
Al_2O_3	9.95	12.05	10.62
TiO_2	1.41	0.84	1.79
FeO	11.87	9.06	11.57
MnO	0.26	0.17	0.26
MgO	12.52	13.48	11.23
CaO	11.49	10.73	9.73
Na_2O	3.15	3.00	2.91
K_2O	0.26	0.34	1.09
P_2O_5	0.06	0.07	0.12
Total	100.00	100.00	100.00
Mg#[2]	55	62	53
Ni	121	39	101
Zr	79	94	97
Ap	0.28	0.32	0.59
Ilm	3.25	1.95	4.15
Or	2.46	2.88	9.23
Ab	18.14	21.81	20.45
An	28.23	36.84	28.14
Di	17.02	6.48	9.64
Hy	0.00	0.00	0.00
Ol	25.88	27.95	25.22
Ne	3.85	1.17	1.61

[2] Ilmenite corrected

2.6 GRAIN SIZE VARIATION IN BOTH GABBROS: TTT DIAGRAMS

Large grain size variations in both the Jomasknutene and Dale gabbro are common. This variation tends to be gradual in the Dale gabbro whereas it is either gradual or abrupt, bounded by sharp contacts in the Jomasknutene gabbro. The grain size increase in the Dale gabbro is accompanied by a decrease in whole rock Mg#. In the Jomasknutene gabbro, the grain size variation does not coincide with the degree of fractionation. The question in need of an answer is how these differences can occur and what their consequence is for the cooling history of the melt. I shall suggest a scenario which gives an explanation for these grain size variations in terms of a Time-Temperature-Transition diagram (TTT-diagram), a new concept in the magmatic igneous petrology to explain grain size variations.

The basic reasons why some magmatic rocks are coarse grained whereas others are fine grained lies in a difference in number density of nuclei formed in a magma. A crystallizing magma will form a coarse grained rock if it contains a few nuclei and a fine grained rock if many nuclei are present. It is therefore important to understand the parameters which influence the number density of nuclei.

Before a magma starts to crystallize, its temperature is above the liquidus. The viscosity of such melt depend mainly on:

- the chemical composition
- the temperature
- the pressure

Formation of nuclei starts below the liquidus, increases with the degree of undercooling and has its maximum at relatively high undercooling. If the degree of undercooling becomes too high, the nucleation rate decreases because diffusion rates in the magma become too low. The growth of crystals from nuclei occur just below the liquidus and finds its maximum at a small degree of undercooling because of its strong dependence on diffusion rates in the magma. The high diffusion rate at low undercooling coincides with a low viscosity in accordance with the Stokes-Einstein relation (Turkdogan 1983). The growth rate decreases with increasing undercooling (increasing viscosity and thus decreasing diffusion rate). An example of a nucleation and growth rate curve is shown in figure 2.6.1[a] modified after Dowty (1980) and de Jong (1989).

Summarized, there are two principle parameters which determine the grain size:

1) Viscosity of the magma
2) Number density of nuclei in the magma

To determine which parameter is responsible for the grain size variation in the Jomasknutene and Dale gabbro, I estimated the viscosity of the gabbroic magmas, using the partial molar viscosity coefficients determined by Bottinga and Weill (1972) and compared these values with the grain size differences. The results are listed in table 2.6.1. These estimates do not necessarily represent true viscosity numbers because the investigated gabbros comprises partly cumulates. It appears that viscosity, which measures about 217 poise, does not change significantly between the coarse, medium and fine grained samples. This leaves the degree of undercooling of the gabbroic magma as the most likely parameter responsible for the observed variations in grain size.

Table 2.6.1 *VISCOSITY*

Mean viscosity values from orthogabbros from th Jomasknutene and Dale calculated from the whole rock chemistry at T = 1250°C using the method of Bottinga and Weill (1972). Minor variations of the viscosity has been observed.

Grain size (mm) Jomasknutene	Mean viscosity (Poise) (T = 1250°C)
Coarse grained > 5	213 (n=10)
Medium grained 1-5	223 (n=9)
Fine grained 1	209 (n=1)
Dale samples ??	149 (n=8)

Before rationalizing the observed grain size variations in the Jomasknutene and Dale gabbro a brief theoretical introduction to TTT-diagrams is presented. TTT-diagram stands for Time-Temperature-Transition diagram. An example of such diagram is shown in figure 2.6.1[b]. These diagrams are well known in industrial material science such as steel, glass and ceramics. TTT-diagrams are not commonly used in geology, except in the exsolution theory of feldspar (Parson and Brown 1984) and pyroxene (Nord and McCallister 1979). The diagrams are used to explain grain size variations in volcanic rocks (Kirkpatrick 1983) as well. The aim here is to construct a similar diagram for plutonic rocks. Although the constructed diagrams (figure 2.6.1[b]) are qualitative only, they give a rationalization for the observed grain size variations (figure 2.6.1[c]) in the Jomasknutene and Dale gabbro and are in agreement with the observed whole rock chemistry. The construction of a TTT-diagram for a magmatic system goes as follows:

- The rate curves (figure 2.6.1[a]) indicate that crystals cannot grow above the liquidus temperature (T_m) or below a certain temperature (T_o). These two temperatures are shown as horizontal lines in the TTT-diagram.
- The maximum growth rate takes place at a temperature just below the liquidus at T_{max}.
- At a residence time 't' of the magma at T_{max} the crystals have a specific size. If 't' is shorter the crystals will not have time to grow and the grain size will be small. If 't' is longer the crystals have enough time to grow resulting in a coarse grained rock.
- If, at a constant residence time, the temperature increases from T_{max} towards T_m, the growth rate decreases and the grain size will be small. If the temperature decreases from T_{max} towards T_o, the growth rate decreases and the nucleation rate increases resulting in a fine grained rock.

With this information it is possible to draw curves in this TTT-diagram which represent the conditions under which equal grain sizes occur. A TTT-diagram shows that grain size variations may occur in a variety of ways. If a magma is gently cooled from T_m to T_o as indicated by line AA', the grain size changes from fine grained to coarse grained with time, concomitant with the fractionation process. This situation has probably occurred in the Dale gabbro. The cooling magma produced initially a fine grained rock (A) with a relatively high Mg# such as occurs in the core of the Dale gabbro. When

crystallization proceeded the Mg# decreased and the grain size increased (A'). During crystallization of the liquid its composition changed due to fractionation. Consequently T_m, T_{max} and T_o will be modified as well and shift the curves to a lower position. The fractionation process is therefore an indirect parameter which modifies the grain size.

To obtain abrupt grain size variations, as observed in the Jomasknutene gabbro, two possible mechanisms can be envisioned. The first one is that the magma cooled very slowly close to T_m followed by an abrupt temperature drop (curve BB') followed again by slow cooling. The second one is that the magma cooled gently followed by a sudden temperature increase (curve CC'). In all likelihood the second scenario (CC') is the one which has been operative in the Jomasknutene gabbro but it is not clear which mechanism produced the (pulsed) temperature increase. Possibilities for such temperature increase are:

1) injection of a new magma pulse
2) liberation of latent heat
3) convecting magma

With this theoretical consideration in mind I constructed figure 2.6.1[c] to illustrates the grain size variation occurring from three different cooling scenarios viz. AA', BB' and CC' The grain size differences, the characteristically sharp contact and the whole rock chemistry suggest a difference in crystallization mechanism for the Jomasknutene and Dale gabbro. This might be a discriminating marker for Gothian and Sveconorwegian gabbros in the central part of the Bamble area. The true implications of the difference in crystallization mechanism on the tectonic history of the Bamble area remain vague.

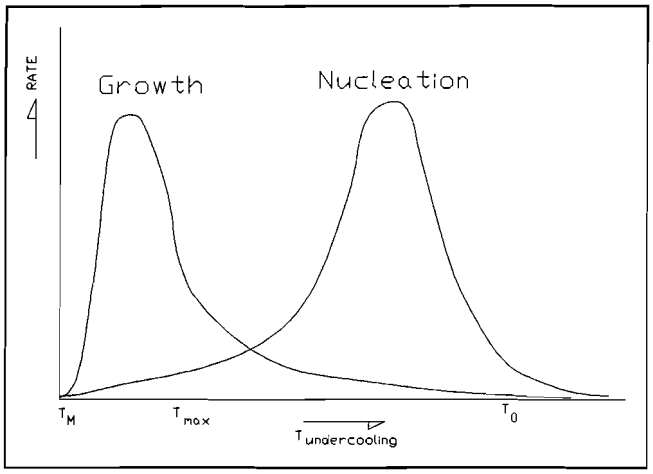

Figure 2.6.1[a]

Curves for the growth rate and nucleation rate of minerals in an undercooled magma modified after Dowty (1980) and de Jong (1989).

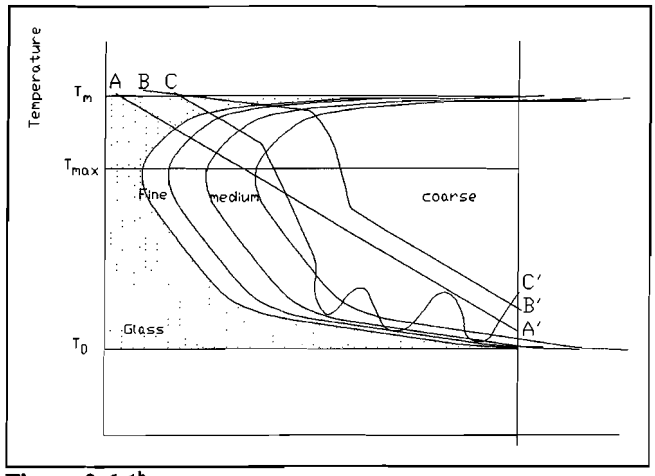

Figure 2.6.1[b]

A theoretical TTT-diagram of a gabbroic magma. T_m represents the liquidus temperature of the magma, T_{max} the temperature at which a mineral find its maximum growth rate and T_0 the temperature at which a mineral stops growing. The vertical line on the right side of the diagram represent the time limit at which the entire magma will be solidified. The 'parabolic' curves represent conditions which forms equal grain sized rocks. The lines AA', BB' and CC' represent three scenario of possible crystallization conditions. AA' is the most likely scenario for the Dale gabbro; CC' for the Jomasknutene gabbro.

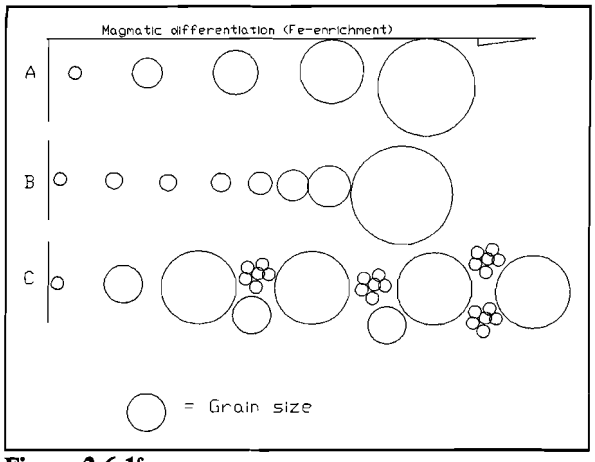

Figure 2.6.1[c]

Grain size variations belonging to the three scenario of crystallization of a magma. Scenario A (Dale gabbro) will have as result a gentle increase of the grain size with the differentiation index. Scenario B' will result in a sudden increase of the grain size with differentiation. Scenario C (Jomasknutene gabbro) will result in a mixture of fine, medium and coarse grained rocks.

2.7 DISCUSSION AND CONCLUSIONS

DISCUSSION

The first aspect which needs discussion is the age of the two gabbros. The interpretation in this thesis concerning the Gothian versus the Sveconorwegian characteristics in the central part of the Bamble area stand or falls with the validity of the age determinations. The age of the Jomasknutene gabbro (1.77 Ga $\pm$0.19 Ga) is the oldest rock ever dated in this area and should need additional affirmation of other dating techniques.

Another discussional aspect concerns the relation between field observations, mineralogy and whole rock chemistry. The Dale gabbro exhibit a relative simple relation between these three aspects. The grain size increases gently from the core towards the rim of the complex. With this grain size variation the fractionation process proceeded as well. In the Jomasknutene gabbro such simple relations seems to be absent. I did not find any significant relations between the grain size variation or geographic position on the one hand and the mineralogy or whole rock chemistry on the other. This makes it impossible to construct a (simple) magmatic history of the Jomasknutene gabbro.

The last aspect which needs discussion is the normative mineral content of both gabbros. It appears from norm calculations that the Jomasknutene gabbro is mainly nepheline normative. This indicates that these rocks are silica undersaturated. However, primary magmatic intercumulus quartz is present in the Jomasknutene gabbro. The Dale gabbro is hypersthene normative which indicates that these rocks are more silica saturated than those from the Jomasknutene gabbro. No quartz has been found in the Dale gabbro. Apparently, the normative mineralogy does not reflect the modal mineralogy. A possible explanation for the silica undersaturated character of the Jomasknutene gabbro is the error in the norm calculation introduced by ignoring magnetite. The consequence of this error is that iron originating from magnetite is bonded by SiO_2 and a relative silica deficiency is introduced in the norm calculations.

CONCLUSIONS

The comparison of petrological aspects of the 1.77 Ga $\pm$0.19 Ga old Jomasknutene gabbro with the 1.11 Ga $\pm$0.14 Ga old Dale gabbro has revealed to some striking similarities and some less striking differences. Table 2.7.1 and 2.7.2 summarizes the main similarities and differences between the Gothian Jomasknutene and Sveconorwegian Dale gabbro.

The magmatic and metamorphic similarities of the Jomasknutene and Dale gabbro makes it difficult to distinguish uniquely between the Gothian and Sveconorwegian period. The following conclusions are drawn:

1) The magmatic history of the Gothian Jomasknutene gabbro must have been more complex than the Sveconorwegian Dale gabbro although the parental magma seems to be similar.
2) The metamorphism accompanying the Gothian and the Sveconorwegian period was not that all encompassing that it altered the entire magmatic mineralogy and texture of the gabbros. Mass transfer during either metamorphic events must have been limited to millimetre scale.
3) Both gabbros exhibit evidence of metamorphism characterized by a relative low partial water pressure.
4) The metamorphic conditions which altered the Jomasknutene gabbro is similar to the Dale gabbro but the intensity differs. This indicates that either:

4[a]) The Gothian metamorphism is similar to the Sveconorwegian one or

4[b]) The Sveconorwegian metamorphism overprinted the Gothian metamorphic features with a variable intensity from place to place.

Table 2.7.1 *MAIN SIMILARITIES BETWEEN THE JOMASKNUTENE AND DALE GABBRO*

Large parts of the gabbros show minor alteration of the primary magmatic minerals
Similar in whole rock chemistry
Similar magmatic and metamorphic mineralogy

Table 2.7.2 *DIFFERENCES BETWEEN THE JOMASKNUTENE AND DALE GABBRO*

JOMASKNUTENE GABBRO	DALE GABBRO
1.77 $\pm$0.19 Ga old (de Haas 1992)	1.1 $\pm$0.14 Ga old (de Haas 1992)
Large gabbro $\sim$7.6 km^2	Small gabbro $\sim$0.3 km^2
Country rock comprising quartzite and albite actinolite gneiss	Country rock comprising granite and migmatite
No back veining is observed	Back veining is present
Major deformation structures are present	No major deformation structures are present
Sheet-like intrusion with a complex magmatic structure	Concentric intrusion with a simple magmatic structure
Nepheline normative	Hypersthene normative
Locally major alteration of the primary magmatic minerals	Minor alteration of the primary magmatic minerals

CHAPTER III
OLIVINE CORONA; A WINDOW TO THE SUBSOLIDUS HISTORY OF THE GABBRO

3.1 INTRODUCTION

In the previous chapter I have presented my results of the comparative study of the Jomasknutene- and Dale gabbro. I discussed their field relations, magmatic- and metamorphic mineralogy, P-T evolution and whole rock chemistry. The gabbros passed the subsolidus regime during cooling from the magmatic to the metamorphic regime. Relics generated in the subsolidus regime of the gabbros provide a window through which we can investigate the prevailing cooling conditions of the gabbroic magmas in the central part of the Bamble area during Gothian as well as Sveconorwegian times. In this chapter I shall look through this window using olivine coronas, a subsolidus spherical shell texture around olivine. I shall discuss the chemical and physical conditions during which these olivine coronas may have formed.

3.2 CONTROVERSIAL THOUGHTS CONCERNING OLIVINE CORONAS

An olivine corona is, in general, a multi layered shell texture around olivine which separates olivine from plagioclase. It is a common texture in most olivine bearing gabbroic rocks. This shell texture, initiated at the olivine plagioclase contact, grows at the expense of olivine and plagioclase. One might ask if these textures have a magmatic, subsolidus or metamorphic origin.

Olivine coronas from the south norwegian gabbro intrusions are well known since the work of Brøgger (1934). Frodesen (1968) and Starmer (1969) have demonstrated that the olivine corona textures from the Bamble area reflect regional metamorphic conditions. Others such as Grieve and Gittins (1975) and Monkoltip and Ashworth (1983) propose a general subsolidus origin for olivine coronas, whereas Joesten (1986) suggested a magmatic origin. Besides this "chronological" discussion, there are differences of opinion concerning the exact nature of the chemical system in which the reaction between olivine and plagioclase takes place. The principal argument circles around the question if a corona system formed under chemically open or closed conditions.

Attempts to apply the isochemical steady state model of Joesten (1977) to olivine corona textures has not been particular successful (Nishiyama, 1983 and Grant, 1988). As it seemed difficult to apply Joestens' model to the olivine corona reaction (Johnson and Carlson 1990) the notion arose that the reaction is non isochemical. Non isochemical behaviour, accompanied by isovolume replacement was suggested by Lamoen (1979). Other workers such as England (1974) and Joesten (1977) concluded that a near isochemical reaction equation between olivine and plagioclase can be obtained. This work will demonstrate that the olivine corona reaction may indeed occur isochemical except for water (see formula 3.2.2).

Literature study indicates that olivine coronas always have an orthopyroxene inner rim. The minerals of the outer rim seem to depend on the regional metamorphic conditions. Typical minerals found in the outer rim are generally:

1) Clinopyroxene, orthopyroxene and spinel $\pm$garnet occurring in terrains with eclogite- and granulite facies conditions (Griffin, 1971). The characteristic reaction producing these minerals is:

Olivine + Plagioclase → Orthopyroxene + Clinopyroxene + Spinel **(3.2.1)**

2) Amphibole ±spinel occurring in terrains with medium amphibolite to hornblende granulite facies conditions (Frodesen 1968). The characteristic reaction producing these minerals is:

Olivine + Plagioclase + Water → Orthopxoxene + Amphibole + Spinel **(3.2.2)**

3.3 PETROGRAPHY OF THE OLIVINE CORONAS

Although controversies on the nature of the olivine corona exist, these shell textures are important sources of information of the geological history of the rocks. For this reason I investigated the corona textures of the Jomasknutene and Dale gabbro. However, in the study of olivine coronas from the Jomasknutene gabbro I encountered to the following limitations:

1) Corona textures in which olivine is still present are rare. Olivine is usually replaced by orthopyroxene ±magnetite. Only four out of sixty five samples show the presence of olivine coronas.
2) The corona textures are small, up to 0.5 cm, and very irregular shaped.

These limitations forced me to study the corona textures from a third gabbro, the Messel gabbro, (Brickwood and Craig 1987). This gabbro exhibits large, up to 1.5 cm in diameter, well developed olivine corona textures similar to those from the Jomasknutene gabbro. Although the similarities between the olivine corona texture from the Messel and Jomasknutene gabbro are striking it remains debatable whether the conclusions drawn from the Messel corona texture are also valid for the Gothian Jomasknutene corona texture. Using the olivine coronas from the Messel and Dale gabbro as model material allows the check upon the validity of chemical and physical models for the corona reaction which I shall discuss below.

MESSEL OLIVINE CORONA

The Messel gabbro, designated in figure 1.3, is a coarse grained gabbro about 10 km south-east of the Dale gabbro. Its geologic description has been given by Brickwood and Craig (1987). This coronitic gabbro contains huge olivine coronas about 1.5 cm in diameter. The corona texture consists of an olivine core, orthopyroxene inner rim and an amphibole spinel outer rim similar to the olivine coronas from the Jomasknutene gabbro. A representative example of a Messel olivine corona is illustrated in figure 3.3.1.

Orthopyroxene grows from the olivine plagioclase contact inward resulting in concave shaped olivine. The orthopyroxene inner rim exhibits a typical columnar or low angle boundary texture from now on designated with l.a.b.. L.a.b. orthopyroxene crystals are elongated, show strong undulatory extinction and vague lamellae. The l.a.b. crystals are radially arranged around the olivine relict. The crystallographic orientation of the crystals make a small angle with each other. A l.a.b. texture is typical for the investigated olivine coronas. Even if olivine has been replaced completely, the l.a.b. texture indicates that olivine had been present.

The outer rim grew outwards replacing mainly plagioclase. It consists of amphibole, either in a polygonal or l.a.b. fabric, intergrown with worm like green spinel. Occasionally amphibole and spinel crystals are arranged in a convex pattern. On the contact with the inner orthopyroxene rim and the outer amphibole rim, a spinel free amphibole zone of a few hundred microns is usually present. Centimeter large plagioclase crystals surround the corona texture. These crystals include minute green spinel inclusions which is responsible for its cloudy character. Especially in the vicinity of olivine corona

texture, the cloudiness of the plagioclase is accentuated.

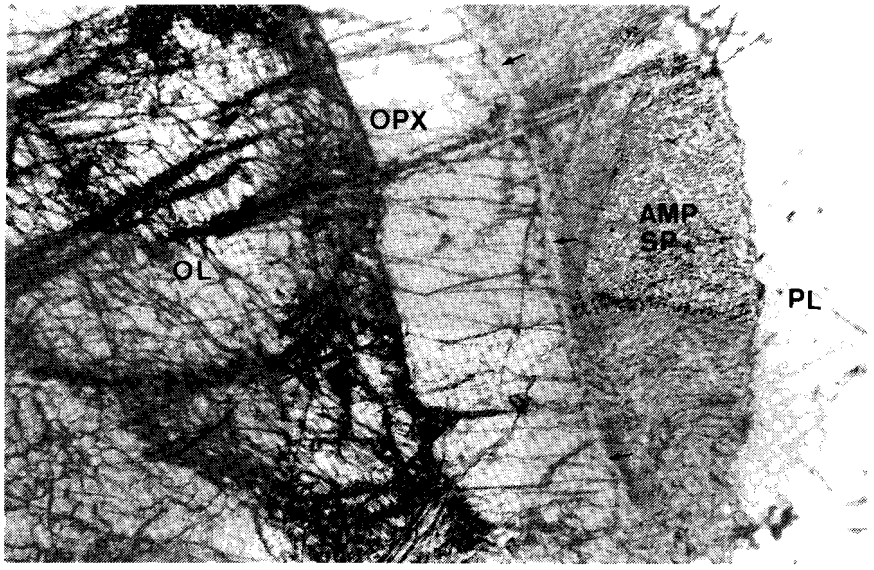

Figure 3.3.1

Olivine corona texture from the Messel gabbro. It consist of an olivine core (OL), an l.a.b. orthopyroxene inner rim (OPX) and an amphibole spinel outer rim (AMP-SP). The olivine corona is surrounded by plagioclase (PL). The small arrows mark a spinel free amphibole zone between orthopyroxene and the amphibole spinel symplectite.

DALE OLIVINE CORONA

Olivine coronas of the Dale gabbro consist of an olivine core, an orthopyroxene inner rim, an amphibole outer rim occasionally replaced by clinopyroxene, orthopyroxene and spinel and plagioclase surrounding it. A representative example of an olivine corona from the Dale gabbro is illustrated in figure 3.3.2. The habitus of olivine and the l.a.b. orthopyroxene inner rim are similar to those in the Messel corona. The outer shell texture is however different. This outer rim grew mainly outwards, away from the original olivine plagioclase contact and consists of amphibole locally replaced by clinopyroxene, orthopyroxene and spinel. The relative time relation between the formation of amphibole on the one hand and the clinopyroxene $\pm$orthopyroxene $\pm$spinel symplectite on the other is often clear; the latter appears to be younger. This dehydration in which amphibole is replaced by an anhydrous mineral assemblage occurred most likely during Sveconorwegian times. I suggest that this dehydration is similar to the one Nijland (1993) found in migmatic rocks around the Ubergsmoen Augen Gneiss. Whether this has any relation with the low partial water pressure discussed in chapter 2.4 is not clear.

Plagioclase crystals are considerably smaller than those found in the Messel gabbro but exhibit the same cloudiness due to minute green spinel inclusions.

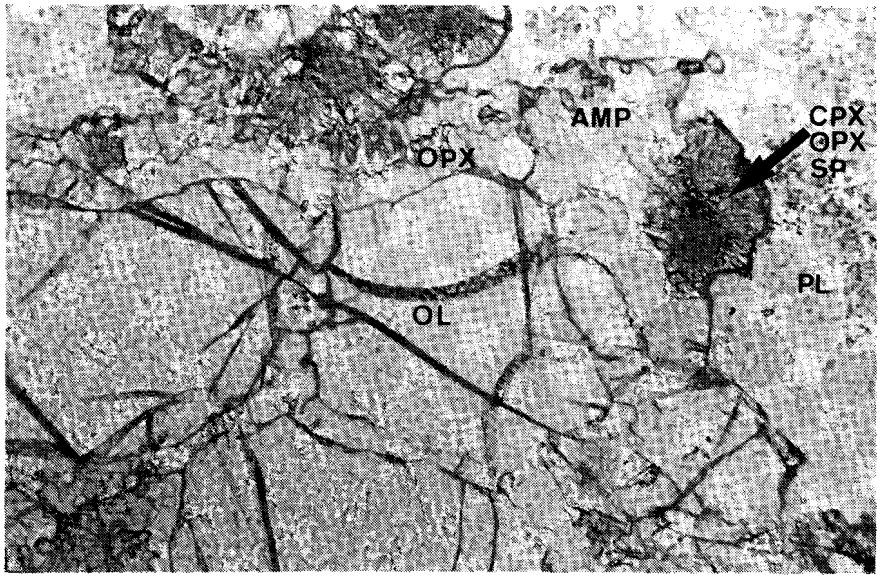

Figure 3.3.2

Olivine corona texture from the Dale gabbro. It consists of an olivine core (OL), an l.a.b. orthopyroxene inner rim (OPX) and an amphibole outer rim (AMP). The olivine corona is surrounded by plagioclase (PL). The amphibole outer rim is partly dehydrated to an orthopyroxene clinopyroxene spinel intergrowth (CPX-OPX-SP). This intergrowth is marked with an arrow.

3.4 ESTIMATED TEMPERATURES CONDITIONS FOR OLIVINE CORONAS

It seems likely from the petrographical description that the orthopyroxene inner rim and amphibole outer rim formed simultaneously due to the reaction between olivine and plagioclase with the addition of water. This reaction has been discussed in chapter 3.2 as being a hydrous-type olivine corona. Thus it is reasonable to assume that these minerals were in equilibrium with one another during their formation. In that case, the iron/magnesium ratio of coexisting amphibole and orthopyroxene can be used to estimate the forming condition of the olivine corona according to the method of Perchuck et al. (1985). Orthopyroxene and amphibole analyses obtained from one corona texture from the Messel gabbro, one from the Jomasknutene gabbro and three from the Dale gabbro all indicate forming conditions of the corona texture around 825°C $\pm$50°C. Such high metamorphic temperatures have not been found in this part of the Bamble area. Therefore the formation of olivine coronas in the central part of the Bamble area are considered to be a subsolidus phenomena.

I mentioned dehydration textures of the outer amphibole rim of the olivine corona in the Dale gabbro. During dehydration of amphibole orthopyroxene, clinopyroxene and spinel is formed. As the chemistry of coexisting orthopyroxene and clinopyroxene is temperature dependent according to Wood and Banno (1973) and Wells (1979), I calculated the temperature at which dehydration took place. The mean temperature lies between 848°C $\pm$18° (Wood and Banno, 1973) and 836°C $\pm$38° (Wells, 1979). These dehydration temperatures are in the same order as those estimated for the olivine corona formation. Therefore I suggest that the dehydration took place in the subsolidus stage of the cooling Dale gabbro. The water activity must have been substantial lowered just after the corona formation.

The dehydration texture, as found in the olivine corona from the Dale gabbro, is most likely a Sveconorwegian phenomenon. The corona formation and the dehydration reaction took place at a similar temperature; the dehydration reaction was accompanied by a substantial lower water activity. This

observation is in agreement with the lowering of the P_{H2O} in the central part of the Bamble area during Sveconorwegian times as mentioned by Nijland (1993). In that case the subsolidus stage of the Dale gabbro coincides with the peak metamorphic conditions of the Sveconorwegian period in the central part of the Bamble area. Olivine coronas from the Messel gabbro and the Jomasknutene gabbro do not show these dehydration textures. Apparently, the dehydration of the amphibole outer rim is a local phenomena in the central part of the Bamble area.

3.5 OLIVINE CORONA MODELS

Now that the timing of the corona growth has been established to be subsolidus, the question of the chemical character of the olivine plagioclase reaction remains. Is the olivine corona reaction, with the exception of water, isochemical or not ? It seems likely that mineral reactions in the investigated gabbros are (close to) isochemical reactions because metamorphism was not that encompassing that it caused major mass transfer in the investigated rocks (chapter 2.5). To verify the possible isochemical character of the olivine corona reaction I considered two extreme models ignoring the role of water:

1) An isochemical one
2) An equal volume replacement one

The isochemical model assumes that the sum of the chemical components remained constant during the reaction and thus, that no or only limited mass transfer occurred out of the chemical corona system. As the densities of the reactants and products are different, the volume of the system must change. The equal volume replacement model assumes no volume change during the reaction. Consequently mass transfer must occur.

Calculations of the two models for olivine coronas from the Messel and Dale gabbro are worked out in appendix B and illustrated in figure 3.5.1. The conclusions from these calculations are summarized in table 3.5.1. An isochemical model is in all likelihood valid for the olivine coronas from the Messel gabbro. An isochemical model for the olivine coronas from the Dale gabbro does not fit equally well. There are two consequences, which are elaborated in appendix B, of the isochemical model:

1) The original olivine plagioclase boundary has to lie in the present amphibole outer rim.
2) A volume decrease has to have occurred during the reaction.

The first consequence can be verified in the spinel free amphibole zone (designated by a small arrow in figure 3.3.1) which occurs as a discontinuous shell around the orthopyroxene inner rim. For the olivine corona from the Dale gabbro, the shell is relatively large and coincides with the spinel free amphibole outer rim as mentioned in chapter 3.3. For the olivine corona from the Messel gabbro the calculated zone is only a few hundred microns thick and coincides with the observations discussed in chapter 3.3 as well.

To verify the second consequence, the one of volume decrease, I investigated the olivine corona with the TEM technique. A volume change in an isochemical system may result in stresses due to contraction or relaxation in the various minerals which can easily be detected by the TEM-technique. The results of this study are discussed below.

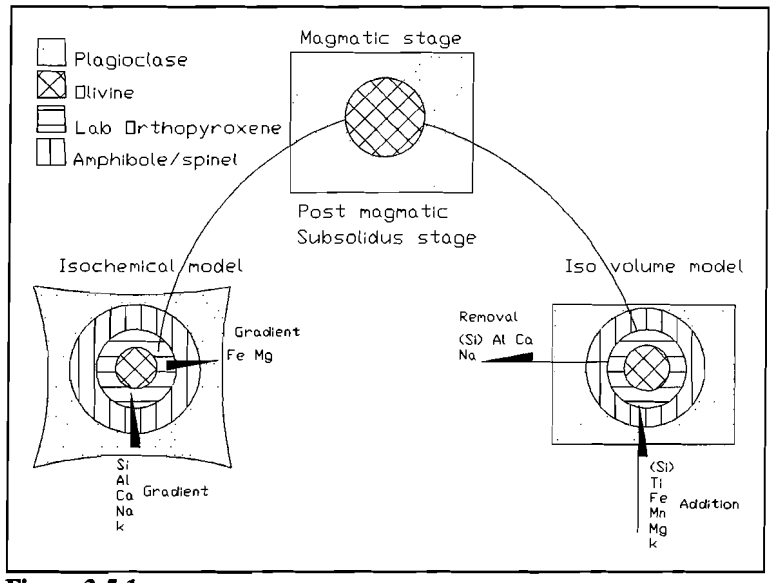

Figure 3.5.1

An illustration of the two models concerning the olivine corona growth. The bent boundaries of the isochemical model illustrate the volume reduction. The arrows illustrate a chemical gradients which caused the element redistribution. The arrows in the isovolume model illustrates the addition or removal of elements to or from the system.

Table 3.5.1 *OLIVINE CORONA MODELS*

Summary of the results of model calculations as presented in appendix B.

	Messel olivine corona	Dale olivine corona
Isochemical model	SSQR = 1.4	SSQR = 4.1
	ΔV = -7%	ΔV = -16%
	Original olivine - plagioclase boundary lies 0.3 mm in the outer amphibole rim (amphibole radius = 1.9 mm).	Original olivine - plagioclase boundary lies 1.6 mm in the outer amphibole rim (amphibole radius = 2 mm).
Isovolume replacement model	9% mass increase	14% mass increase
	All elements are mobile	All elements are mobile

SSQR = Sum of SQuare of Residuals; a measure for isochemistry.

ΔV = relative volume change before and after the reaction.

3.6 CLINOENSTATITE LAMELLAE IN L.A.B ORTHOPYROXENE FROM THE MESSEL OLIVINE CORONA

In the petrographical description of the olivine corona (3.3) I mentioned the existence of lamellae and the undulated extinction of the orthopyroxene inner rim. These textures may have formed due to stress adaption in orthopyroxene crystals. A TEM-study of these textures resulted in the following observations.

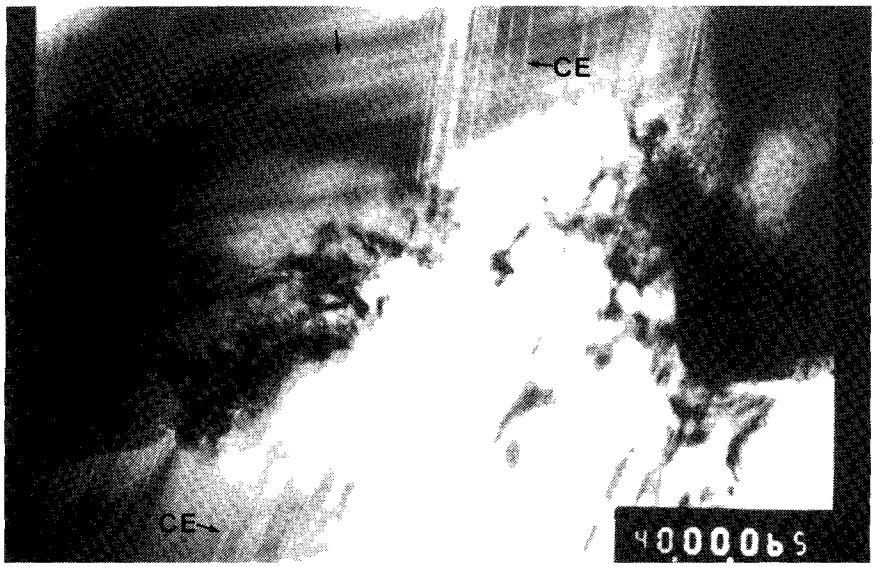

Figure 3.6.1

TEM photograph of two orthopyroxene crystals (OE) making a small angle contact with one another (large arrows). There is no unique crystallographic relation between the two crystals. The clinoenstatite lamellae (CE) as well as the braided exsolution texture (small arrows) are clearly visible and make a large angle with each other.

A lamellar texture (CE) parallel to the $(100)_{opx}$ plane has been found in the l.a.b. orthopyroxene (OE) outer rim and are illustrated in figure 3.6.1. The thickness of the individual lamellae is about 0.1 μm, too small for chemical analysis. These lamellae are mainly concentrated in zones of about 0.5 to 1 μm wide in which the individual lamellae can still be distinguished. The interface between lamellae and host orthopyroxene is straight and always coherent. Diffraction patterns of the lamellar zones show additional faint spots between the transmitted $(000)_{opx}$ and diffracted beam $(200)_{opx}$ and streaking spots in the (100) direction. The additional diffraction spots are indicative of intergrowth of pyroxene polymorphs as reported by Buseck et al. (1980). Similar textures were interpreted as clinoenstatite (CE) inversion lamellae from an orthoenstatite (OE) host by Boland (1974), Coe & Kirby (1975) and McLaren & Etheridge (1976). The transition from an orthoenstatite of presumably high temperature to clinoenstatite of presumably low temperature is still open to debate. Grover (1972) stated that this transition occurs at about 600°C and is pressure dependent. Rapidly cooled high temperature orthopyroxene have been investigated with TEM by Carlson et al. (1988). They found regions in an orthopyroxene host consisting of isochemical clinoenstatite lamellae. These lamellae are supposed to originate from shearing during anisotropic contraction of the cooling orthoenstatite. If clinoenstatite lamellae are the result of anisotropic

contraction the density of clinoenstatite should be higher that of orthoenstatite. The density of orthoenstatite is 3.198 gr/cm^{-3}; the density of clinoenstatite is 3.190 gr/cm^{-3} (Robie and Bethke 1966). Unfortunately, these densities do not support the volume decrease. On the other hand, the total volume of the olivine corona minerals is smaller than the original magmatic assemblage. Thus after the corona growth there is a volume surplus in the system which could initiate minerals with a lower density, e.g. clinoenstatite lamellae in the orthopyroxene host.

Another texture which is observed, illustrated in figure 3.6.1 as well, is a braided lamellar texture, irregular shaped and short in wave length. This braided texture is interpreted as an exsolution texture formed during a period of relatively fast cooling of orthopyroxene. The exact nature of these exsolution lamellae is not clear.

3.7 LOW ANGLE BOUNDARIES IN THE ORTHOPYROXENE INNER RIM

In the petrographic description of olivine coronas in chapter 3.3 I mentioned the typical columnar or low angle boundary texture (l.a.b.) occurring in the orthopyroxene inner rim and occasionally in the amphibole outer rim. These textures are important because they are often the only evidence that olivine has been present in gabbroic rocks. In this paragraph I would like to present a possible mechanism for the formation of these typical textures, analogous to the crystallization experiment described by Ashby and Jones (1988). These authors made a saturated ammonium chloride solution of 50°C, heated up to 75°C and poured in a cold vessel. As the solution touches the cold vessel wall it cools fast and becomes supersaturated. Initially, tiny chill crystals are formed on the wall of the vessel with a random crystallographic orientation. The chill crystals act as a stratum on which dendritic crystals start to grow with similar crystallographic orientations as the tiny chill crystals. The liquid between the dendrites solidifies resulting in complete solid, columnar grain texture.

In analogy with this experiment but concerning different phases, I made a hypothesis which describes the formation of the typical l.a.b. texture in the olivine corona. Contacting magmatic olivine and plagioclase are initially stable at elevated P-T conditions. Upon cooling the olivine plagioclase contact becomes metastable. After triggering this metastable situation, initially tiny "chill" crystals are formed on the olivine plagioclase contact with a random crystallographic orientation. Orthopyroxene crystals grow relatively fast, using the crystallographic orientation of the tiny "chilled" crystals, towards the core of the olivine corona texture and amphibole grew outwards. Orthopyroxene and amphibole crystals kept their crystallographic orientation during their growth which resulted in a columnar, l.a.b., texture. The adjacent crystals have no crystallographic relation to each other.

If this hypothesis is correct, I should be able to observe the following features in the olivine corona:

1) There should be no crystallographic relation between orthopyroxene and olivine.
2) There should be no crystallographic relation between adjacent columnar orthopyroxene crystals.
3) There should be evidence for fast cooling in orthopyroxene (adaption after metastability).
4) Similar considerations counting for orthopyroxene should also count for the amphibole outer rim.

To find evidence for these features I carried out a TEM study on all minerals in the olivine corona from the Messel gabbro. This study resulted in the following conclusions:

1) Olivine orthopyroxene contacts are always sharp and there is no unique crystallographic relation between olivine and orthopyroxene.
2) Orthopyroxene crystals do not share main crystallographic orientations. An example of orthopyroxene crystals contacting each other is shown in figure 3.6.1.
3) Most orthopyroxene crystals from the l.a.b. inner rim of the olivine corona exhibit a braided lamellar texture as shown in figure 3.6.1. The texture is irregular and has a short wavelength. This braided texture is interpreted as an exsolution texture in orthopyroxene. The small size of the exsolution lamellae and short wavelength indicates a rapid adaption of orthopyroxene to its physical and chemical environment (Nord and McCallister 1979).
4) Evidences for this corona growth mechanism similar to those found in orthopyroxene have not been observed in the outer amphibole rim. Amphibole is nearly dislocation free and no exsolution textures have been observed.

The first three conclusions endorse the suggested hypothesis for the formation of the l.a.b. texture in the olivine corona. The olivine corona texture could have grown from triggered metastability. Relatively fast growth rates of the corona texture suggest that only a relatively short time existed for elemental diffusion. This enhances the isochemical model of olivine coronas as discussed above.

3.8 CONCLUSIONS

The principal conclusions of this olivine corona study are:

1) The olivine coronas from both the Jomasknutene and the Messel gabbro are similar and consist of the following mineral sequence from core to rim:

   Olivine | Orthopyroxene | Amphibole + Spinel | Plagioclase ±Spinel

   The olivine coronas from the Dale gabbro are different consisting of the following minerals from core to rim:

   Olivine | Orthopyroxene | Amphibole (±Opx ±Cpx ±Spinel) | Plagioclase ±Spinel
2) The olivine plagioclase reaction forming the corona texture in the Messel gabbro can be most properly described by an isochemical reaction with the exception of water. The olivine plagioclase reaction forming the corona texture in the Dale gabbro is not equally well isochemical. Both the Gothian and Sveconorwegian metamorphic periods were not that encompassing that large mass transfer occurred in the investigated gabbros.
3) Temperature conditions of the olivine corona formation in both the Messel- and in the Dale gabbro range between 775°C and 875°C. The outer amphibole rim in the Dale gabbro shows in addition evidence of dehydration which I estimate to have occurred around 850°C. The metamorphism during the Sveconorwegian period is characterized by a substantial lowering of the water pressure at a nearly constant (subsolidus) temperature.

CHAPTER IV
METAMORPHIC FLUID COMPOSITION INFERRED FROM THE AMPHIBOLITIZATION PROCESS

4.1 INTRODUCTION

It is commonly held that fluids accompany magmatic- and metamorphic activities in the crust. These fluids are thought to contain various elements and chemical complexes. The composition of such fluid phase constraints on the chemistry of the magmatic or metamorphic minerals which are formed in their presence. In fact, the composition of these minerals mirrors the fluid composition. To investigate and distinguish between the nature of the fluids operational during the Gothian and Sveconorwegian metamorphic period, I used two approaches:

1) an investigation of the metamorphic minerals such as amphibole and, to a lesser extent, biotite from the Gothian Jomasknutene and Sveconorwegian Dale gabbro. These two minerals are able to incorporate halogens and halogen like complexes such as hydroxyl, chlorine and fluorine which are thought to be present in fluid phases accompanying magmatic and metamorphic processes. I focused on amphibole because it occurs in nearly all samples from both gabbros.
2) an investigation of fluid inclusions formed during the formation of the amphibole-quartz symplectite in the Jomasknutene gabbro.

I shall demonstrate in this chapter that the metamorphic fluid penetrating the Jomasknutene gabbro after solidification was poor in fluorine, rich in chlorine and consequently acidic. This acidity de-aluminized amphibole from rim samples. Silica and alkalis in amphibole were modified as well.

Apart from this aqueous brine-like fluid considerable amounts of CO_2 and N_2 were detected and are thought to be coexistent with the brine-like fluid. This suggests that the water pressure at the time of amphibolitization must have been substantial lower, $P_{H2O} \sim 1$ kbar, than the estimated metamorphic pressure which measures about 7 kbar. The metamorphic fluid penetrating the Dale gabbro tend to resemble, qua chlorine content, the metamorphic fluid which penetrated the outer margin of the Jomasknutene gabbro.

4.2 THEORETICAL CONSIDERATION

The composition of magmatic and metamorphic fluids can be investigated indirectly via minerals such as amphibole and biotite which are able to exchange elements with such fluids or directly via fluid inclusions. The latter will be discussed in detail in chapter 4.7; the former will be discussed below.

It is commonly held that amongst others, halogens, alkalis and hydroxyl are present in variable amounts in magmatic and metamorphic fluids. The exchange of these elements between liquid and minerals is determined by the pressure and temperature dependent equilibrium coefficient K (formula 4.2.2). The minerals I shall focus on are amphibole and biotite. The equilibrium coefficient for amphibole or biotite and a fluid depends mainly on five variables:

1) The temperature at which the exchange reaction takes place. Volfinger et al. (1985) suggest that a decreasing temperature facilitates chlorine incorporation in amphibole, in analogy to biotite.
2) The iron content of amphibole and biotite. An increase in iron content facilitates the incorporation of chlorine and alkalis in amphibole and biotite (Volfinger et al. 1985).

3) The concentration of the elements present in the fluid.
4) The fluid/rock ratio.
5) The acidity of the fluid.

I shall first discuss the parameters which influence the chlorine and alkali content in amphibole and biotite. Thereafter, I shall apply this knowledge to amphibole from the Jomasknutene- and Dale gabbro with as goal to constrain the character of the metamorphic fluids affecting the mineralogy of the Jomasknutene- and Dale gabbro.

The exchange of elements between a fluid (^{aq}) and a solid phase, such as amphibole, is characterized by an equilibrium coefficient K. Focusing on Cl and the OH complex the following equilibrium equation can be written:

$$OH^{amphibole} + Cl^{aq} \rightleftharpoons OH^{aq} + CL^{amphibole} \quad \textbf{(4.2.1)}$$

which has an equilibrium coefficient K defined as:

$$K = \frac{[Cl^{amphibole} \times OH^{aq}]}{[Cl^{aq} \times OH^{amphibole}]} \quad \textbf{(4.2.2)}$$

This chemical equilibrium coefficient concerning OH and Cl is thought to be temperature dependent and equilibrium conditions move to the right with decreasing temperature according to Volfinger et al. (1985). These authors also suggest that iron affects the internal structure of amphibole such that the relatively large chlorine ion is able to be incorporated in the amphibole structure at the expense of a hydroxyl ion at high iron contents. There is however another factor which may influence this equilibrium coefficient. Seyfried et al. (1986) have suggested a mechanism for the removal of chlorine from a hydrothermal fluid with increasing temperature based on an experimental study of basalt-fluid interaction. The results of this study, summarized below, are applied to conditions around 400°C and 400 bar but may very well be applicable to more elevated metamorphic conditions. The principal results of the experiments carried out by Seyfried and co-workers are:

1) Chlorine, originating from a fluid, in the presence of olivine or other iron magnesium rich phases, such as amphibole, is progressively incorporated in a solid Fe/Mg hydroxyl chloride phase as the temperature increases from 400° to 425°. They suggest the following reaction:

$$3Cl^- + H_2O + Fe^{2+} + Mg^{2+} \rightleftharpoons FeMgOHCl_3^{solid} + H^+ \quad \textbf{(4.2.3)}$$

This reaction equation indicates that with the shift of the equilibrium towards the right the remaining fluid becomes relatively poor in chlorine and thus less chlorine is available to be incorporated in a solid phase such as amphibole. This is in agreement with the theory of Volfinger et al. (1985) but explained via another mechanism. As hydroxyl is removed from the fluid as well, the remaining fluid becomes more acidic. In the light of the amphibole chemistry a low pH favours for the solubility of the amphotheric element Al instead of Si resulting in a de-aluminization.

2) The solid Fe-Mg hydroxyl chloride complex dissolves progressively with decreasing temperature. The equilibrium condition (formula 4.2.3) shifts towards the left and the fluid becomes relatively chlorine rich again.

3) A Na-K-Ca-Cl fluid in the presence of plagioclase and olivine, fixes Na over Ca at 425°C resulting in an albitization of plagioclase. Ca is preferentially incorporated relative to Na in solid phases at 400°C.

4.3 ORIGIN OF AMPHIBOLE FROM THE JOMASKNUTENE AND DALE GABBRO

Amphibole from the Jomasknutene and Dale gabbro is generally formed either from primary magmatic minerals or from other metamorphic minerals as discussed in chapter 2.3. It is the main metamorphic mineral in the Jomasknutene gabbro which, together with scapolite and biotite, is able to exchange chlorine with a fluid. The origin and timing of amphibole put constraints on the timing of the chlorine influx.

There are four possible origins for amphibole:

1) A metamorphic one
2) A metasomatic one
3) A subsolidus one
4) A primary magmatic one

Most amphibole from the Jomasknutene gabbro is definitely a metamorphic mineral as discussed in chapter 2.3. This statement is based on the common observation that amphibole overgrows other metamorphic minerals such as biotite, amphibole and occasionally garnet. Amphibole is often polygonized especially in strongly amphibolitized gabbros. Some amphibole is formed during metasomatism or affected by it. I have inferred this from the comparison between chemical amphibole analyses from the core and rim samples and will be discussed below. Amphibole associated with olivine coronas may well be a subsolidus product. However, occasionally coronitic amphibole seems to overgrow metamorphic garnet, indicating that at least some of the corona related amphibole has a metamorphic origin. Finely it is unlikely that amphibole has a primary magmatic origin because there is no evidence for the occurrence of amphibole as a primary magmatic cumulus or intercumulus phase; nor has an increase of amphibole with fractionation been observed as asserted in chapter II.

Thus most amphibole tends to be a metamorphic mineral with or without a metasomatic signature. Therefore the origin or redistribution of chlorine in amphibole is also a metamorphic or metasomatic process.

4.4 THE AMPHIBOLE CHEMISTRY

Before discussing the chemistry of amphibole from the Jomasknutene and Dale gabbro I shall discuss its general structure and chemistry first.

The standard amphibole formula may be written as:

$A_{0-1}B_2C_5T_8O_{22}(OH,F,CL)_2$

A = Na^+,K^+

B = Na,Li,Ca,Mn,Fe,Mg

C = Mg,Fe^{2+},Mn,Al,Fe^{3+},Ti

T = Si,Al

Elements in the amphibole structure are limited to some specific sites each with their own occupancy. From the amphibole formula it is easy to calculate the maximum weight percentages OH^-, Cl^- and F^- which can theoretically be incorporated in amphibole. Amphibole with the structural formula:

$Na_{0.5}K_{0.5}Ca_2Fe_2Mg_2AlSi_6Al_2O_{22}(OH,Cl,F)_2$

can incorporate a maximum of 3.7 Wt% OH or 7.4 Wt% Cl or 4.1 Wt% F. Typical chlorine values which are found in nature are listed in table 4.4.1. In addition, similar calculations can be made for biotite. Biotite with the structural formula:

$K_2Fe_3Mg_3Si_6Al_2O_{20}(OH,Cl,F)_4$

can incorporate a maximum of 7.1 Wt% OH or 13.7 Wt% CL or 7.8 Wt% F. From these values it seems reasonable to assume that biotite is able to incorporate more halogens or halogen like elements than amphibole.

Table 4.4.1 *CHLORINE CONTENT IN NATURAL AMPHIBOLE*

Some literature values of chlorine in natural amphibole from various geological settings to compare it with values from amphibole in the Jomasknutene gabbro. Amphibole from literature is characterized by a high iron content; usually ferric iron.

Reference	Geological setting	Max. Wt% Chlorine
Krutov (1936)	Skarn	7.24
Jacobson (1975)	Ultramafic intrusion	6.51
Schiffries and Skinner (1987)	Bushveld: hydrothermal	5.00
Karmineni et al. (1982)	Granulite	4.18
Vanko (1986)	Basic rock under greenschist facies metamorphism	4.0
Shuma et al. (1987)	Calcareous pegmatite	3.27
Dick and Robins (1979)	Skarn	3.09
Geijer (1959)	Skarn	1.42
This work	Metagabbro	1.95

AMPHIBOLE FROM THE JOMASKNUTENE GABBRO

I investigated amphibole from eight gabbro samples and one country rock sample. Two gabbro samples are located close to the gabbro country rock contact viz. Ga315 and Ga342 and are designated rim samples; the other gabbro samples (Ga153, Ga159, Ga336, Ga357, Ga358 and Ga364) are located more towards the centre of the gabbro and are designated core samples. Figure 4.4.1 presents the appropriate locations of the sample numbers in the Jomasknutene gabbro.

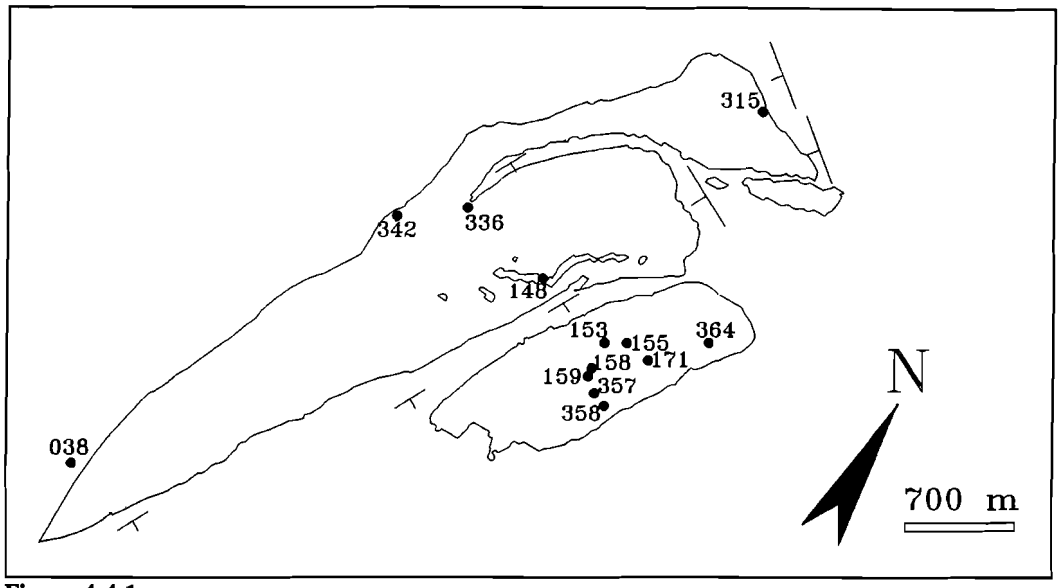

Figure 4.4.1

The sample map of the Jomasknutene gabbro. The numbers represent the samples from which amphibole analyses are obtained. For a detailed geological description of the Jomasknutene gabbro I refer to chapter II.

Mean chemical amphibole analyses from samples from the Jomasknutene gabbro are listed in table 4.4.2. Amphibole from the Jomasknutene, as well as from the Dale gabbro, is high in calcium (> 1.74 p.f.u), lower in B-sited sodium ($\sim Na+K-1 < 0.67$ p.f.u) and therefore belong to the group of calcic amphibole (Leake 1978). The chemical variability of amphibole within one sample depends, as mentioned in chapter 2.3, on the mineral from which it is derived. The Mg# of amphibole from the core samples ranges from 28 to 71; the silica content from 5.5 to 6.3 atoms per formula unit (p.f.u.). Amphibole from the core samples is usually relatively low in silica whereas amphibole from the outer margin has a higher silica content with a maximum of 7.3 atoms p.f.u.. These variations in silica content and Mg# are illustrated in figure 4.4.2. The sum of sodium and potassium atoms p.f.u. is close to one in amphibole sampled from the core of the gabbro whereas this sum decreases in amphibole from the rim of the gabbro. This variation is illustrated in figure 4.4.3. It indicates that the amphibole from the core of the gabbro has probably filled its complete A-site whereas amphibole from the rim samples has not. Amphibole from the rim samples is thus relatively depleted in alkalis.

Chemical composition of amphibole sampled from the outer margin of the Jomasknutene gabbro is compared to that of the core of the gabbro relatively poor in aluminium, rich in silica and consequently poor in alkali elements as predicated to charge balance requirements. The decrease of alkalis in amphibole from the rim samples continues in amphibole from the country rocks which surround the gabbro; this is best demonstrated in figure 4.4.3.

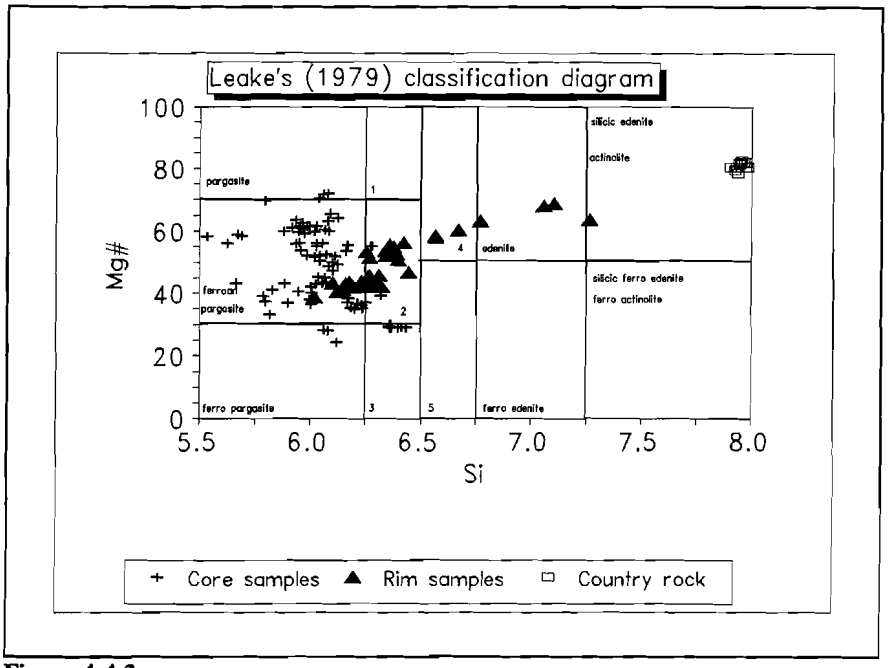

Figure 4.4.2

Amphibole analyses plotted in the classification diagram of Leake (1978). The sum of sodium and potassium is in general > 0.5 p.f.u., titanium is lower the 0.5 p.f.u. and the calcium content is higher than 1.74 p.f.u.. Thus amphibole from the Jomasknutene gabbro belong to the group of calcic amphibole. The core samples (n_{core}= 54) are ferro-pargasite whereas the rim samples (n_{rim}= 37) shows an increase in their silica content towards an edenitic- or actinolitic composition. The amphibole chemistry of the rim samples tend toward the amphibole composition from the country rock($n_{country\ rock}$= 12).

1= pargasitic hornblende, 2= ferroan pargasitic hornblende, 3= ferro pargasitic hornblende, 4= edenitic hornblende, 5= ferro edenitic hornblende.

The maximum chlorine content of amphibole from the Jomasknutene gabbro is 0.54 p.f.u.; the maximum fluorine content 0.15 p.f.u. The maximum occupation of chlorine on the monovalent anion site is about 25%; the maximum occupation of fluorine 8%. Thus more than 70% of the monovalent anion site in amphibole from the Jomasknutene is occupied by hydroxyl. The F to Cl molar ratio is in general smaller than 1. This indicates that the fluid, which equilibrated with amphibole from the core and rim samples, was chlorine rich relatively to fluorine especially because fluorine is preferential incorporated over chlorine in amphibole (Volfinger et al. 1985). The chlorine activity of the fluid, affecting the outer margin of the Jomasknutene gabbro, must have been slightly higher than that of the fluid affecting the core of the gabbro. This is inferred from figure 4.4.4 which shows a slight enrichment of chlorine in amphibole from the outer margin samples compared to the core samples. Due to the de-aluminization of amphibole from the rim samples, and consequently charge balance requirements, alkali elements were removed as well. To find out which alkali element is preferentially removed from amphibole during de-aluminization, I plotted potassium and sodium against their Mg#, in figure 4.4.5 and 4.4.6 respectively, and distinguished between core and rim samples. It appears that potassium is slightly depleted in rim samples compared to core samples. Sodium does not follow this trend entirely. Amphibole from rim samples exhibits a negative correlation between the Mg# and sodium content whereas amphibole from the core samples exhibit the opposite correlation. What is the reason for this paradoxical behaviour ?

First of all a negative correlation of sodium and potassium with an increasing Mg# is suggested by the theoretical consideration of Volfinger et al. (1985). Alkali elements are incorporated in the amphibole structure, mainly on the A-site. This site has its maximum occupancy at 1 alkali atom p.f.u.. If the total alkali supply is larger than 1 p.f.u., the residual has to be removed, for example to the B-site. In amphibole from the core samples an excess of alkali elements must have been present. The sum of sodium and potassium is equally or larger than 1. Potassium is then preferential incorporated on the A site of the amphibole structure to sodium. This has as consequence that potassium has a negative correlation with the Mg# in a alkali saturated environment whereas sodium has not.

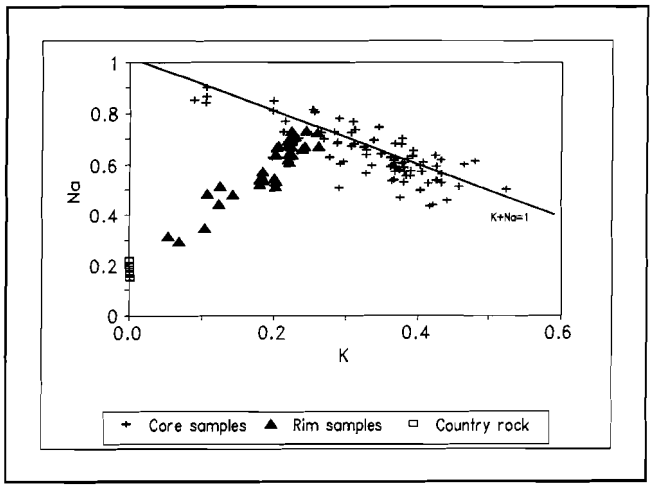

Figure 4.4.3

Alkali elements in amphibole from the Jomasknutene gabbro. The core samples lie close to the line Na+K=1 whereas the rim samples are in general lower in alkali elements and tend towards the alkali characteristics of amphibole from the country rock.

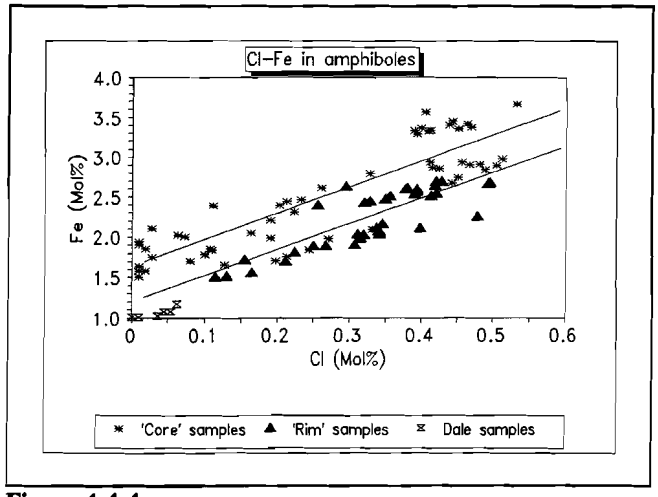

Figure 4.4.4

Amphibole plot of Cl versus Fe. The mean chlorine content of amphibole from the rim samples is slightly higher than the mean chlorine content of core samples at a similar iron content but the deviation from the mean values overlap. Amphibole analyses from the Dale gabbro are low in chlorine.

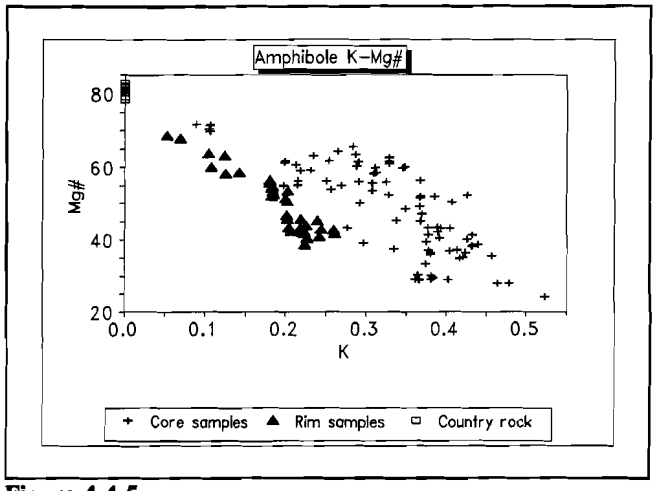

Figure 4.4.5

The potassium content of amphibole from the Jomasknutene gabbro. The rim samples (triangle) are slightly depleted in potassium compared to the core samples (cross).

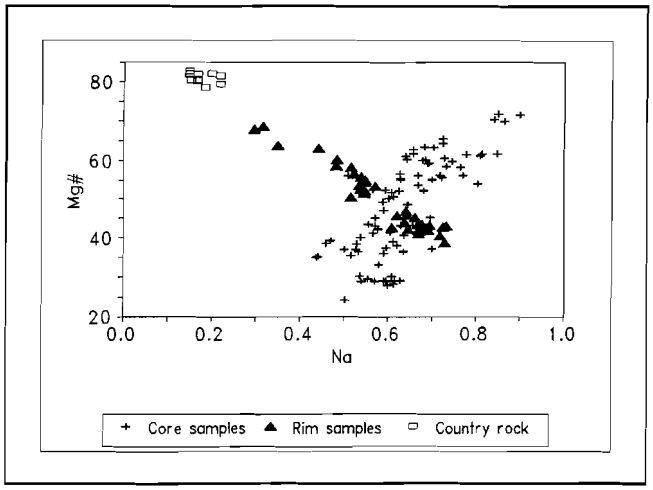

Figure 4.4.6

The sodium content of amphibole from the Jomasknutene gabbro. The rim samples show a negative correlation with the Mg#. The core samples show a positive correlation with the Mg# probably due to the limited ability of amphibole to incorporate alkalies on the A-site.

AMPHIBOLE FROM THE DALE GABBRO

Amphibole associated with olivine coronas from three samples of the Dale gabbro has been analyzed among others for their chlorine content. The sum of alkalies in amphibole from the Dale gabbro is usually close to one and thus resembles mostly those from the core of the Jomasknutene gabbro. The chlorine content is in general lower than 0.06 p.u.f. and the fluorine content usually negligible. Mean amphibole analyses from the Dale gabbro are listed in table 4.4.2 and plotted together with amphibole analyses from the Jomasknutene gabbro in figure 4.4.4. The small variation in iron content of the analyzed amphibole makes it difficult to draw valid conclusions about the precise nature of the fluid associated with the formation of amphibole in the Dale gabbro. The chlorine content in amphibole from the Dale gabbro is lower than those from the Jomasknutene gabbro. More amphibole analyses with a larger range in Mg# are needed to establish the true behaviour of chlorine in the Dale gabbro.

Table 4.4.2 *CHEMICAL ANALYSES OF AMPHIBOLE FROM THE JOMASKNUTENE GABBRO*

Mean amphibole analyses from the Jomasknutene and Dale gabbro. Most amphibole belong to the group of pargasite according to the nomenclature of Leake (1978). The oxide values are in weight percentages; the element values are the number of atoms based on a negative charge of 46 (Cl⁻ and F⁻ encountered). Samples Ga315 and Ga342 are from the rim of the complex; the other Ga- samples are from the core of the gabbro; the TK sample is obtained from the country rock. All iron is calculated as divalent iron. WT samples are obtained from the Dale gabbro. The Cl/Fe ratio is multiplied by 1000.

#	n=6	n=7	n=4	n=10	n=5	n=3	n=4	n=2	n=2	n=8	n=7	n=4
Sample	Ga153	Ga153	Ga159	Ga315	Ga315	Ga315	Ga336	Ga336	Ga336	Ga342	Ga342	Ga342
Origin	Ilm	Augite	Ilm	Augite	Poly	Augite	Ilm	Opx	Opx	Poly	Opx/Cpx	Poly
SiO_2	39.13	39.53	39.03	46.04	41.56	41.58	37.95	42.07	40.15	40.10	41.18	39.53
TiO_2	2.78	1.91	1.42	1.28	1.42	1.60	1.55	0.00	0.39	1.50	1.89	1.36
Al_2O_3	14.00	11.63	12.01	9.57	12.44	11.96	16.42	14.05	15.20	12.73	11.80	13.55
FeO	18.38	21.88	21.39	14.19	16.20	17.06	19.71	16.12	16.78	20.31	19.53	19.96
MnO	0.00	0.00	0.00	0.10	0.06	0.00	0.00	0.00	0.00	0.00	0.10	0.31
MgO	7.80	7.15	7.35	12.82	10.47	10.14	6.85	11.07	9.85	8.24	8.80	8.09
CaO	11.09	10.93	10.94	11.42	11.28	11.30	11.12	11.61	11.47	10.77	10.98	10.45
Na_2O	1.95	1.68	1.59	1.51	1.85	1.81	2.03	2.17	1.98	2.29	2.13	2.36
K_2O	2.00	2.04	2.11	0.61	0.94	1.02	1.61	1.08	1.64	1.16	1.13	1.18
Cl	0.42	1.72	1.69	0.85	1.27	1.57	0.86	0.28	0.70	1.60	1.26	1.59
F	0.00	0.00	0.00	0.08	0.06	0.09	0.06	0.18	0.12	0.08	0.08	0.14
Negative charge	46	46	46	46	46	46	46	46	46	46	46	46
Si	6.03	6.22	6.20	6.77	6.33	6.35	5.86	6.28	6.09	6.20	6.31	6.13
Ti	0.32	0.23	0.17	0.14	0.16	0.18	0.18	0.00	0.05	0.18	0.22	0.16
Al	2.54	2.16	2.25	1.66	2.23	2.15	2.99	2.47	2.72	2.32	2.13	2.48
Al^{IV}	1.97	1.78	1.80	1.24	1.67	1.65	2.14	1.73	1.91	1.80	1.70	1.87
Al^{VI}	0.58	0.38	0.45	0.43	0.57	0.50	0.85	0.74	0.80	0.52	0.43	0.61
Fe	2.37	2.88	2.84	1.75	2.06	2.18	2.55	2.01	2.13	2.62	2.50	2.59
Mn	0.00	0.00	0.00	0.01	0.01	0.00	0.00	0.00	0.00	0.00	0.01	0.04
Mg	1.79	1.68	1.74	2.81	2.38	2.31	1.58	2.46	2.23	1.90	2.01	1.87
Ca	1.83	1.84	1.86	1.80	1.84	1.85	1.84	1.86	1.86	1.78	1.80	1.74
Na	0.58	0.51	0.49	0.43	0.55	0.53	0.60	0.63	0.58	0.68	0.64	0.71
K	0.39	0.41	0.43	0.12	0.19	0.20	0.32	0.21	0.31	0.23	0.22	0.23
Cl	0.11	0.46	0.49	0.21	0.33	0.41	0.23	0.07	0.18	0.42	0.33	0.42
F	0.00	0.00	0.00	0.04	0.03	0.04	0.03	0.08	0.06	0.04	0.04	0.07
$(Cl/Fe)*10^3$	47	160	161	122	160	187	89	34	84	160	130	162
F/Cl	0.00	0.00	0.00	0.18	0.09	0.11	0.12	1.19	0.33	0.09	0.12	0.16
Mg#	37	38	48	62	54	51	38	55	51	42	45	42

Table 4.4.2 *(continued)*

#	n=2	n=2	n=4	n=6	n=3	n=6	n=6	n=11	n=8
Sample	Ga357	Ga357	Ga357	Ga358	Ga358	Ga364	Ga364	TK038	WT10/WT203/WT208
Origin	Opx	Ilmenite	Ol/Ilm	Ol/Aug	Augite	Aug/Qtz	Augite	Country rock	Olivine
SiO_2	40.23	40.71	39.42	40.60	40.07	39.98	39.91	57.02	41.52
TiO_2	0.93	1.09	0.71	0.68	3.03	1.54	1.50	0.00	0.95
Al_2O_3	14.76	15.68	16.80	15.53	13.95	9.73	10.06	0.55	16.06
FeO	16.03	13.99	14.68	13.30	15.48	25.46	25.48	8.41	8.76
MnO	0.00	0.00	0.08	0.07	0.00	0.17	0.29	0.00	0.00
MgO	11.04	11.72	10.81	12.00	10.77	5.88	5.73	20.11	14.11
CaO	11.15	11.51	11.19	11.19	10.84	10.64	10.71	11.54	11.60
Na_2O	2.30	2.49	2.21	2.53	2.62	1.87	1.88	0.65	2.68
K_2O	1.73	1.19	1.52	1.57	1.26	1.83	1.97	0.00	1.23
Cl	1.17	0.59	0.73	0.06	0.05	1.67	1.57	0.01	0.20
F	0.03	0.12	0.24	0.00	0.00	0.22	0.20	0.22	0.04
Negative charge	46	46	46	46	46	46	46	46	46
Si	6.10	6.02	5.92	6.06	6.01	6.38	6.35	7.95	6.08
Ti	0.10	0.12	0.08	0.08	0.34	0.19	0.18	0.00	0.11
Al	2.64	2.73	2.98	2.73	2.47	1.83	1.89	0.09	2.78
AL^{IV}	1.90	1.98	2.08	1.95	1.99	1.62	1.65	0.05	1.92
Al^{VI}	0.74	0.75	0.89	0.79	0.48	0.21	0.24	0.04	0.86
Fe	2.03	1.73	1.85	1.66	1.94	3.40	3.39	0.98	1.07
Mn	0.00	0.00	0.01	0.01	0.00	0.02	0.04	0.00	0.00
Mg	2.27	2.58	2.42	2.67	2.41	1.40	1.36	4.18	3.08
Ca	1.81	1.83	1.80	1.79	1.74	1.82	1.83	1.73	1.82
Na	0.68	0.71	0.64	0.73	0.76	0.58	0.58	0.18	0.76
K	0.34	0.22	0.29	0.30	0.24	0.37	0.40	0.00	0.23
Cl	0.30	0.15	0.19	0.01	0.02	0.45	0.42	0.01	0.05
F	0.01	0.05	0.12	0.00	0.00	0.12	0.10	0.10	0.02
$(Cl/Fe)*10^3$	150	85	100	8	7	133	125	5	47
F/Cl	0.04	0.37	0.62	0.00	0.00	0.24	0.24	21	0.40
Mg#	53	60	57	62	55	29	29	81	74

4.5 TIMING AND POSSIBLE SOURCES FOR HALOGENS IN AMPHIBOLE FROM THE JOMASKNUTENE GABBRO

I shall discuss here the timing and possible origin of the halogen bearing fluid in the Jomasknutene gabbro which exchanged with amphibole during or after its formation. There are two alternatives for the timing of the chlorine influx:

1) The halogens were already present in the gabbroic magma.
2) The halogens entered an already solidified gabbro.

I prefer the second alternative because firstly there is no evidence that large amounts of halogen- or hydroxyl carrying minerals were formed during crystallization of the gabbroic magma and secondly that no increase in the halogen content is observed with increased fractionation as discussed in chapter II.

There are two principally different sources for halogens:

1) a magmatic one.
2) a metasomatic/metamorphic one

Certainties about the origin of halogens in metamorphosed igneous rocks are difficult to obtain. A metamorphic fluid can become enriched in halogens by a number of processes such as boiling, selective removal of water during mineral forming reactions or heredity of already halogen rich pre-metamorphic fluid. To investigate the origin of these concentrated halogen-bearing fluids one should investigate a guiding element, isotopic composition or element ratio which is characteristic for possible halogen sources and compare these values with values from the metamorphosed igneous rocks.

The reigning idea about the origin of a halogen-rich metamorphic fluid in the Bamble area is based on studies of specific rocks such as cordierite-orthoamphibole rocks and tourmaline-rich rocks (Visser 1993) and fluid inclusion studies (Touret, 1985). Cordierite-orthoamphibole rocks have been interpreted as being the result of metamorphism of an hydrothermally altered marine sediment; the tourmaline rich rocks as a metamorphosed leaching product of evaporitic rocks (Touret, 1985). In both examples, the pre-metamorphic fluid may have become rich in halogen- and alkali elements and subsequently effected other rocks such as gabbros. In order to evaluate this reigning idea I used chemical data from seawater and basaltic rocks as reference material and compared them with data obtained from the Jomasknutene gabbro.

The chlorine (isotope) analyses were carried out by Eggenkamp (1994). Whole rock chlorine data were extrapolated from analyses of two amphibole rich samples from the Jomasknutene gabbro; one core (Ga159) and one rim sample (Ga342). Both whole rock chlorine contents measure about 5000 ppm (Eggenkamp, pers. comm). Such high chlorine content in whole rock samples suggests an other than magmatic source for this element. Glassy basaltic rocks usually do not exceed 1400 ppm chlorine (Ito et al. 1983). Molar fluorine to chlorine ratios in amphibole from the Jomasknutene gabbro are usually smaller than one and close to zero. These ratios are not in accordance with the molar fluorine to chlorine ratio of about 4 from back arc basin basalt (Sanders and Tarney 1991). Boudreau et al. (1986) confirms this with the statement that melts with extremely high chlorine to fluorine ratios are unknown. Thus, it is unlikely that fluorine and chlorine in amphibole from the Jomasknutene gabbro originate a primary magmatic source.

Another attempt to determine the chlorine source involved determining the chlorine isotope ratio from two amphibole bearing samples from the Jomasknutene gabbro (Eggenkamp, 1994). The preliminary results of this isotope study indicate a similarity with standard seawater. $\delta^{37}Cl$ values ranges between -0.26 ($\sigma_{n-1}=0.12$) and -0.06 ($\sigma_{n-1}=0.02$). As chlorine isotope ratios are in general modified from standard

seawater by relatively low temperature processes such as evaporitization, I suggest that chlorine does not originate from an evaporitic sources but rather from a normal seawater source. This suggestion strengthens the idea that the metamorphic fluid has formed from a hydrothermal system rather than from an evaporitic leaching mechanism. There are no indications that the hydrothermal system was initiated by underlying gabbro intrusions.

This conclusion is preliminary and open for debate because the chlorine isotope composition at earlier times, its composition in the lower crust and mantle and its behaviour in magmatic and metamorphic systems are unknown.

4.6 BIOTITE; ANOTHER INDICATOR FOR THE FLUID COMPOSITION

Biotite and scapolite are minerals in the Jomasknutene gabbro which also can incorporate halogens and hydroxyl complexes. Unfortunately, there are no chemical scapolite analyses available in which chlorine or fluorine have been measured. However, there are chlorine and fluorine data for biotite. It is of interest to compare the chlorine and fluorine content of amphibole with that of biotite in order to determine whether these minerals have formed under similar conditions. In chapter 2.3 I demonstrated that biotite is probably older than amphibole. Thus differences in halogen content between amphibole and biotite may be caused by variations in halogen activity with time. Volfinger et al. (1985) demonstrated that the chlorine content in biotite should be higher than that of a coexisting amphibole. Mean chemical biotite analyses are listed in table 4.6.1. It appears that, in general, the chlorine content of biotite is lower than that of amphibole from the same sample. The fluorine content is low as well. Thus, biotite has probably equilibrated either under higher temperature conditions or with a fluid containing less halogens compared to the conditions prevailing during amphibole formation. The high chlorine to fluorine molar ratio in biotite indicates that the fluid has been rich in chlorine and relatively poor in fluorine, analogous to the fluid which equilibrated with amphibole. The comparison of the halogen content between amphibole and biotite in the Jomasknutene gabbro indicates that the halogen activity of the metamorphic fluid in the Jomasknutene gabbro must have been variable with time.

Table 4.6.1 *CHEMICAL ANALYSES OF METAMORPHIC BIOTITE*

Mean biotite analyses from the Jomasknutene gabbro. Biotite is always low in halogen elements compared to amphibole (table 4.4.2).

#	n=11	n=2	n=3	n=4	n=2	n=4
Sample	Ga153	Ga155	Ga159	Ga342	Ga357	Ga358
SiO_2	35.77	35.00	36.34	36.61	36.45	35.90
TiO_2	4.17	3.35	5.21	3.12	4.24	3.08
Al_2O_3	14.99	15.87	13.41	14.38	15.53	15.96
FeO	17.75	17.90	22.16	18.65	14.69	14.47
MnO	0.01	0.05	0.02	0.00	0.00	0.00
MgO	12.48	12.14	9.34	13.10	15.18	14.81
Na_2O	0.20	0.34	0.11	0.27	0.31	0.13
K_2O	9.18	9.33	9.57	9.31	9.09	8.21
Cl	0.04	0.00	0.54	0.97	0.43	0.07
F	0.00	0.00	0.00	0.15	0.21	0.00
Negative charge	44	44	44	44	44	44
Si	5.47	5.40	5.60	5.57	5.42	5.47
Ti	0.48	0.39	0.60	0.36	0.47	0.35
Al	2.70	2.89	2.43	2.58	2.72	2.87
Fe	2.28	2.31	2.85	2.37	1.83	1.84
Mn	0.00	0.01	0.00	0.00	0.00	0.00
Mg	2.83	2.79	2.14	2.97	3.36	3.37
Na	0.06	0.10	0.03	0.08	0.09	0.04
K	1.79	1.84	1.88	1.80	1.72	1.60
Cl	0.01	0.00	0.14	0.25	0.11	0.02
F	0.00	0.00	0.00	0.07	0.10	0.00
Mg#	55	55	43	56	65	65
F/Cl	0.00	-	0.00	0.28	0.92	0.00

4.7 PRELIMINARY RESULTS OF A FLUID INCLUSION STUDY

Fluid inclusions in gabbroic rocks are not commonly studied because suitable minerals which are able to trap and hold pervasive metamorphic fluids are usually absent. Fortunately, intercumulus augite in the Jomasknutene gabbro is locally replaced by amphibole and quartz (chapter 2.3 and 2.4). It is this quartz which has trapped and kept considerable amounts of the metamorphic fluid. The physical and chemical data provided by the study of these inclusions will tell us more about the metamorphic parameters at time of the amphibolitization of the augite. These data are combined with data derived from theoretical considerations of the replacement of augite by amphibole and quartz, discussed in chapter 2.4, and the peak metamorphic P-T conditions discussed by Nijland (1993). It is to be expected that considerable aqueous brine-like inclusions might be found based on the intensive amphibolitization of the augite and the high chlorine content of amphibole. Furthermore, non aqueous fluid inclusions are expected as well based on the theoretical approach of the replacement of augite by amphibole and quartz as discussed in chapter 2.4. These considerations suggest that $P_{H2O} < P_{total}$

4.7.1 INTRODUCTION TO PREVIOUS WORK

A regional fluid inclusion study in south-east Norway was carried out by Touret (1985). His study focused on the amphibolite to granulite transition zone in the Bamble area. His principal conclusions are:

- Phase separation between CO_2 and aqueous brine fluids.
- Aqueous brine inclusions occur throughout the entire (central) Bamble area and are thought to have a pre-metamorphic origin. They re-equilibrated during several stages of their (metamorphic) history.
- $CO_2(\pm N_2)$ inclusions are restricted to the granulite facies area near Tromøy and near isolated granulite facies domains in the amphibolite facies region. These inclusions are the best indicators to delineate the peak metamorphic conditions.
- Several exceptions to these granulite facies related $CO_2(\pm N_2)$ inclusions have been observed notably in relatively late metamorphic segregation. These exceptions may be related to deep seated intrusions responsible for the heat supply during peak metamorphism.
- Low density N_2 inclusions have been observed but their origin and history are not clear.

4.7.2 SAMPLE DESCRIPTION

In this study I investigated fluid inclusion from one sample Ga364. The fluid inclusions found in this sample are thought to represent fluids responsible for the amphibolitization of augite in the Jomasknutene gabbro. The location of this sample is marked in figure 4.4.1 and lies in the eastern part of the Jomasknutene gabbro. Amphibole from this sample is not 'chemically altered' as the ones from the rim of the gabbro. They exhibit a 'normal' chemistry as discussed in chapter 4.4. Quartz is formed on the original augite plagioclase contact (chapter 2.4). The idealized reaction concerning the formation of quartz out of augite and plagioclase is:

Augite + *Plagioclase* + *Periclase* + *Water* → *Amphibole* + *Quartz* **(4.7.1)**

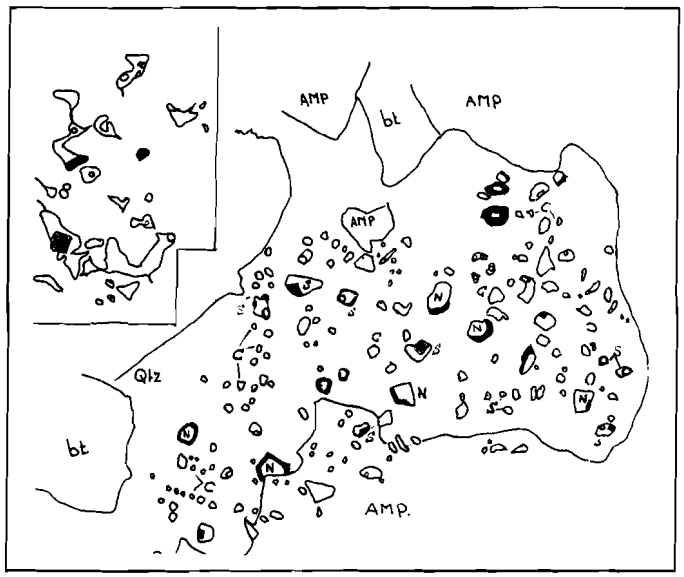

Figure 4.7.1

A representative drawing of fluid inclusions trapped in a quartz grain. The quartz formed together with amphibole out of augite and plagioclase (sample Ga364). Bt= biotite, Qtz= quartz, Amp= amphibole, N= low density N_2 inclusion, C= high density CO_2-N_2 inclusion, S= salt bearing aqueous inclusion.
The inset drawing shows an example of an imploded aqueous inclusion.

The quartz grains included in amphibole, contain the fluid inclusions which are investigated. Figure 4.7.1 represents a quartz grain which illustrates the typical shapes and distribution of the fluid inclusions. The fluid inclusions are distributed homogeneously and occur isolated. These inclusions are therefore interpreted as being primary in their host mineral. The trapped fluid accompanied in all likelihood the amphibolitization of augite.

Two main types of fluid inclusions have been recognized:

Type 1) Aqueous, often salt bearing inclusions (probably similar to the brine like inclusions discussed by Touret, 1985). The size of the inclusions ranges from 0.5 up to 20 microns. The small inclusions are usually round whereas the large ones are angular. This angularity of some of the aqueous inclusions indicate they have been imploded (inset in figure 4.7.1). The implosion theory is made plausible in chapter 4.7.4. The salinity of the aqueous inclusions varies. Some inclusions contain salt cubes comprising about 70 volume % of the inclusions whereas others have no salt cube at all.

Type 2) Gaseous inclusions. Their size range between 0.5 and 20 microns and are usually more idiomorphically shaped than the aqueous ones. These gaseous inclusions contain locally salt cubes as well. No visible trace of water has been observed in these inclusions.

As both types of inclusions are intermingled at all scales in the quartz grain they warrant the assumption that the inclusions are formed from an immiscible fluid system consisting of a gaseous CO_2-N_2 phase and an aqueous phase with a high salt concentration. That a chemical system, consisting of H_2O, CO_2 and NaCl can exsolve under various metamorphic conditions has been demonstrated by Johnson (1991) and Trommsdorff and Skippen (1987). Touret (1985) suggested that the highly saline

aqueous phase has initially a pre-metamorphic origin (already discussed in chapter 4.5) whereas the CO_2 rich gaseous phase has a peak metamorphic origin either related magmatic intrusions or metamorphic mineral reactions.

4.7.3 THE PHYSICAL PROPERTIES OF THE FLUID INCLUSIONS

MELTING AND HOMOGENIZATION TEMPERATURES

The method I used to determine the melting- and homogenization temperatures (respectively T_m and T_h) of the fluid inclusions is by recording the temperatures at which phase transitions occur during heating of an inclusion cooled down to about -190°C. The measured melting temperature (T_m) and homogenization temperature (T_h) are summarized and illustrated in figure 4.7.2[a,b]. With this method, I have distinguished three types of inclusions. The first one corresponds aqueous inclusions; the second and third one correspond gaseous inclusions. Upon heating the cooled inclusion exhibit the following phase transformations:

Type 1) Salt bearing aqueous inclusions:

Melting of the cooled inclusion occurs occasionally below -50°C but usually between -19.1°C and -12.4°C. A vapour phase is present as soon as the solid-liquid transition occurs. The disappearance of the vapour phase does not occur below +50°C (homogenization temperature has not been determined). Frequently aqueous inclusions include a solid phase (salt cube) at room temperature.

Type 2[a]) High density mixed CO_2-N_2 inclusions:

Melting temperature ranges between -61.4°C and -58.8°C (mean T_m = -59.5°C; n=20). In the molten state of the inclusion a gas bubble is present and disappears (homogenizes) in the liquid phase between -25.9°C and -5.7°C (mean T_h = -16.4°C; n=20). These data are illustrated in figure 4.7.2[a,b].

Type 2[b]) Low density N_2 inclusions:

Homogenization of the fluid phase occurs at -47.5°C, close to the critical point of N_2. The gas bubble is then dissolved into the liquid phase. Similar low density N_2 inclusions have been found in the Bamble area by Touret and Dietvorst (1983) but their origin and interpretation remains unclear.

The conclusions which are drawn from these observations are:

1) the low melting temperature (< -50°C) of several aqueous fluid inclusions indicates a multi component ionic system in which Ca^{2+} and Na^{+} dominate with probably minor amounts of other ions such as Mg^{2+} and K^{+}.
2) The depression of the melting temperature of the CO_2 inclusions indicate that these inclusions are mixed with other gaseous species. Raman spectrometry analyses, as discussed below indicate a CO_2-N_2 mixture with a molar proportion of about 9:1.

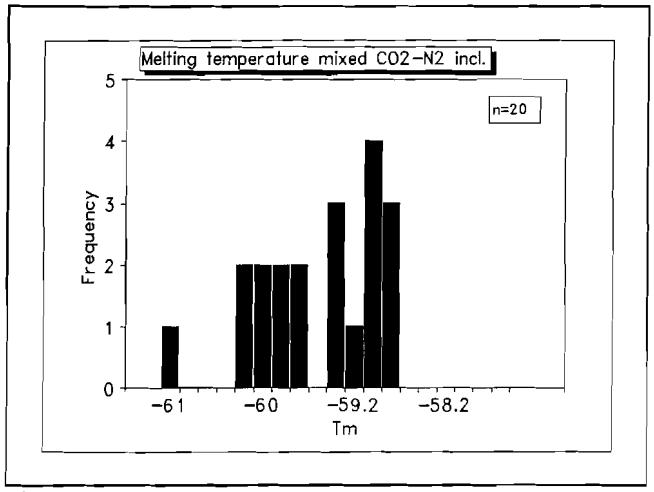

Figure 4.7.2[a]

Histogram of T_m values for mixed CO_2-N_2 fluid inclusions in quartz. The deviation from the melting temperature of pure CO_2 (-56.6°C) indicate an mixture with another species.

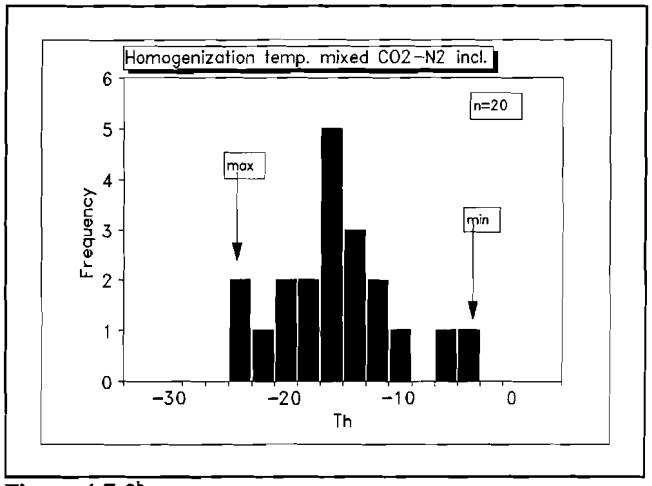

Figure 4.7.2[b]

Histogram of T_h values for mixed CO_2-N_2 fluid inclusions in quartz. The variation of the homogenization temperature indicate a variation in density considering the chemical composition to be equal. The density ranges from 0.86 gr/cm^3 to 0.96 gr/cm^3.

RAMAN SPECTROMETRY

To investigate the (im)purity of the gaseous inclusions I used the Raman spectrometry analyzing technique. The analyses where made by a Dilor Microdil-28 multichannel laser Raman microspectrometer using a 514 nm Ar ion laser as source of excitation. The instrument and measurement conditions of this method have been described by Burke and Lustenhouwer (1987). The results of this study are:

1) The mixed CO_2-N_2 inclusions contain 88 $\pm$1 mole% CO_2 and 12 $\pm$1 mole% N_2 on the average (n=3). Neither CH_4 nor H_2S has been detected.
2) In the low density N_2-inclusions no other type of molecule than N_2 has been detected.

4.7.4 INTERPRETATION

With the homogenization temperatures and composition of the CO_2-N_2 inclusions established it is possible to calculate isochores of this system. To calculate them, first the molar volume of the mixture must be determined. This can be done graphically using a diagram which illustrates the CO_2-N_2 composition as function of the temperature. Such TX-diagram for the system CO_2-N_2 is constructed by van den Kerkhof (1990). It appears that a mixture of 88 mole% CO_2 and 12 mole% N_2 with a homogenization temperature between -25.9°C and -5.7°C has a molar volume between 44 cm^3 (density 0.96 gr/cm^3) and 49 cm^3 (density 0.86 gr/cm^3). The results of the isochore calculations are summarized in figure 4.7.3 and joined with the theoretical approach of the formation of the amphibole quartz symplectite and the metamorphic P-T path of Nijland (1993).

It has been suggested previously that the fluid at peak metamorphic conditions must have been an immiscible system containing a saline aqueous and gaseous CO_2-N_2 bearing phase. Johnson (1991) and Trommsdorff and Skippen (1987) demonstrated the possibility of immiscibility in the system H_2O-CO_2-NaCl along most temperature-depth paths in metamorphic rocks if the chloride content of the fluid system is adequate. This immiscible character of the peak metamorphic fluid in the Jomasknutene gabbro is proven by the occurrence of salt cubes in these gaseous CO_2-N_2 inclusions. In principle, it would now be possible to determine the unique P-T conditions by intersecting the isochores of the aqueous and gaseous system. Unfortunately, the initially isobaric metamorphic cooling path re-equilibrated the aqueous inclusions, more than the gaseous one. The reason for this selective re-equilibration lies in the steepness of the isochores. Isochores from the aqueous inclusions are steep whereas those from the high density gaseous inclusions runs more or less parallel to the isobaric metamorphic cooling path (figure 4.7.3). As the rocks cooled down, the metamorphic conditions caused an overpressure with respect to the inclusions. This overpressure is larger for the aqueous inclusions than it is for the high density gaseous inclusions as can be deduced from figure 4.7.3. Thus re-equilibration of aqueous inclusions is more likely than of gaseous ones. The result of this re-equilibration is visualized by the implosion textures drawn in the inset of figure 4.7.1. Apparently, high density gaseous inclusions represent the best remnants of the peak metamorphic fluid conditions. The pressure recorded in these CO_2-N_2 inclusions is about 1 or 2 kbar lower than the estimated peak metamorphic pressure conditions of Nijland (1993). Deviation from the peak metamorphic pressure conditions can be explained by selective water leakage from H_2O bearing gaseous CO_2-N_2 inclusions or undetected H_2O in the gaseous inclusions.

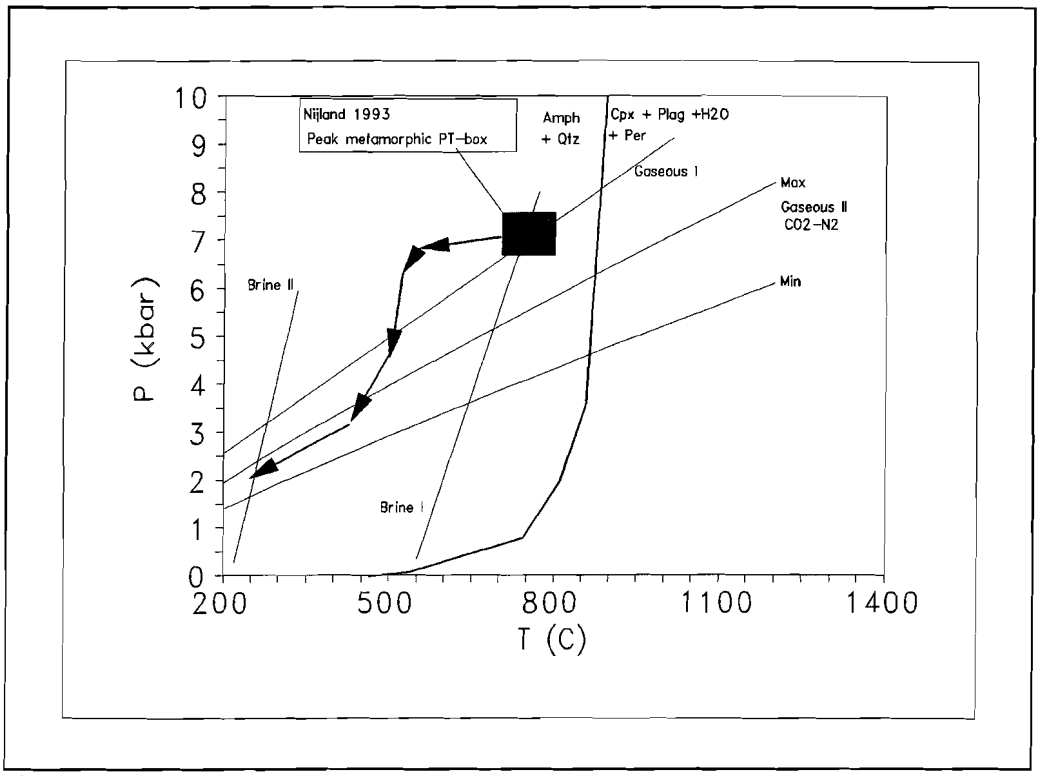

Figure 4.7.3

P-T restrictions for the Nelaug area in the central part of the Bamble area. The box represent peak metamorphic conditions; the arrows the metamorphic cooling path. Brine I and Gaseous I represent the most probable isochore positions of the aqueous and gaseous CO_2-N_2 phase respectively during peak metamorphic conditions. Brine II (Touret, pers. comm) and Gaseous II (Max and Min) represent the isochores of aqueous and gaseous CO_2-N_2 phase respectively after re-equilibration. It appears that the difference between the pressure in the inclusions and the metamorphic pressure is larger for the brine inclusions than for the gaseous ones. Therefore the brine inclusions re-equilibrated probably more than the gaseous ones. The thick solid line corresponds to the theoretical P-T values for the formation of amphibole and quartz out of clinopyroxene and plagioclase.

4.8 CONCLUSIONS

I investigated amphibole from the Jomasknutene and Dale gabbro in order to pinpoint the nature of the metamorphic fluid penetrating the two gabbros. I reached the following principal conclusions:

1) The high chlorine to fluorine ratio in metamorphic amphibole from the Jomasknutene gabbro suggests a metamorphic fluid relatively rich in chlorine and poor in fluorine.
2) The chlorine content of amphibole from the outer margin of the Jomasknutene gabbro is in general slightly higher than that of samples from the core. Amphibole from the rim samples equilibrated either at lower temperature with the same chlorine containing fluid or at a similar temperature with a higher chlorine containing fluid.
3) Amphibole from samples from the rim of the Jomasknutene gabbro are de-aluminized and depleted in divalent iron due to an acid fluid with as consequence a relative enrichment in silica and a depletion in alkali elements in the amphibole.
4) The chemistry of amphibole from the Jomasknutene gabbro indicates that the ability to incorporate chlorine in amphibole depends on their iron content.
5) Amphibole from the Dale gabbro resemble, qua chlorine content, amphibole from the outer margin of the Jomasknutene gabbro as inferred from a small number of amphibole analyses.
6) The halogen content and the chlorine isotopic composition, in amphibole from the Jomasknutene gabbro suggests a seawater origin rather than a magmatic or evaporitic one.
7) Three main types of fluid inclusions are recognized:
    - Aqueous salt-bearing fluid inclusions, intensively re-equilibrated during metamorphic retrogradation.
    - Mixed CO_2-N_2 inclusions, representing best the peak metamorphic P-T conditions.
    - Low density N_2 inclusions
8) The partial water pressure during amphibolitization of augite must have been substantial lower (1 kbar) than the total pressure of about 7 kbar.

CHAPTER V
A GEODYNAMIC MODEL FOR THE BAMBLE AREA

5.1 INTRODUCTION

In this concluding chapter I shall discuss a generalized metamorphic model for the Bamble area based on theoretical heat distribution parameters in the lithosphere. This model forms a reference for earlier determined Gothian and Sveconorwegian metamorphic parameters. Finally I shall compile the data presented in this thesis to illustrate my ideas upon the geodynamic evolution of the south norwegian area during Gothian and Sveconorwegian times and the role of the Bamble area in it.

5.2 METAMORPHIC MODEL

The regional metamorphic conditions during the Gothian and Sveconorwegian period are caused primary by burial metamorphism. Maximum pressure estimates of both metamorphic periods reached between 6 and 8 kbar, agreeing with an average rock pile of about 25 km on top of the present day exposed Bamble rocks. The metamorphism caused by such rock pile is principally dependant on two variables:

1) The heat production above the investigated area.
   This variable depends mainly on distribution of heat producing elements in the overlying crust. The relation between the amount of heat produced by these elements and the depth is an exponential one as discussed by Lachenbruch (1970).
2) The heat production underneath the investigated area.
   This variable depends on the underlying heat source and its distance from the investigated area. The relation between the amount of heat production and the distance from the heat source (mantle) is thought to be a linear one.

Staring from these two principles, Turcotte and Schubert (1982) suggested the following formula which describes the temperature as function of the depth:

$$T(z) = T_m + \frac{q_m * z}{K} + \left(\frac{A * L}{K} * \left(1 - e^{-\frac{z}{L}}\right)\right) * 10^4 \quad \textbf{(5.1)}$$

T(z)	=	Temperature at depth z	(°C)
T_s	=	Temperature at the surface	(0°C)
q_m	=	"Mantle" heat flux	(0.03 W/m^2)
z	=	Depth	(m)
K	=	Thermal conductivity	(2.25 W/(mK))
A	=	Volumetric heat production rate	(2*10^{-6} W/m^3)
L	=	Characteristic length scale	(10,000 m)

The values for the various parameters used in formula 5.1 are obtained from the paper by England and Thompson (1984). They have discussed the possible ranges for these parameters in a stable continental crust and presented mean values. A "mantle" heat flux is generally not less than 0.02 W/m^2 and, except in regions where extensive magmatism is occurring, it does not exceeds 0.04 W/m^2 (Sclater et al. 1980, 1981). Using formula 5.1, I have calculated three theoretical steady state geotherms using three different "mantle" heat fluxes i.e. 0.03 W/m^2, 0.06 W/m^2, 0.08 W/m^2. The results of these calculations are illustrated in figure 5.1. Using these three geotherm as base I plotted the Gothian and Sveconorwegian metamorphic P-T values in figure 5.1 as well. Now it is possible to discuss and compare the metamorphic conditions in terms of variation in "mantle" heat flux at a constant thickness of the crust during Gothian and Sveconorwegian times.

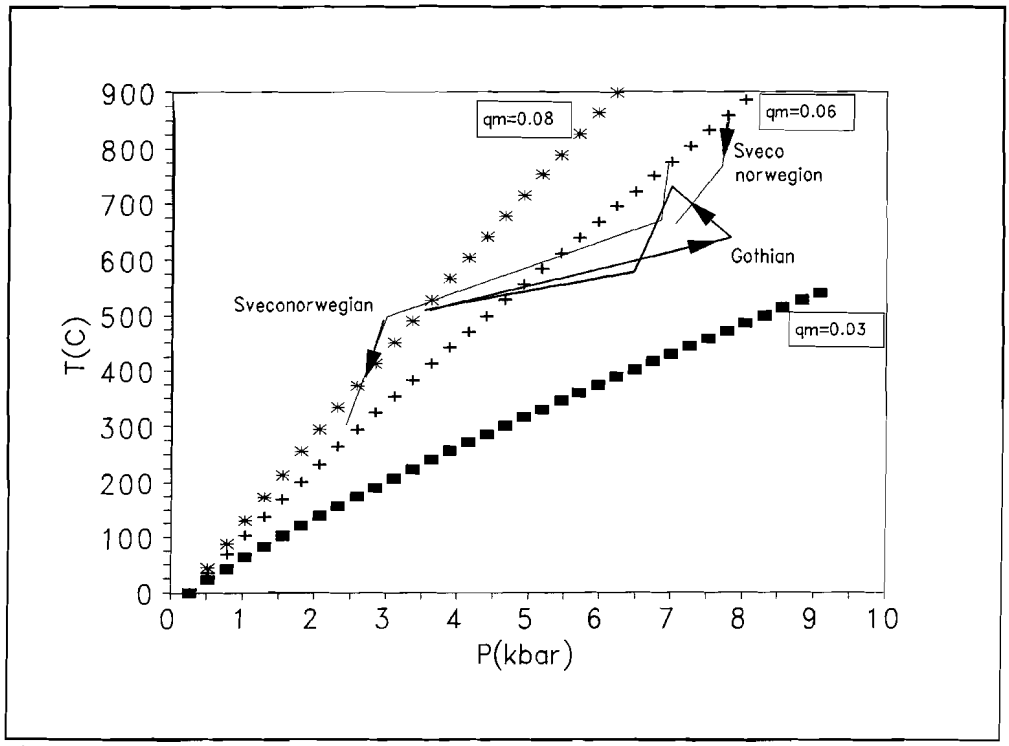

Figure 5.1

The Gothian P-T estimates from Visser (1993) the Sveconorwegian P-T estimates from Nijland (1993) designated by the thick and thin lines respectively. For comparison three steady state geotherms are drawn with different heat flow values.

Figure 5.1 suggest the metamorphic conditions of both periods are characterized by elevated "mantle" heat fluxes. Peak metamorphic conditions during the Gothian period coincide with a heat flux of about 0.05 W/m^2; the heat flux during the Sveconorwegian period may reached even 0.06 W/m^2. The question rises what caused these elevated conditions and what is the geodynamic implication of it. A plausible explanation is, in my opinion, a rift configuration of the Bamble crust starting at Gothian times and lasted until the end of the Sveconorwegian period. Although I suggested in chapter I (table 1.1) the Bamble area was alternately subjected to extensional and compressional activities, accompanying metamorphic signatures of the latter have not been found and possibly wiped out by extensional

metamorphism and tectonism. This idea fits in the model of 'caterpillar tectonics' discussed by James and Ding, 1988.

An elevated heat flux caused by a mantle plume or an underplating magma have already been suggested by Touret (1969), de Haas (1992) and Nijland (1993). Because there is no evidence for major changes in heat flow activity in the Bamble area, the rift configuration may have existed from the start of the Gothian period and sustained until the end of the Sveconorwegian period. This rift system underneath the Bamble area must have been overruled during various compressional episodes during the Bamble history. The gabbroic intrusions are, in this scenario, most likely the result of attempted rifting of the continental Bamble crust. The cooling trajectory, which is thought to be of Sveconorwegian age (Visser 1993 and Nijland 1993) indicate that during uplift of the Bamble crust, the "mantle" heat flux increased even more (q_m=0.08 W/m^2). The attempted rift of the Bamble crust may have caused the actual uplift of the Bamble area. Whether true rifting of the crust did occur after the Sveconorwegian period remains unclear.

5.3 GEODYNAMIC MODEL

My opinion upon the geodynamics of south Norway, and the Bamble area in particular, is based on results of this thesis and a literature study, mainly presented in chapter I. I shall discuss this geodynamic model below in a chronological order.

In the pre or early Gothian period Bamble sediments were deposited. The Nidelva quartzite complex must have been deposited close or on the continental mainland (Nijland et al. 1993). Other sedimentary complexes, such as the Selås banded gneiss has been interpreted as a turbidite system (Touret, 1969) indicating the existence of a deep marine basin. Before the onset of the deformation of these sediments during the Gothian period a more or less stabilized "Telemark protocontinent" (Telemark Banded Gneiss Complex) must have been present west of the Bamble area. This idea is based on the oldest, Gothian, deformation structures in the Bamble and Kongsberg area (Starmer, 1993). East of this sediment deposits, the Svecofennian mainland must have been present. Whether the sedimentary Bamble basin was rift related is not clear. 1.77 Ga $\pm$0.19 Ga ago sediments in the Bamble area were intruded by gabbroic magmas, among which the Jomasknutene gabbro. These intrusions could be the result of a (rift-related) elevating heat flux from underneath the Bamble area. In the period after the intrusion of Gothian gabbroic magmas the area remained probably buried and was continuously subjected to amphibolite facies metamorphism. Rift related dikes intruded some specific parts of the south scandinavian area. Before the onset of the early Sveconorwegian compressional period sediments were deposited in the Rogaland area. These sediments were subsequently squeezed between a stabilized continental bloc in the west, known as the Laurentian Shield, against the stabilized Svecofennian and Gothian continent in the east. This compressional regime opposed the rifting system. The metasediments of the Bamble area were subjected to major deformation again. Before the main Sveconorwegian deformation period started, a period of anorogeny occurred in the Bamble area accompanied again with intrusion of gabbroic magmas among which the Dale gabbro. Because this period is also characterized by high heat fluxes is seems likely that the rift system was initiated again. The gabbro intrusions were subsequently subjected to deformation and metamorphism of the main Sveconorwegian period.

In conclusion I suggest that the crust of the Bamble area is continuously subjected to a high "mantle" heat flux and interpreted as a rifting system. This resulted in various gabbroic intrusions among which the Jomasknutene and Dale gabbro. The attempted rifting was alternated with periods of compression, now recognizable as orogenic periods which opposed true rifting of the Bamble crust.

APPENDIX A
WHOLE ROCK DATA SET

Whole rock analyses from the Dale and Jomasknutene gabbro are presented in weight percentages.

- The Mg# (magnesium number) is defined here as the molar ratio of MgO and MgO+FeO. It is not corrected for normative ilmenite (chapter 2).
- The dimension of the trace elements is ppm.
- **nd** indicates that the element has not been analyzed for that particular sample.

-Location: D = Dale gabbro
JKN = Jomasknutene gabbro

-Name: A = Amphibolite
C = Coronite
G = Gabbro
U = Ultramaphic rock (unit D)

-Size: the grain size variation has been divided into three groups based on macroscopic field observations. C = Coarse grained
M = Medium grained
F = Fine grained

-Quality: a measure of the original magmatic texture and mineralogy.
O = altered gabbroic texture and mineralogy
S = major scapolitization
\+ = metamorphosed gabbro sample
++++ = fresh, only slightly altered, gabbro sample

APPENDIX A

Sample	WT216	WT3	WT209	WT221	WT222	WT211	WT210	WT220	WT215	WT225	WT214	WT217
Location	DALE	DALE	DALE	DALE	DALE	DALE	DALE	DALE	DALE	DALE	DALE	DALE
Name	G	G	G	G	G	G	G	G	G	G	G	G
Size												
Quality	+++	+++	+++	+++	+++	+++	+++	+++	+++	+++	+++	+++
SiO_2	46.62	49.60	48.87	45.83	47.50	46.21	48.02	47.29	42.77	44.35	45.35	42.56
TiO_2	1.84	1.22	1.20	0.88	0.88	1.10	0.87	0.67	0.78	0.84	0.91	0.80
Al_2O_3	12.96	14.24	15.81	18.20	17.46	13.69	15.10	18.11	10.93	10.86	11.15	9.66
FeO	13.64	11.28	11.13	10.01	9.87	11.35	10.93	9.54	14.77	15.88	13.87	16.47
MnO	0.22	0.18	0.19	0.17	0.17	0.19	0.19	0.15	0.21	0.24	0.22	0.25
MgO	7.12	6.87	8.03	7.96	7.98	9.45	9.29	9.79	16.79	18.25	15.99	19.39
CaO	10.79	11.89	11.80	10.86	10.98	11.14	11.45	11.12	7.77	6.73	8.80	6.42
Na_2O	2.32	2.72	2.50	2.13	2.42	1.77	2.06	2.10	1.64	1.71	1.74	1.40
K_2O	0.67	0.57	0.45	0.78	0.54	0.90	0.70	0.29	0.35	0.33	0.31	0.30
P_2O_5	0.15	0.16	0.16	0.14	0.14	0.13	0.12	0.14	0.13	0.13	0.13	0.14
Total	96.33	98.73	100.14	96.96	97.94	95.93	98.73	99.20	96.14	99.32	98.47	97.39
Mg#	48	52	56	59	59	60	60	65	67	67	67	68
Co	65	97	72	73	62	81	76	72	149	131	133	121
Ni	69	59	93	136	122	115	115	156	408	400	315	449
Cu	113	62	71	61	37	70	62	39	50	61	49	55
Rb	19	10	8	30	11	35	27	4	3	6	6	6
Sr	288	271	307	317	328	236	289	324	197	214	217	194
Y	25	21	21	16	16	19	16	13	15	16	17	16
Zr	68	55	71	59	55	55	50	46	55	60	60	57
Nb	3	2	4	2	3	3	2	3	2	3	3	3
Ba	153	161	185	206	134	173	195	121	125	151	148	138
La	7	7	7	0	0	0	4	2	0	5	0	4
Ce	17	17	13	nd	nd	nd	10	nd	nd	11	nd	11
Sm	3	3	3	nd	nd	nd	2	nd	nd	2	nd	2
Eu	1	nd	1	nd	nd	nd	1	nd	nd	1	nd	1
Tb	1	1	1	nd	nd	nd	0	nd	nd	1	nd	0
Yb	2	2	2	nd	nd	nd	1	nd	nd	1	nd	1
Hf	2	2	2	nd	nd	nd	1	nd	nd	2	nd	1

Sample	WT208	WT223	WT203	WT204	WT10	GA385	GA325	GA335	GA369	GA368	GA347	GA370
Location	DALE	DALE	DALE	DALE	DALE	JKN	JKN	JKN	JKN	JKN	JKN	JKN
Name	G	G	G	G	G	U	U	U	U	U	U	U
Size												
Quality	+++	+++	+++	+++	+++	0	0	O	O	O	O	O
SiO_2	44.19	43.93	45.29	46.51	40.77	45.17	42.17	44.39	43.31	48.38	43.39	43.58
TiO_2	0.53	0.41	0.52	0.55	0.28	2.52	1.36	1.62	1.05	2.23	1.08	0.63
Al_2O_3	12.92	15.05	13.11	14.08	8.19	16.71	13.00	13.28	13.39	6.25	14.65	15.54
FeO	13.89	11.46	12.92	11.48	16.16	13.59	16.15	17.22	15.71	18.78	14.04	12.85
MnO	0.21	0.18	0.20	0.19	0.24	0.22	0.28	0.32	0.23	0.37	0.27	0.21
MgO	16.48	13.64	17.37	15.74	25.45	5.98	13.58	11.85	12.82	16.57	13.60	15.56
CaO	8.18	9.12	9.01	9.30	5.15	8.04	6.68	6.10	9.46	4.24	9.07	7.63
Na_2O	1.50	1.71	1.33	1.84	0.80	4.97	3.17	2.32	1.97	0.87	1.97	2.21
K_2O	0.21	0.25	0.20	0.31	0.10	0.98	1.65	0.77	0.31	0.12	0.26	0.21
P_2O_5	0.11	0.10	0.10	0.00	0.09	0.31	0.16	0.23	0.01	0.10	0.12	0.16
Total	98.22	95.85	100.05	100.00	97.23	98.49	98.20	98.10	98.26	97.91	98.45	98.58
Mg#	68	68	71	71	74	44	60	55	59	61	63	68
Co	138	111	11	105	nd	124	74	129	101	120	117	113
Ni	369	322	364	307	nd	311	110	198	114	95	252	272
Cu	34	25	29	7	nd	62	91	70	28	52	34	30
Rb	0	1	3	0	nd	52	21	4	0	1	0	0
Sr	251	271	233	213	nd	85	338	56	84	48	137	100
Y	11	9	11	12	nd	18	29	22	41	24	16	10
Zr	42	33	39	42	nd	70	125	102	59	186	66	40
Nb	2	2	2	2	nd	1	4	1	1	2	0	0
Ba	103	97	89	0	nd	nd	nd	nd	nd	nd	nd	nd
La	0	0	3	0	nd	nd	nd	nd	nd	nd	nd	nd
Ce	nd	nd	0	nd	nd	nd	nd	nd	nd	nd	nd	nd
Sm	nd	nd	1	nd	nd	nd	nd	nd	nd	nd	nd	nd
Eu	nd	nd	1	nd	nd	nd	nd	nd	nd	nd	nd	nd
Tb	nd	nd	0	nd	nd	nd	nd	nd	nd	nd	nd	nd
Yb	nd	nd	1	nd	nd	nd	nd	nd	nd	nd	nd	nd
Hf	nd	nd	1	nd	nd	nd	nd	nd	nd	nd	nd	nd

APPENDIX A

Sample	GA148	GA395	GA372	GA371	GA373	GA144	GA176	GA339	GA329	GA179	GA379	GA145
Location	JKN	JKN	JKN	JKN	JKN	JKN	JKN	JKN	JKN	JKN	JKN	JKN
Name	U	U	U	U	U	A	G	G	G	G	C	G
Sizc						C	C	C	C	C	C	C
Quality	O	O	O	O	O	O	S+	S++	S++	S++	S++	S++
SiO_2	44.01	43.66	43.93	47.04	43.14	44.16	47.60	44.09	50.84	45.93	46.91	47.06
TiO_2	0.86	0.95	0.65	0.42	0.47	1.90	1.92	5.44	1.51	1.72	1.67	1.03
Al_2O_3	14.20	14.43	15.10	10.68	13.83	14.74	15.65	10.94	18.33	15.84	17.25	18.59
FeO	13.51	12.74	11.54	14.98	13.17	15.24	12.16	19.92	8.96	13.33	11.31	10.86
MnO	0.20	0.21	0.19	0.30	0.24	0.27	0.24	0.27	0.18	0.27	0.21	0.19
MgO	16.38	15.45	15.52	20.97	19.32	10.40	6.18	4.25	3.58	7.99	7.03	7.19
CaO	6.95	7.82	9.23	2.49	6.47	7.89	9.79	8.03	10.05	10.03	10.68	9.16
Na_2O	2.25	2.98	2.27	1.36	1.69	2.51	4.09	4.30	4.88	3.01	3.06	3.75
K_2O	0.19	0.24	0.21	0.06	0.17	1.14	0.94	0.21	0.43	0.42	0.51	0.95
P_2O_5	0.10	0.10	0.07	0.05	0.02	0.24	0.21	0.34	0.24	0.13	0.13	0.14
Total	98.65	98.58	98.71	98.35	98.52	98.49	98.78	97.79	99.00	98.67	98.76	98.92
Mg#	68	68	71	71	72	55	48	28	42	52	53	54
Co	127	133	120	144	127	123	69	85	59	2	76	79
Ni	345	277	248	376	344	321	65	31	19	121	101	75
Cu	17	35	15	19	20	76	75	85	69	79	54	26
Rb	6	0	0	0	0	27	19	2	9	16	14	32
Sr	81	75	91	42	88	270	313	151	299	181	269	257
Y	16	13	9	4	5	20	26	34	22	23	20	19
Zr	63	62	40	30	31	92	96	199	95	84	94	89
Nb	1	1	1	0	0	2	4	4	1	2	6	2
Ba	0	nd	nd	nd	nd	nd	311	nd	nd	85	nd	nd
La	4	nd	nd	nd	nd	10	nd	nd	nd	nd	nd	nd
Ce	10	nd	nd	nd	nd	22	nd	nd	nd	nd	nd	nd
Sm	2	nd	nd	nd	nd	4	nd	nd	nd	nd	nd	nd
Eu	1	nd	nd	nd	nd	2	nd	nd	nd	nd	nd	nd
Tb	1	nd	nd	nd	nd	1	nd	nd	nd	nd	nd	nd
Yb	2	nd	nd	nd	nd	2	nd	nd	nd	nd	nd	nd
Hf	1	nd	nd	nd	nd	2	nd	nd	nd	nd	nd	nd

Sample	GA346	GA146	GA375	GA392	GA350	GA157	GA330	GA340	GA397	GA316	GA356	GA153
Location	JKN	JKN	JKN	JKN	JKN	JKN	JKN	JKN	JKN	JKN	JKN	JKN
Name	C	G	C	G	C	G	C	G	G	G	C	G
Size	C	C	C	C	C	C	C	C	C	C	C	C
Quality	S++	++	++	++	++	++	++	+++	+++	+++	+++	+++
SiO_2	46.48	44.40	46.48	46.72	46.09	46.92	44.44	40.48	48.11	49.82	46.45	47.14
TiO_2	1.14	3.82	2.13	2.08	0.77	1.66	0.76	5.85	3.38	2.15	2.40	2.17
Al_2O_3	17.29	11.87	18.16	16.95	15.69	17.07	16.88	9.42	14.15	17.63	17.22	16.74
FeO	12.15	18.12	12.24	12.39	15.16	12.04	14.16	23.73	13.63	10.42	12.86	13.06
MnO	0.23	0.29	0.22	0.25	0.41	0.22	0.33	0.40	0.15	0.18	0.22	0.24
MgO	8.15	5.65	6.04	6.59	8.79	7.16	9.92	4.62	3.63	3.01	5.36	6.51
CaO	9.16	9.99	9.04	8.46	8.79	9.96	9.22	8.68	9.45	9.98	10.10	9.07
Na_2O	3.46	3.39	3.23	3.95	2.20	3.32	2.32	3.43	4.87	4.57	3.21	2.91
K_2O	0.48	0.44	0.82	0.97	2.76	0.34	0.32	0.33	0.66	0.74	0.60	0.65
P_2O_5	0.10	0.22	0.27	0.26	0.40	0.11	0.08	0.43	0.45	0.34	0.16	0.21
Total	98.64	98.19	98.63	98.62	101.06	98.80	98.43	97.37	98.48	98.84	98.58	98.70
Mg#	54	36	47	49	51	51	56	26	32	34	43	47
Co	74	104	67	75	96	77	127	138	54	56	79	99
Ni	79	35	94	100	82	79	138	55	35	29	77	97
Cu	33	89	64	89	78	68	47	132	133	50	182	86
Rb	14	15	17	12	7	8	5	5	22	10	10	15
Sr	221	178	414	415	157	205	151	151	251	290	366	348
Y	16	30	27	25	21	22	18	51	50	43	17	23
Zr	50	102	111	92	45	87	50	197	258	220	65	89
Nb	1	3	4	3	1	2	0	4	18	12	2	3
Ba	nd	107	nd	nd	nd	nd	nd	nd	nd	nd	nd	379
La	nd	7	nd	nd	nd	nd	nd	nd	nd	nd	nd	nd
Ce	nd	18	nd	nd	nd	nd	nd	nd	nd	nd	nd	nd
Sm	nd	5	nd	nd	nd	nd	nd	nd	nd	nd	nd	nd
Eu	nd	2	nd	nd	nd	nd	nd	nd	nd	nd	nd	nd
Tb	nd	1	nd	nd	nd	nd	nd	nd	nd	nd	nd	nd
Yb	nd	3	nd	nd	nd	nd	nd	nd	nd	nd	nd	nd
Hf	nd	3	nd	nd	nd	nd	nd	nd	nd	nd	nd	nd

APPENDIX A

Sample	GA151	GA155	GA315	GA318	GA159	GA358	GA355	GA456	GA450	GA455	GA391	GA457
Location	JKN	JKN	JKN	JKN	JKN	JKN	JKN	JKN	JKN	JKN	JKN	JKN
Name	G	G	C	G	G	G	G	D	D	D	G	D
Size	C	C	C	C	C	C	C	F	F	F	F	F
Quality	+++	+++	+++	+++	+++	++++	++++	O	O	O	O	O
SiO_2	47.54	46.43	47.53	46.35	47.04	46.33	42.82	46.49	47.74	46.18	51.79	47.80
TiO_2	1.94	2.17	1.15	1.66	1.05	1.78	1.40	2.80	2.89	2.10	2.71	1.96
Al_2O_3	15.44	15.68	18.12	16.19	19.14	16.32	11.22	14.97	15.21	14.94	15.64	15.95
FeO	12.00	13.05	10.56	11.44	10.15	12.78	17.48	14.44	13.07	13.37	7.80	8.84
MnO	0.19	0.24	0.22	0.23	0.19	0.30	0.28	0.25	0.22	0.23	0.09	0.12
MgO	6.32	7.40	7.27	8.27	8.48	7.92	13.97	5.56	5.61	6.58	6.10	7.38
CaO	10.06	9.96	10.26	10.26	9.38	8.56	8.48	8.19	8.69	10.00	9.21	11.51
Na_2O	4.31	3.21	3.07	3.52	2.90	3.34	2.00	4.27	3.88	4.48	4.78	4.21
K_2O	0.81	0.37	0.53	0.65	0.50	1.05	0.39	1.25	1.11	0.62	0.62	1.17
P_2O_5	0.18	0.20	0.12	0.16	0.15	0.21	0.22	0.34	0.27	0.17	0.31	0.20
Total	98.79	98.71	98.83	98.73	98.98	98.59	98.26	98.56	98.69	98.67	99.05	99.14
Mg#	48	50	55	56	60	52	59	41	43	47	58	60
Co	68	80	71	69	73	77	131	nd	nd	nd	36	nd
Ni	48	99	95	127	39	136	203	nd	nd	nd	62	nd
Cu	43	63	66	97	161	85	100	nd	nd	nd	27	nd
Rb	35	9	8	16	10	18	13	nd	nd	nd	18	nd
Sr	247	208	273	241	317	364	285	nd	nd	nd	243	nd
Y	26	32	16	21	24	22	22	nd	nd	nd	23	nd
Zr	123	123	74	102	94	86	93	nd	nd	nd	127	nd
Nb	9	3	5	7	3	3	2	nd	nd	nd	6	nd
Ba	171	99	nd	nd	nd	nd	nd	nd	nd	nd	nd	nd
La	nd	4	nd	nd	nd	nd	nd	nd	nd	nd	nd	nd
Ce	nd	12	nd	nd	nd	nd	nd	nd	nd	nd	nd	nd
Sm	nd	4	nd	nd	nd	nd	nd	nd	nd	nd	nd	nd
Eu	nd	2	nd	nd	nd	nd	nd	nd	nd	nd	nd	nd
Tb	nd	1	nd	nd	nd	nd	nd	nd	nd	nd	nd	nd
Yb	nd	3	nd	nd	nd	nd	nd	nd	nd	nd	nd	nd
Hf	nd	3	nd	nd	nd	nd	nd	nd	nd	nd	nd	nd

Sample	GA452	GA336	GA451	GA174	GA386	GA363	GA164	GA357	GA367	GA364	GA342	GA338
Location	JKN	JKN	JKN	JKN	JKN	JKN	JKN	JKN	JKN	JKN	JKN	JKN
Name	C	G	G	G	G	G	G	G	U	G	G	G
Size	F	F	F	M	M	M	M	M	M	M	M	M
Quality	++	++++	++++	O	O	O	O	O	O	S++	S++	+
SiO_2	47.38	45.64	47.45	45.95	45.54	46.10	47.19	46.41	43.66	48.28	45.67	44.08
TiO_2	1.80	2.16	1.76	1.70	1.58	1.58	1.49	1.30	1.02	4.26	2.42	4.36
Al_2O_3	18.22	19.75	18.16	16.01	18.62	17.06	18.48	18.11	13.68	12.27	16.17	11.76
FeO	11.75	13.18	11.94	13.42	11.73	12.13	10.13	10.50	13.92	16.82	14.77	18.65
MnO	0.21	0.25	0.22	0.27	0.25	0.26	0.18	0.21	0.25	0.36	0.27	0.33
MgO	6.42	4.59	6.20	7.79	7.59	8.18	7.42	8.57	14.50	3.40	6.39	5.28
CaO	9.26	9.35	9.00	9.90	8.89	9.75	9.14	10.69	8.63	7.08	8.15	9.14
Na_2O	2.93	2.99	3.14	2.89	3.68	3.08	3.40	2.48	2.34	3.59	3.27	2.87
K_2O	0.68	0.27	0.74	0.42	0.64	0.36	1.28	0.43	0.31	1.63	0.98	1.07
P_2O_5	0.17	0.37	0.18	0.11	0.18	0.14	0.17	0.13	0.13	0.45	0.01	0.39
Total	98.82	98.55	98.79	98.46	98.70	98.64	98.88	98.83	98.44	98.14	98.10	97.93
Mg#	49	38	48	51	54	55	57	59	65	26	44	34
Co	nd	87	nd	10	95	91	64	78	117	81	81	97
Ni	nd	45	nd	29	174	141	83	157	237	18	95	38
Cu	nd	105	nd	2	55	61	58	43	40	50	221	117
Rb	nd	3	nd	5	10	8	21	13	1	25	16	13
Sr	nd	267	nd	15	415	206	265	273	137	267	332	219
Y	nd	25	nd	33	19	25	22	18	16	50	26	39
Zr	nd	85	nd	158	76	93	100	81	66	216	113	156
Nb	nd	2	nd	13	2	1	7	5	1	7	4	6
Ba	nd	nd	nd	0	nd	nd	113	nd	nd	nd	nd	nd
La	nd	nd	nd	nd	nd	nd	3	nd	nd	nd	nd	nd
Ce	nd	nd	nd	nd	nd	nd	nd	nd	nd	nd	nd	nd
Sm	nd	nd	nd	nd	nd	nd	nd	nd	nd	nd	nd	nd
Eu	nd	nd	nd	nd	nd	nd	nd	nd	nd	nd	nd	nd
Tb	nd	nd	nd	nd	nd	nd	nd	nd	nd	nd	nd	nd
Yb	nd	nd	nd	nd	nd	nd	nd	nd	nd	nd	nd	nd
Hf	nd	nd	nd	nd	nd	nd	nd	nd	nd	nd	nd	nd

APPENDIX A

Sample	GA324	GA352	GA327	GA354	GA365	GA394	GA343	GA158	GA360	GA353	GA326	GA398
Location	JKN	JKN	JKN	JKN	JKN	JKN	JKN	JKN	JKN	JKN	JKN	JKN
Name	G	C	G	G	G	C	C	G	G	G	G	G
Size	M	M	M	M	M	M	M	M	M	M	M	M
Quality	+	++	++	++	++	++	+++	+++	+++	+++	+++	+++
SiO_2	45.45	46.77	47.55	47.39	47.70	46.76	46.34	48.60	46.23	46.75	47.05	47.28
TiO_2	1.91	2.68	1.71	1.71	1.83	2.19	2.61	1.51	2.80	1.58	1.55	1.71
Al_2O_3	17.25	16.45	19.32	18.76	17.42	16.63	16.06	22.81	14.40	18.84	18.65	16.79
FeO	13.01	13.99	10.65	10.76	12.11	12.77	14.29	7.21	13.90	10.65	11.16	11.22
MnO	0.27	0.24	0.21	0.17	0.22	0.28	0.26	0.14	0.21	0.17	0.22	0.24
MgO	8.23	5.09	4.84	5.70	6.42	6.95	5.89	3.05	6.66	5.15	5.72	6.86
CaO	8.14	8.19	11.41	9.31	9.31	8.38	8.59	12.05	8.99	10.46	10.32	11.03
Na_2O	3.25	3.70	2.86	3.59	2.79	2.78	3.14	3.54	4.16	4.40	3.65	2.98
K_2O	0.81	0.90	0.18	0.26	0.67	1.57	0.94	0.23	0.65	0.60	0.27	0.50
P_2O_5	0.25	0.43	0.11	0.25	0.18	0.27	0.29	0.15	0.16	0.21	0.18	0.15
Total	98.57	98.44	98.84	97.90	98.65	98.58	98.41	99.29	98.16	98.81	98.77	98.76
Mg#	53	39	45	49	49	49	42	43	46	46	48	52
Co	91	70	54	71	81	72	80	45	91	62	60	64
Ni	186	61	53	86	64	101	78	34	106	57	55	83
Cu	90	95	50	101	72	60	193	54	94	85	61	118
Rb	17	20	1	10	17	50	16	1	18	13	3	11
Sr	396	339	247	345	212	344	320	234	292	246	252	268
Y	21	34	18	21	29	25	28	20	32	25	23	20
Zr	95	148	56	77	105	97	113	80	127	96	77	89
Nb	3	5	1	2	1	3	4	2	4	1	1	6
Ba	nd	nd	nd	nd	nd	nd	nd	nd	nd	nd	nd	nd
La	nd	nd	nd	nd	nd	nd	nd	4	nd	nd	nd	nd
Ce	nd	nd	nd	nd	nd	nd	nd	11	nd	nd	nd	nd
Sm	nd	nd	nd	nd	nd	nd	nd	3	nd	nd	nd	nd
Eu	nd	nd	nd	nd	nd	nd	nd	1	nd	nd	nd	nd
Tb	nd	nd	nd	nd	nd	nd	nd	1	nd	nd	nd	nd
Yb	nd	nd	nd	nd	nd	nd	nd	2	nd	nd	nd	nd
Hf	nd	nd	nd	nd	nd	nd	nd	2	nd	nd	nd	nd

Sample	GA156	GA393
Location	JKN	JKN
Name	G	C
Size	M	M
Quality	+++	++++
SiO_2	46.41	46.83
TiO_2	1.61	2.10
Al_2O_3	17.06	17.01
FeO	12.41	12.38
MnO	0.24	0.22
MgO	7.86	6.64
CaO	9.67	8.75
Na_2O	3.12	3.61
K_2O	0.25	0.84
P_2O_5	0.14	0.24
Total	98.77	98.62
Mg#	53	49
Co	73	77
Ni	112	114
Cu	71	79
Rb	3	13
Sr	182	378
Y	24	25
Zr	95	93
Nb	2	3
Ba	nd	nd
La	nd	nd
Ce	nd	nd
Sm	nd	nd
Eu	nd	nd
Tb	nd	nd
Yb	nd	nd
Hf	nd	nd

APPENDIX B
OLIVINE CORONA MODELS

This appendix presents the calculation on olivine coronas from the Messel and Dale gabbro. The calculations represent a numeric example of two extreme models; an isochemical and an isovolume one. The principal goal of these calculations is to determine which of the two model fits best and discuss the consequence of the models.

THE OLIVINE CORONA FROM THE MESSEL GABBRO

I made the following assumptions in constructing a model for the genesis of olivine coronas:

1) The reaction between olivine and plagioclase is as follows:

Olivine + *Plagioclase* → *Orthopyroxene* + *Amphibole* + *Spinel* **(*B*.1)**

2) Influx of water is ignored.
3) The investigated corona has an ideal spherical shell texture. The diameter of the olivine is 5 mm, the orthopyroxene inner layer is 2 mm thick and an outer amphibole spinel symplectite layer 1.9 mm. These values are obtained from measurements of the olivine corona shown in figure B.1.
4) The Ca/(Ca+Na+K) ratio of amphibole is similar to that of the replaced plagioclase.

In addition to these assumptions I used the following data:

1) The densities of the mineral phases concerned the olivine corona are listed below.
   $D_{olivine\ (69\%Fo)} = 3.50\ gr/cm^3$
   $D_{plagioclase\ (75\%An)} = 2.72\ gr/cm^3$
   $D_{orthopyroxene\ (73\%En)} = 3.42\ gr/cm^3$
   $D_{pargasite\ (mean)} = 3.15\ gr/cm^3$
   $D_{spinel\ (mean)} = 4.05\ gr/cm^3$
2) The chemical analyses of olivine, orthopyroxene, amphibole, spinel and plagioclase, which are used for the model calculations, are listed in table B.1.
3) There are three main boundaries distinguished in the investigated olivine corona:
   Olivine Orthopyroxene boundary at 5.0 mm from the centre.
   Orthopyroxene Amphibole boundary at 7.0 mm from the centre.
   Amphibole Plagioclase boundary at 8.9 mm from the centre.

APPENDIX B

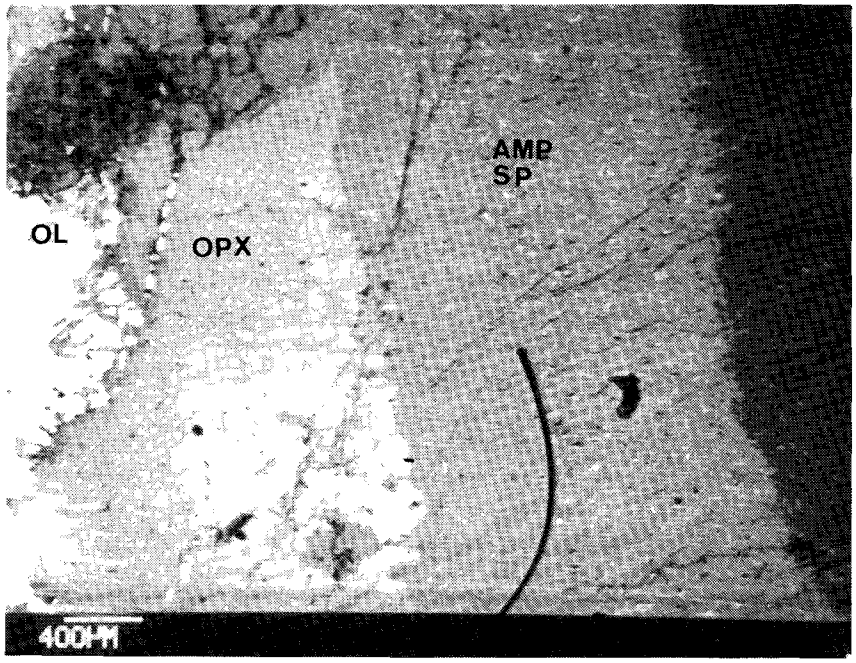

Figure B.1

SEM photograph of an olivine corona from the Messel gabbro. I used this photograph to obtain volume data for calculations on the models. A small spinel free amphibole rim on the outside of the orthopyroxene inner rim may indicate that the original olivine plagioclase boundary laid inside the amphibole layer.

The volume of the orthopyroxene layer is therefore:

$$\frac{4}{3} \times \pi \times (7^3\ mm - 5^3\ mm) = 913\ mm^3 \qquad \textbf{(B.2)}$$

The volume of the amphibole-spinel symplectite layer is:

$$\frac{4}{3} \times \pi \times (8.9^3\ mm - 7^3\ mm) = 1516\ mm^3 \qquad \textbf{(B.3)}$$

Table B.1 *CHEMICAL ANALYSES OF OLIVINE CORONA PHASES FROM THE MESSEL GABBRO*

Chemical microprobe analyses of the corona phases from the Messel gabbro. The plagioclase has a fictive composition with an anorthite percentage of 75 which is similar to the $^{Ca}/_{Ca+Na}$ *ratio of amphibole.*

Mineral	Olivine	Orthopyroxene	Amphibole	Spinel	Plagioclase
SiO_2	37.33	54.60	43.22	0.00	49.66
TiO_2	0.00	0.12	0.00	0.00	0.00
Al_2O_3	0.00	1.51	15.82	61.37	32.77
FeO	27.74	17.83	11.50	26.76	0.00
MnO	0.40	0.00	0.22	0.31	0.00
MgO	35.32	26.36	13.81	11.16	0.00
CaO	0.07	0.20	10.94	0.00	14.72
Na_2O	0.01	0.00	1.85	0.03	2.85
K_2O	0.00	0.00	0.23	0.00	0.00
Cl	0.00	0.00	0.00	0.00	0.00
F	0.00	0.00	0.00	0.00	0.00
Total	101.04	100.62	97.69	100.05	100.00
Negative charge	8	12	46	8	16
Si	0.99	1.95	6.28	0.00	2.25
Ti	0.00	0.00	0.00	0.00	0.00
Al	0.00	0.05	2.70	1.96	1.75
Fe	0.62	0.54	1.40	0.61	0.00
Mn	0.01	0.01	0.03	0.01	0.00
Mg	1.395	1.44	2.99	0.45	0.0
Ca	0.00	0.02	1.70	0.00	0.75
Na	0.00	0.00	0.52	0.00	0.25
K	0.00	0.00	0.04	0.00	0.00
Cl	0.00	0.00	0.02	0.00	0.00
F	0.00	0.00	0.00	0.00	0.00
Total	3.02	4.02	15.66	3.03	5.00
Mg#	69.4	72.81	68.19	42.65	-

APPENDIX B

ISOCHEMICAL MODEL FOR THE MESSEL CORONA

In this model I assume that the reaction between olivine and plagioclase is isochemical. I used the chemical composition listed in table B.1 to calculate the weight percentages of olivine, plagioclase, orthopyroxene, amphibole and spinel needed to balance an isochemical reaction (LeMaitre 1979; GENMIX computer program). An indication for the degree of isochemistry is represented by the SSQR number. This number is calculated by summing the squares of differences between the weight percentages of the oxides of reactants and products. A low SSQR number suggests isochemistry. The SSQR number for the olivine corona reaction in the Messel gabbro is 1.4 indicating isochemistry. The result of these calculations is presented in equation B.4. The weight percentages are recalculated to volume percentages. The total volume decrease associated with the corona formation is about 7%.

$$\begin{array}{lrcll} Wt\% & 52.1\ Ol + 47.8\ Plag & \rightarrow & 31.2\ Opx + 60.2\ Amph + 8.6\ Sp & \\ Vol(cm^3) & 14.89\ Ol + 17.61\ Plag & \rightarrow & 9.12\ Opx + 19.11\ Amph + 2.12\ Sp & \\ & \sum 32.5\ cm^3 & \rightarrow & \sum 30.35 cm^3 \qquad \Delta V = 7\% & \textbf{(B.4)} \end{array}$$

The calculated volume ratio Sp/(Sp+Amph) is about 11. The observed volume ratio Sp/(Sp+Amph) in the outer rim of the olivine corona, determined by point counting figure B.1, is about 6.8. This discrepancy between the calculated and observed spinel concentration may be due to neglecting the spinel in the surrounding plagioclase (cloudiness), which is in fact also part of the corona system.

The volume coefficients from equation B.4 are used to calculate the location of the original olivine plagioclase boundary with the following formula:

$$\frac{4}{3} \times \pi \times (R^3 - 5^3 mm) = \frac{4}{3} \times \pi \times (8.9^3 mm - 5^3 mm) \times Ol^{reacted\ fraction} \qquad \textbf{(B.5)}$$

In this formula, R is the radius of the original olivine grain. The fraction of olivine which reacted is obtained from equation B.4 and measures 45.8 Vol%. The value for R, the original size of the olivine crystal is thus 7.31 mm. As the distance from the centre of the olivine grain to the orthopyroxene amphibole boundary is 7 mm, I conclude that original olivine plagioclase boundary lies 0.31 mm in the present amphibole layer. It is thus very likely that the outer boundary of the spinel free amphibole layer coincides with the original olivine plagioclase contact.

EQUAL VOLUME REPLACEMENT MODEL FOR THE MESSEL CORONA

This model assumes a reaction between olivine and plagioclase in which the volume of orthopyroxene generated is equal to the volume depletion due to the reacted olivine. The volume of the amphibole spinel symplectite generated is equal to the consumed volume of plagioclase. The model is based on the assumption that the original olivine plagioclase boundary coincides with the orthopyroxene amphibole boundary. I calculated that 37.6 volume percentage olivine and 62.4 volume percentage plagioclase reacted according to the following formula:

$$\frac{913}{913+1516} \times 100\% = 37.6 \; Vol\% \; Olivine$$

$$\frac{1516}{913+1516} \times 100\% = 62.4 \; Vol\% \; Plagioclase \qquad (B.6)$$

The reaction products are 37.6 volume percentage orthopyroxene and 62.4 volume percentage of an amphibole spinel symplectite. The observed volume ratio Sp/(Sp+Amph) is about 6.8 and thus the volume percentage of amphibole in this model is 58.0 % and that of spinel is 4.4 %. These volume percentages due to reacting olivine and plagioclase to orthopyroxene, amphibole and spinel are used to calculate the corresponding weight percentages.

$$\begin{array}{l} 131.6 \; gr \; Ol + 169.7 \; gr \; Plag \rightarrow 128.6 \; gr \; Opx + 182.7 \; gr \; Amph + 17.82 \; gr \; Sp \\ \sum 301.3 \; gr \qquad\qquad \rightarrow \sum 329.12 \; gr \qquad (9\% \; mass \; increase) \end{array} \qquad (B.7)$$

This model calculation demonstrates that corona formation is associated with a mass transfer of 9%. I determined the mass transport of each element separately and listed the gains and losses in table B.2.

Table B.2 *MASS TRANSPORT IN OLIVINE CORONAS FROM THE MESSEL GABBRO*

Mass transport according to the equal volume model from an olivine corona from the Messel gabbro. The mean weighted chemistry before the olivine corona is listed in column 2 whereas the weighted chemistry of the corona products after the reaction is listed in column 3. The difference between these two columns is indicative for the mass transport and is listed in column 4.

	Reactant (Ol+Pl)	Product (Opx+Amph+Sp)	% adding(+) or removing(-)
SiO_2	49.1+84.3= 133.4	70.2+79.0+0= 149.2	+11.8%
TiO_2	0+0= 0	0.2+0+0= 0.2	+
Al_2O_3	0+55.6= 55.6	1.9+28.9+10.9= 41.7	-25.0%
FeO	36.5+0= 36.5	22.9+21.0+4.8= 48.7	+33.4%
MnO	0.1+0= 0.1	0+0.4+0.1= 0.5	+400%
MgO	46.5+0= 46.5	33.9+25.2+2.0= 61.1	+31.4%
CaO	0.1+25.0= 25.1	0.3+20.0+0= 20.3	-19.1%
Na_2O	0+4.8= 4.8	0+3.4+0= 3.4	-29.2%
K_2O	0+0= 0	0+0.4+0= 0.4	+

These results imply that in an open system considerable gains and losses of the elements occur during reaction between olivine and plagioclase which is in contrast to the conclusions reached earlier in chapter II.

THE OLIVINE CORONA FROM THE DALE GABBRO

Analogous to the two models applied on the Messel olivine coronas I modelled the olivine corona from the Dale gabbro. The assumptions I made are similar to those of the Messel olivine gabbro except:

1) The diameter of the olivine is 0.8 mm, the orthopyroxene inner layer is 1.8 mm thick and an outer amphibole-spinel symplectite layer 2 mm. These values are obtained from measurements of the corona shown in figure B.2.

The data used in the model for the Dale olivine corona differ from the data used for the Messel gabbro in:

2) The chemical analyses of the olivine, orthopyroxene, amphibole, spinel and plagioclase, which are used for the calculations, are listed in table B.2.
3) There are three main boundaries distinguished in the investigated olivine corona:
   Olivine Orthopyroxene boundary at 0.8 mm from the centre.
   Orthopyroxene Amphibole boundary at 2.6 mm from the centre.
   Amphibole Plagioclase boundary at 4.6 mm from the centre.

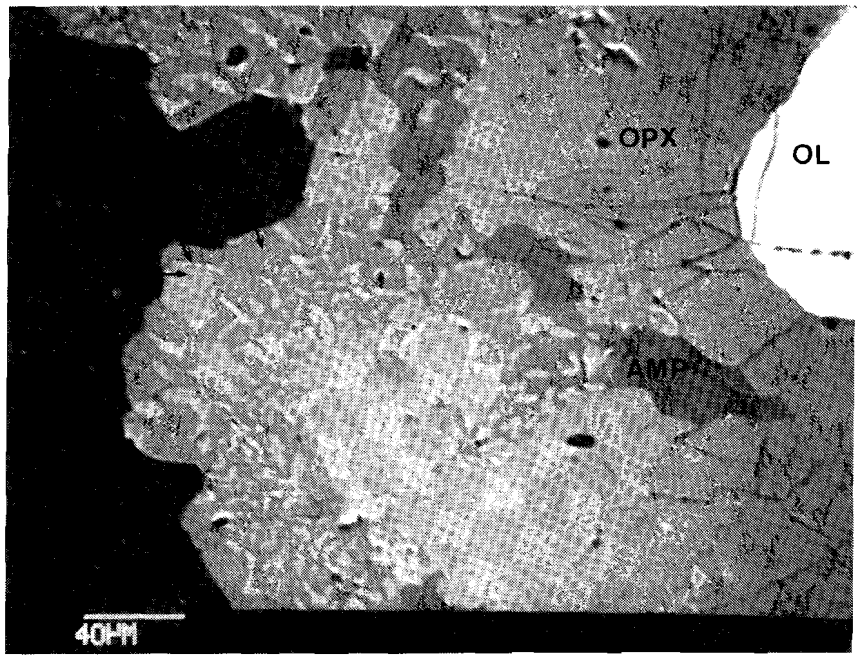

Figure B.2

SEM photograph of an olivine corona from the Dale gabbro. I used this photograph to obtain volume data for calculations on the models. The dehydration structure of the outer amphibole rim resulting in an orthopyroxene clinopyroxene symplectite is clearly visible.

Table B.3 *CHEMICAL ANALYSES OF OLIVINE CORONA PHASES FROM THE DALE GABBRO*

Chemical microprobe analyses of the corona phases from the Dale gabbro. The plagioclase has a fictive composition with an anorthite percentage of 75 which is close to the $^{Ca}/_{Ca+Na}$ ratio of amphibole (72).

Mineral	Olivine	Opx	Amph	Spinel	Plag	Augite
SiO_2	37.48	53.23	41.31	0.19	49.66	53.33
TiO_2	0.00	0.00	0.30	0.28	0.00	0.00
Al_2O_3	0.00	2.28	16.74	63.87	32.77	3.34
FeO	29.45	17.99	9.62	22.54	0.00	6.07
MnO	0.68	0.68	0.00	0.00	0.00	0.23
MgO	32.62	24.99	14.08	12.72	0.00	14.74
CaO	0.00	0.41	11.81	0.20	14.72	22.16
Na_2O	0.00	0.00	2.59	0.00	2.85	0.82
K_2O	0.00	0.00	1.35	0.00	0.00	0.00
Cl	0.00	0.00	0.25	0.00	0.00	0.00
F	0.00	0.00	0.00	0.00	0.00	0.00
Total	100.23	100.12	97.80	99.80	100.00	100.69
Negative charge	8	12	46	8	16	12
Si	1.01	1.94	6.02	0.01	2.25	1.95
Ti	0.00	0.00	0.04	0.01	0.00	0.00
Al	0.00	0.21	2.88	1.98	1.75	0.14
Fe	0.66	0.55	1.17	0.50	0.00	0.18
Mn	0.02	0.02	0.00	0.00	0.00	0.01
Mg	1.31	1.36	3.06	0.50	0.0	0.80
Ca	0.00	0.02	1.85	0.01	0.75	0.87
Na	0.00	0.00	0.74	0.00	0.25	0.06
K	0.00	0.00	0.25	0.00	0.00	0.00
Cl	0.00	0.00	0.06	0.00	0.00	0.00
F	0.00	0.00	0.00	0.00	0.00	0.00
Total	3.00	4.00	16.00	3.00	5.00	4.01
Mg#	66.36	71.27	72.25	50.15	-	81.36

The volume of the orthopyroxene layer is therefore:

$$\frac{4}{3}\times\pi\times(2.6mm^3-0.8mm^3)=71.5\,mm^3 \qquad \textbf{(B.8)}$$

The volume of the amphibole/spinel symplectite layer is:

$$\frac{4}{3}\times\pi\times(4.6mm^3-2.6mm^3)=334.1\,mm^3 \qquad \textbf{(B.9)}$$

ISOCHEMICAL MODEL FOR THE DALE CORONA

Two reactions are considered in the formation of the olivine coronas from the Dale gabbro. The first reaction is described by the following equation:

Wt%	55.0 *Ol*	+	45.0 *Plag*	→	58.0 *Opx* + 30.0 *Amph* +	12.0 *Sp*	
Vol(cm^3)	15.71 *Ol*	+	16.54 *Plag*	→	16.96 *Opx* + 9.52 *Amph* +	0.54 *Sp*	
	$\sum$ 32.25 cm^3			→	$\sum$ 27.02cm^3	$\Delta V=16\%$	**(B.10)**

The volume change associated with the corona reaction is about 2.5 times higher then in the model of olivine corona from the Messel gabbro. The reaction is substantial less isochemical than in the Messel olivine corona as can be deduced from an SSQR number of 4.1.

Analogous to previous calculations, the original olivine plagioclase boundary in the Dale gabbro olivine corona is calculated by using the following equation:

$$\frac{4}{3}\times\pi\times(R^3-0.8^3mm)=\frac{4}{3}\times\pi\times((4.6^3mm-0.8^3mm))\times Ol^{reacted\ fraction} \qquad \textbf{(B.11)}$$

In this formula R is the radius of the original olivine grain. The fraction of olivine which reacted can be calculated from equation B.8 and is 48.7 Vol%. R is thus 3.63 mm indicating that the location of the original olivine plagioclase boundary was situated about 1.63 mm in the present amphibole layer. This is a relative high value in relation to the total size of the corona texture and to the calculations in olivine coronas from the Messel gabbro. This may explain the presence of the spinel free amphibole outer rim in some olivine coronas from the Dale gabbro.

The second reaction concerns the dehydration of the amphibole outer rim and is shown in the next equation:

$$Amphibole \rightarrow Orthopyroxene + Augite + Spinel(+albite) + Water \qquad \textbf{(B.12)}$$

Amphibole should react, in an isochemical model, to 44 Wt% augite, 26 Wt% orthopyroxene, 21 Wt% Spinel and 9 Wt% plagioclase. The SSQR number is ~20 indicating that the reaction laid down in equation B.12 is far from isochemical.

EQUAL VOLUME REPLACEMENT MODEL FOR THE DALE CORONA

Analogous to the calculations on the olivine coronas from the Messel gabbro I calculated the mass transfer from the olivine coronas from the Dale gabbro in the model of equal volume replacement. The volumes of concern in this model are:

$$\frac{71.5}{71.5+334.1} \times 100\% = 17.6 \; \textit{Vol\% Olivine}$$

$$\frac{334.1}{71.5+334.1} \times 100\% = 82.4 \; \textit{Vol\% Plagioclase} \qquad \textbf{(B.13)}$$

The Sp/(Sp+Amph) ratio has been determined by point counting a magnified photograph of an amphibole spinel symplectite from an olivine corona from the same sample and is 9.1. Thus the volume percentage amphibole is 74.9% and the volume percentage spinel is 7.5%. These volume percentages are used in the following equation:

$$\begin{aligned} &61.7 \; gr \; Ol + 224.1 \; gr \; Plag \rightarrow 60.3 \; gr \; Opx + 235.9 \; gr \; Amph + 30.4 \; gr \; Sp \\ &\textstyle\sum 285.8 \; gr \qquad\qquad \rightarrow \sum 326.6 \; gr \qquad (14\% \; \textit{mass increase}) \end{aligned} \qquad \textbf{(B.14)}$$

Analogous to the Messel olivine corona model I calculated the mass transfer for each element which is listed in table B.4. If the equal volume model had been operative, considerable mass transfer must have occurred which is in contrast to previous observations.

In conclusion, it is most likely that the isochemical model has been operative in the formation of olivine coronas in the Messel gabbro and to lesser extent in the Dale gabbro. The isochemical model may also be applied to the olivine coronas from the Jomasknutene gabbro. Although this appendix presents only two numeric examples, olivine coronas from the investigated gabbros are likely to have formed more or less isochemically.

Table B.4 *MASS TRANSPORT IN OLIVINE CORONAS FROM THE DALE GABBRO*

Mass transport during the olivine corona reaction of the Dale gabbro according to equal volume model. The mean weighted chemistry before the olivine corona is listed in column 2 whereas the weighted chemistry of the corona products after the reaction is listed in column 3. The difference between these two columns is indicative for the mass transport and is listed in column 4.

	Reactant (Ol+Pl)	Product (Opx+Amph+Sp)	% adding(+) or removing(-)
SiO_2	23.3+117.7=140.0	32.1+98.8+0.1 =131.0	-7.0%
TiO_2	0+0.4= 0.4	0+0.7+0.1= 0.8	+
Al_2O_3	0+68.6= 68.6	1.7+39.8+19.4= 60.9	-11.2%
FeO	18.2+0= 18.2	10.9+19.7+6.9= 37.5	+106.0%
MnO	0.4+0= 0.4	0.4+0.8+0= 1.2	+200%
MgO	20.1+0= 20.1	15.1+34.8+3.9= 53.8	+167.7%
CaO	0.0+28.6= 28.6	0.0+28.0+0= 28.0	-2.1%
Na_2O	0+9.7= 9.7	0+6.3+0= 6.3	-35.0%
K_2O	0+0.13= 0.13	0+2.88+0= 2.88	+

REFERENCES

Ashby, M.F. and **Jones**, D.R.H. 1988.
Engineering materials 2; an introduction to microstructures, processing and design.

Boland, J.N. 1974.
Lamellar Structures in low-calcium orthopyroxenes.
Contribution to Mineralogy and Petrology, 47, 215-222.

Bottinga, Y. and **Weill**, D.F. 1972.
The viscosity of magmatic silica liquids: a model for calculation.American Journal of Science, 272, 438-475.

Boudreau, A.E., **Mathez**, E.A. and **McMallum**, I.S. 1986.
Halogen Geochemistry of the Stillwater and Bushveld complex: evidence for transport of the platinum-group elements by Cl-rich fluids.
Journal of Petrology, 27 (4), 967-986.

Bowen, N.L. and **Schairer**, J.F. 1935.
The system MgO-FeO-SiO_2.
American Journal of Science, 29, 151-217.

Brickwood, J.D. and **Craig**, J.W. 1987.
Primary and re-equilibrated mineral assemblages from the Sveconorwegian mafic intrusions of the Kongsberg and Bamble areas, Norway.
Norsk Geologisk Undersøkelse, 410, 1-23.

Brøgger, W.C. 1934.
On several Archean rocks from the south coast of Norway II. The south norwegian hyperites and their metamorphism.
Skr. Nor. Vid. Ak. Mat. Nat. Kl. 1, 1-421.

Brueckner, H.K. 1972.
Interpretation of Rb-Sr ages from the Precambrian and Palaeozoic rocks of southern Norway.
American Journal of Science, 272, 334-358.

Bugge, J.A.W. 1943.
Geological and petrological investigations in the Kongsberg Bamble formations.
Norsk Geologisk Undersøkelse, 160, 1-150.

Burke, E.A.J. and **Lustenhouwer**, W.J. 1987.
The application of a multichannel laser Raman microprobe (Microdil-28®) to the analysis of fluid inclusions.
Chemical Geology, 61, 11-17.

Buseck, P.R, **Nord**, G.L. and **Veblen**, D.R. 1980.
Subsolidus phenomena in pyroxenes.
Reviews in Mineralogy, Pyroxenes, Volume 7, 117-211.
Editor: C.T. Prewitt.

Carlson, W.D., **Swinnea**, J.S., and **Miser**, D.E. 1988.
Stability of orthoenstatite at high temperature and low pressure.
American Mineralogist, 73, 1255-1263.

Carmichael, I.S.E, **Turner**, F.J. and **Verhoogen**, J. 1974.
Igneous petrology.

Claesson, S., **Huhma**, H., **Kinny**, P. and **Williams**, I.S., 1991.
Provence of Svecofennian metasediments: U-Pb dating of detrital zircons.
Terra abstracts, 3, 505.

Coe, R.S. and **Kirby**, S.H. 1975
The orthoenstatite to clinoenstatite transformation by shearing and reversion by annealing: mechanism and potential applications.
Contribution to Mineralogy and Petrology, 52, 29-55.

Daly, J.S. **Park**, R.G. and **Cliff**, R.A., 1983.
Rb-Sr isotopic equilibrium during Sveconorwegian (=Grenville) deformation and metamorphism of the Orust dykes, S.W. Sweden
Lithos, 16, 307-318.

Dam, B.P. and van **Roermund**, H.L.M. 1989.
The thermal and metamorphic history of intercumulus augite from the Bamble area, SE Norway.
Ultramicroscopy, 17, 201-202.

Dick, L.A. and **Robinson**, G.W. 1979.
Chlorine-bearing potassian hastingsite from a sphalerite skarn in southern Yukon.
Canadian Mineralogy, 17, 25-26.

Dowty, E. 1980.
Crystal growth and nucleation theory and the numerical simulation of igneous crystallization.
Physics of magmatic processes.
Editor: Hargraves, R.B.

Eggenkamp, H.G.M., 1994.
δ^{37}Cl. The geochemistry of chlorine isotopes.
PhD Thesis; University of Utrecht.
Geologica Ultraiectina 116.

England, R.N. 1974.
Corona structures formed by near-isochemical reaction between olivine and plagioclase in a metamorphosed dolerite.
Mineralogical Magazine, 39, 816-818.

England, P.C. and **Thompson**, A.B. 1984.
Thermal requirements for crustal melting in continental collision zones.
Journal Geological Society of London.

Falkum, T. 1985
Geotectonic evolution of southern Scandinavia in the light of late-proterozoic plate-collision.
The deep proterozoic crust of the North Atlantic provinces, NATO ASI Series C Volume 158, 309-322.
Editors: Tobi, A.C. and Touret, J.L.R.

Falkum, T. 1990.

REFERENCES

The Proterozoic evolution of southwestern Fennoscandia - crustal accretion or ensialic rejuvenation.

Second symposium on the Baltic Shield, Lund, Sweden, 10.

Falkum, T. and **Petersen**, J.S., 1980.

The Sveconorwegian orogenic belt, a case of late-Proterozoic plate-collision.

Geologische Rundschau, 69, 622-647.

Field, D. and **Råheim**, A. 1979.

Rb-Sr total whole rock isotope study on Precambrian charnockitic gneiss from south Norway: evidence for isochron resetting during a low-grade metamorphic deformational event.

Earth and Planetary Science Letters, 45, 32-44.

Field, D. and **Råheim**, A. 1981.

Age relationship in the Proterozoic high-grade gneiss regions of southern Norway.

Precambrian Research, 14, 261-275.

Field, D., **Smalley**, P.C., **Lamb**, R.C. and **Råheim**, A., 1985.

Geochemical evolution of the 1.6 - 1.5 Ga old amphibolite-granulite facies terrain, Bamble sector, Norway: dispelling the myth of Grenvillian high grade reworking.

The deep proterozoic crust of the North Atlantic provinces, NATO ASI Series C Volume 158, 567-578.

Editors: Tobi, A.C. and Touret, J.L.R.

Frodesen, S. 1968.

Coronas around olivine in a small gabbro intrusion, Bamble area, south Norway.

Norsk Geologisk Tidsskrift, 48, 201-206.

Gaál, G. and **Gorbatschev**, R., 1987.

An outline of the Precambrian evolution of the Baltic Shield.

Precambrian Research, 35, 15-52.

Geijer, P. 1959.

The distribution of halogens in skarn amphiboles in central Sweden.

Ark. Mineralogy and Geology, 2: 482-504.

Gorbatschev, R. and **Gaál**, G. 1987.

The Precambrian history of the Baltic Shield.

in: A. Krõner (ed), Proterozoic Lithospheric Evolution

American Geophysical Union, Geodynamics series.

Grant, S.M. 1988.

Diffusion models for corona formation in metagabbros from the western Grenville province, Canada.

Contribution to Mineralogy and Petrology, 98, 49,63.

Grieve, R.A.F. and **Gittins**, J. 1975.

Composition and formations of coronas in the Hadlington Gabbro, Ontario, Canada.

Canadian Journal of Earth Sciences, 12, 289-299.

Griffin, W.L. 1971.

Genesis of coronas in anorthosites of the upper Jotun Nappe, Indre Sogn, Norway.

Journal of Petrology, 12, 219-243.

Grover, J. 1972.

The stability of low-clinoenstatite in the system $Mg_2Si_2O_6$-$CaMgSi_2O_6$.

EOS, Trans American Geophysical Union, 53, 539.

Haas, G.J.L.M de, 1992.

Source evolution, and age of the coronitic gabbros from the Arendal-Nelaug area, Bamble, southeast Norway.

PhD Thesis; University of Utrecht, 1-129.

Geologica Ultraiectina 86.

Hagelia, P., 1989.

Structure, metamorphism and geochronology of the Skagerrak Shear Belt, as revealed by studies in the Hovdefjell-Ubergsmoen area, South Norway.

Unpublished M.Sc. thesis; University of Oslo, 1-238.

Hageskov, B. and **Pedersen**, S., 1988.

Rb/Sr age determination in the Kattsund-Koster dyke swarm in the Østfold-Marstrand belt of the Sveconorwegian province, W. Sweden-SE Norway.

Bulletin of the Geological Society of Denmark, 37, 51,51.

Hargraves, R.B., 1986.

Faster spreading or greater ridge length in the Archean.

Geology, 14, 750-752.

Harley, S.L. 1984.

An experimental study of the partitioning of Fe and Mg between garnet and orthopyroxene.

Contributions to Mineralogy and Petrology, 86, 359-373.

Holland, T.J.B. and **Powell**, R. 1990.

An enlarged and updated internally consistent thermodynamic data set with uncertainties and correlations: the system K_2O-Na_2O-CaO-MgO-MnO-FeO-Fe_2O_3-Al_2O_3-TiO_2-SiO_2-C-H_2-O_2.

Journal of Metamorphic Geology, 8, 89-124.

Huebner, J.S. and **Turnock**, A.C. 1980.

The melting relation at 1 bar of pyroxenes composed largely of Ca-, Mg-, and Fe-gearing components.

American Mineralogist, 65, 225-271.

Ito, E., **Harris**, D.M. and **Anderson**, A.T. 1983.

Alteration of oceanic crust and geological cycling of chloride and water.

Geochimica et Cosmochimica Acta, 47, 1613-1624.

Jacobson, S.S. 1975.

Dashkessanite: high-chlorine amphibole from St.Paul's rocks, Equatorial Atlantic Transcaucasia, U.S.S.R.

Mineral Science Investigation, Contribution to Earth Science Smithonian Institute, 14, 17-20.

Jacobson, S.B. and **Heier**, K.S., 1978.

Rb-Sr isotope systematics in metamorphic rocks, Kongsberg sector, south Norway.

Lithos, 11, 257-276.

James, P.R. and **Ding**, P. 1988.

'Caterpillar tectonic' in the Harts Range area: a kinship between two sequential Proterozoic extension-collision orogenic belts within the eastern Arunta inlier of central Australia.

Precambrian Research, 40/41, 199-216.

Joesten, R. 1977.
Evolution of mineral assemblage zoning in diffusion metasomatism.
Geochimica et Cosmochimica Acta, 41, 649-670.

Joesten, R. 1986.
The role of magmatic reaction, diffusion and annealing in the evolution of coronitic microstructures in troctolitic gabbro from Risør, Norway.
Mineralogical Magazine 50, 441-467.

Johnson, E.L. 1991.
Experimentally determined limits for H_2O-CO_2-NaCl immiscibility in granulites.
Geology, 19, 925-928.

Johnson, C.D. and **Carlson**, D. 1990.
The origin of olivine-plagioclase coronas in metagabbros from the Adirondack mountains, New York.
Journal of Metamorphic Petrology, 8, 697-717.

Jong, B.H.W.S. de 1989.
Glass.
Ullmann's Encyclopedia of Industrial Chemistry.
Volume A 12, 365-432.
VCH Verlagsgesellschaft.

Karmineni, D.C., **Bonardi**, M. and **Rao**, A.T. 1982.
Halogen-bearing minerals from the Airport Hill, Visaskhapatnam, India.
American Mineralogist, 67, 1001-1004.

Kerkhof, A.M. van den, 1990.
Isochoric phase diagrams in the system CO_2-CH_4 and CO_2-N_2: Application to fluid inclusions.
Geochimica et Cosmochimica Acta, 54, 621-629.

Kirkpatrick, R.J. 1983.
Theory of nucleation in silica melts.
American Mineralogist, 68, 66-77.

Krutov, G.A. 1936.
Dashkessanite-a new chlorine amphibole of the hastingsite group.
Dokl. Akad. Nauk. S.S.S.R., 341-373.

Kullerud, L and **Machado**, N. 1991.
End of a controversy: U-Pb geochronological evidence for significant Grenvillian activity in the Bamble area, Norway.
Terra Abstracts., 3, 504.

Kushiro, I. 1973.
The system diopside-anorthite-albite: determination of compositions of coexisting phases.
Yb. Carnegie Instn Wash., 72, 502-507.
In:The interpretation of igneous rocks.
Editors: Cox, K.G., Bell, J.D. and Pankhurst, R.J.

Lachenbruch, A.H. 1970.
Crustal temperature and heat production: Implications of the linear heat-flow relation.
Journal of Geology, 75, 3291-3300.

Lamb, R.C., **Smalley**, P.C. and **Field**, D., 1986.
P-T conditions for the Arendal granulites, southern Norway: implications for the role of P, T and CO_2 in deep crustal LILE-depletion.
Journal of Metamorphic Geology, 4, 143-160.

Lamoen, H. van 1979.
Phase relations in metamorphosed iron ore bearing gabbros from SW Finland.
PhD Thesis; Free University of Amsterdam, 1-112.

Leake, B.E. 1978.
Nomenclature of amphiboles.
American Mineralogist, 63, 1023-1053.

Lee, H.Y. and **Ganguly**, J. 1988.
Equilibrium compositions of coexisting garnet and orthopyroxene: Experimental determination in the system FeO-MgO-Al_2O_3-SiO_2 and applications.
Journal of Petrology, 29, 93-113.

LeMaitre, R.W. 1979.
A new generalized petrological mixing model.
Contribution to Mineralogy and Petrology, 71, 133-137.

Lindh, A., 1987.
Westward growth of the Baltic Shield.
Precambrian Research, 35, 53-70.

Maijer, C. 1990.
Metamorphism in the Froland-Nelaug-Tvedestrand Arendal area, Bamble: reevaluation of the Sveconorwegian as a high grade event.
Geonytt, 17, 75.

McLaren, A.C. and **Etheridge**, M.A. 1976.
A transmission electron microscope study of natural deformed orthopyroxene.
Contribution to Mineralogy and Petrology, 57, 163-177.

Monkoltip, P. and **Ashworth**, J.R. 1983.
Quantative estimation of an open-system symplectite-forming reaction: restricted diffusion of Al and Si in coronas around olivine.
Journal of Petrology 24, 635-661.

Morimoto, N., **Fabries**, J, **Ferguson**, A.K., **Ginzburg**, I.V., **Ross**, M., **Seifert**, F.A. and **Zussman**, J. 1988.
Nomenclature of pyroxene.
Mineralogical Magazine, 52, 535-550.

Munz, I.A. and **Morvik**, R. 1991.
Metagabbros in the Modem Complex, southern Norway: an important heat source for Sveconorwegian metamorphism.
Precambrian Research, 52, 97-113.

Nijland, T.G. 1993.
The Bamble amphibolite to granulite facies transition zone, Norway.
PhD Thesis; University of Utrecht, 1-166.
Geologica Ultraiectina 101.

REFERENCES

Nijland, T.G. and **Maijer**, C. 1992.

Lower crustal transition I. Changing mineral assemblage and thermobarometric estimates over a classical amphibolite to granulite transition zone Bamble, Norway.

First Netherlands Earth Scientific Congres, April 23-24, 1992.

Nijland, T.G., **Maijer**, C., **Senior**, A. and **Verschure**, R.H., 1993.

Primary sedimentary structures and composition of the high grade Nidelva Quartzite Complex [Bamble, Norway], and the origin of nodular gneisses.

Proc. Kon. Ned. Akad. van Wetensch., 96(2), 217-232.

Nijland,T.G. and **Senior**, A. 1991.

Sveconorwegian granulite facies metamorphism of polyphase migmatites and basic dikes, south Norway.

Journal of Geology, 99, 515-525.

Nishiyama, T. 1983.

Steady diffusion model for olivine-plagioclase corona growth.

Geochimica et Cosmochimica Acta, 47, 283-294.

Nord, G.L. and **McCallister**, R.H. 1979.

Kinetics and mechanism of decomposition in Wo_{25} En_{31} Fs_{44} clinopyroxene.

Geological Society of America, 11, 488.

O'Nions, R.K. and **Baadsgaard**, H., 1971.

A radiometric study of polymetamorphism in the Bamble region, Norway.

Contribution to Mineralogy and Petrology, 34, 1-21.

Parson, I. and **Brown**, W.L. 1984.

Feldspars and the thermal history of igneous rocks.

Feldspar and Feldspatoids, Structures, Properties and Occurrences, Nato ASI Series C Volume 137, 317-371.

Editor: Brown, W.L.

Pasteels, P.J. and **Michot**, J., 1975.

Geochronological investigation of the metamorphic terrain of SW Norway.

Norsk Geologisk Tidskrift, 55, 111-134.

Perchuck, L.L., **Aranovich**, L.Ya., **Podlesskii**, K.K., **Lavranteva**, I.V., **Gerasimov**, V.Yu., **Fed'kin**, V.V., **Kitsul**, V.I., **Karsakov**, L.P. and **Berdnikov**, N.V. 1985.

Precambrian granulites of the Aldan shield, eastern Siberia, USSR.

Journal of Metamorphic Geology, 3, 265-310.

Poorter, R.P.E., 1981.

Precambrian palaeomagnetism of Europe and the position of the Balto-Russian plate relative to Laurentia.

in: A. Kröner (ed), Precambrian plate tectonics

Elsevier, Amsterdam, Dev. Precam. Geol., 4, 599-622.

Richter, F.M., 1988.

A major change in the thermal state of the earth at the Archean-Proterozoic Boundary: consequences for the nature and preservation of continental lithosphere.

Journal of Petrology, Special Lithosphere Issue, 39-52.

Robie, R.A. and **Bethke**, P,M. 1966.

Molar volumes and densities of minerals.

Handbook of physical constrains, 60-73.

Editor: Clark, S.P.Jr.

Sanders, A. and **Tarney**, J. 1991.

Chapter 10: Back arc basins.

in: P.A. Floyd (ed), Oceanic basalts.

Blackie Glasgow & London.

Schiffries, C.M. and **Skinner**, B.J. 1987

The Bushveld hydrothermal system: field and petrological evidence.

American Journal of Science, 287, 566-595.

Sclater, J.G., **Jaupart**, C. and **Galson**, D. 1980.

Heat flow through oceanic and continental crust, and heat loss of the Earth.

Reviews Geophysical Space Physics, 81, 269-312.

Sclater, J.G., **Parson**, B.E. and **Jaupart**, C. 1981.

Oceans and continents: similarities and differences in the mechanism of heat loss.

Sen, S.K. and **Bhattacharya**, A. 1984.

An orthopyroxene-garnet thermometer and its applications to the Madras charnockites.

Contribution to Mineralogy and Petrology, 88, 64-71.

Sengupta, P., **Dasgupta**, S., **Bhattacharya**, P.K. and **Mukkerjee**, M. 1990

An orthopyroxene-biotite geothermometer and its application in crustal granulites and mantle derived rocks.

Journal of Metamorphic Geology, 8, 191-216.

Seyfried, W.E.Jr, **Berndt**, M.E. and **Janecky**, D.R. 1986.

Chloride depletions and enrichments in seafloor hydrothermal fluids: Constrains from experimental basalt alteration studies.

Geochimica et Cosmochimica Acta, 50, 469-475.

Shuma, K. , **Enami**, M. and **Horiuchi**, T. 1987.

Chlorine-rich potassium hastingsite from west Ongul island, Lutzow-Holm Bay, east Antarctica.

Mineralogical Magazine, 51, 709-714.

Solyom, Z., **Lindqvist**, J.E. and **Johansson**, I., 1992

The geochemistry, genesis and geotectonic setting of Proterozoic mafic dike swarms in southern and central Sweden.

Geologiska Föreningens i Stokholm Föhandlinger, 14, 47-65.

Starmer, I.C. 1969.

Basic plutonic intrusions of the Risør-Sondeled area, South Norway: The original lithologies and their metamorphism.

Norsk Geologisk Tidsskrift, 49, 403-431.

Starmer, I.C. 1985.

The evolution of the South Norwegian Proterozoic as revealed by major and mega-tectonics of the Kongsberg and Bamble sectors.

The deep proterozoic crust of the North Atlantic provinces, NATO ASI Series C Volume 158, 259-290.

Editors: Tobi, A.C. and Touret, J.L.R.

Starmer, I.C. 1987.

Geological Map of the Bamble Sector, South Norway (1:100.000): 3 sheets.

The Geology of southernmost Norway. An excursion guide.

Norsk Geologisk Tidsskrift, 1987.

Editors: Maijer, C. and Padget, P.

Starmer, I.C., 1991.

The Proterozoic evolution of the Bamble sector shear belt, south Norway: correlation across southern Scandinavia and the Grenvillian controversy.

Precambrian Research, 49, 107-139.

Starmer, I.C., 1993.

The Sveconorwegian orogeny in southern Norway, relative to deep crustal structures and events in the north Atlantic Proterozoic supercontinent.

Norsk Geologisk Tidsskrift, 73, 109-132.

Theullngs, W.T., van **Ditshuizen**, G.P. 1987.

De coronitische gabbro van Vestre Dale.

Unpublished M.Sc. thesis; University of Utrecht.

Torske, T., 1985.

Terrane displacement and Sveconorwegian rotation of the Baltic Shield: a working hypothesis.

The deep proterozoic crust of the North Atlantic provinces, NATO ASI Series C Volume 158, 333-343.

Editors: Tobi, A.C. and Touret, J.L.R.

Touret, J.L.R. 1969.

Le socle Precambrian de la Norvège méridionale.

Unpubl. PhD Thesis, University of Nantes, 1-609.

Touret, J.L.R. 1985.

Fluid regime in southern Norway: the record of fluid inclusions.

The deep proterozoic crust of the North Atlantic provinces, NATO ASI Series C Volume 158, 517-549.

Editors: Tobi, A.C. and Touret, J.L.R.

Touret, J.L.R. and **Dietvorst**, P. 1983.

Fluid inclusions in high grade anatectic metamorphites.

Journal of Geology, 140-4, 635-649.

Trommsdorff, V. and **Skippen**, G. 1987.

Metasomatism involving fluids in CO_2-H_2O-NaCl.

Chemical transport in metasomatic processes, 133-152.

Editor: Helgeson, H.C.

Turcotte, D.L. and **Schubert**, G. 1982.

Geodynamics: application of continuum physics to geological problems.

J.Wiley & Sons, N.Y., 1-450.

Turkdogan, E.T. 1983.

Physicochemical properties of molten slags and glasses.

The metals Society, London.

Editor: Turkdogan, E.T.

Vanko, D.A. 1986.

High-chlorine amphiboles from oceanic rocks: product of highly saline hydrothermal fluids ?

American Mineralogist, 71, 51-59.

Verschure, R.H. 1985.

Geochronological frame work for the late Proterozoic evolution of the Baltic Shield in south Scandinavia.

The deep proterozoic crust of the North Atlantic provinces, NATO ASI Series C Volume 158, 381-410.

Editors: Tobi, A.C. and Touret, J.L.R.

Visser, D. 1993.

The metamorphic evolution of the Bamble sector, south Norway.

PhD Thesis; University of Utrecht, 1-159.

Geologica Ultraiectina 103.

Vlaar N.J., 1985.

Precambrian geodynamical constrains.

The deep proterozoic crust of the North Atlantic provinces, NATO ASI Series C Volume 158, 3-20.

Editors: Tobi, A.C. and Touret, J.L.R.

Volfinger, M. , **Robert**, J.-L. and **Neiva**, A.M.R. 1985.

Structural control of the chlorine content of OH-bearing silicates (mica and amphiboles).

Geochimica et Cosmochimica Acta, 49, 37-48.

Wahlgren, C.H., 1981.

The Stora-Busjön conglomerate- an indication of granitoid basement in the gneiss complex of south-western Sweden.

Sver. Geologisk Undersökelse, C781:31-37.

Ward, P., 1987.

Early Proterozoic deposition and deformation at the Karelian craton margin in southeastern Finland.

Precambrian Research, 35, 71-93.

Wells, P.R.A. 1979.

Pyroxene thermometry in simple and complex systems.

Contribution to Mineralogy and Petrology, 62, 129-139.

Wood, B.J. and **Banno**, S. 1973.

Garnet orthopyroxene and orthopyroxene clinopyroxene relationships in simple and complex systems.

Contribution to Mineralogy and Petrology, 42, 109-124.

Yoder, H.S. and **Tilley**, C.E. 1962.

Origin of basalt magmas: an experimental study of natural and synthetic rock systems.

Journal of Petrology, 3, 342-532.

Åhäll, K.I. and **Daly**, J.S., 1989.

Age, tectonic setting and provenance of Östfold-Marstrand Belt supracrustals: westward crustal growth of the Baltic Shield at 1760 Ma.

Precambrian Research, 45: 45-61.

CURRICULUM VITAE

PERSONALIA

Name:	Bastiaan Pieter Dam
Address:	Iepstraat 8
Residence:	3581 LL Utrecht, the Netherlands
Telephone:	+(0)30-545245
Born:	4th January 1964

CAREER

1994 Completion of my dissertation.

1991-1993 **Database specialist**

I participated the development of complex relational database applications on an IBM-RS6000 computer, a UNIX operating system and an INFORMIX database management system.

1986-1990 **Research co-worker**

I participated a research project at:

State University of Utrecht, the Netherlands
Institute of Earth Sciences
Group: Geochemistry, Petrology

EDUCATION

1982-1986 **University**

I studied geology at:

State University Utrecht, the Netherlands
Institute of Earth Sciences
Group: Geochemistry, Petrology

- Main subject: Petrology
- Additional subjects: Geophysical exploration methods (seismics, electro magnetic methods)
  Scanning and Transmitting electron microscopy

1976-1982 **Secondary school**

Subjects: Dutch, English, Mathematics, Physics, Chemistry and Biology.